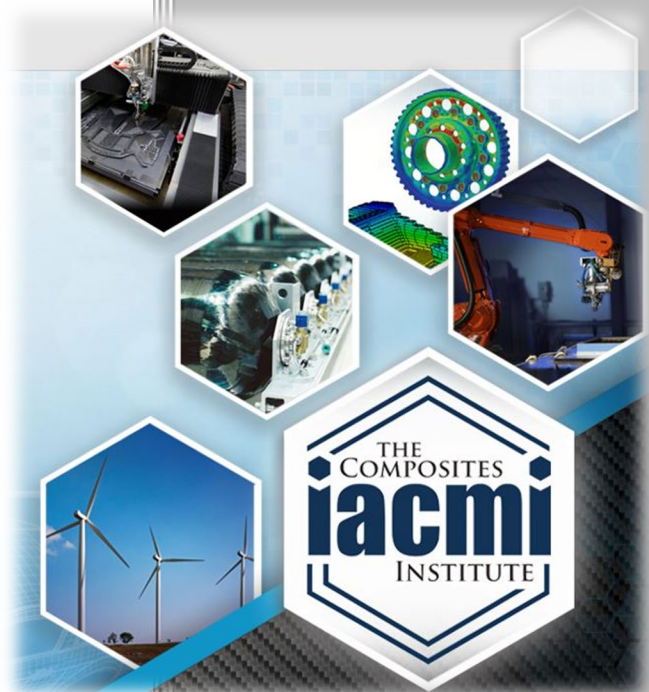# Development of Additively Manufactured Complex Tools for Autoclave Cure Composites

Author: Donald W. Radford
Date: November 2, 2021

Final Technical Report
PA16-0349-4.9-01

Approved for Public Release.
Distribution is Unlimited.

Acknowledgments

Development of Additively Manufactured Complex Tools for Autoclave Cure Composites

Principal Investigator: Donald W. Radford

Organization: Composite Manufacture, Materials, and Structure Laboratory, Colorado State University

Address: 3317 W. Vine Dr., Fort Collins, CO, 80521

Phone:

Email:

Industry Partner: Frank Roundy, Ability Composites

Date Published: (July, 2021)

Production and Evaluation of Tooling prepared by: Isaac M. Morris & Donald W. Radford
Colorado State University (CSU)

Techno-Economic Modeling prepared by: Paul Murdy, David Snowberg & Derek Berry
National Renewable Energy Laboratory (NREL)

Project Period:
(11/2019 – 04/2021)

TABLE OF CONTENTS

LIST OF ACRONYMS/TERMINOLOGY

3D	three dimensional
AQ-120	Aquasys 120
AQ-180	Aquasys 180
BVOH	Butenediol Vinyl Alcohol
CAD	Computer Aided Design
CL-130	Chamberlay 130
CNC	Computer Numerical Control
CTE	Coefficient of Thermal Expansion
CMMS	Composite Materials, Manufacture and Structures Laboratory
CSU	Colorado State University
HDT	Heat Deflection Temperature
IACMI	Institute for Advanced Composites Manufacturing Innovation
PETG	Polyethylene terephthalate glycol
PPE	Personal Protective Equipment
PTFE	Polytetrafluoroethylene
Road	The printed bead, or path of plastic on the surface
T_g	Glass Transition Temperature
TEM	Techno-Economic Model
TSP	Trisodium Phosphate

LIST OF FIGURES

LIST OF TABLES

EXECUTIVE SUMMARY

IACMI Project 4.9, Tooling for Composites with Washout Features Produced by Additive Manufacturing, assembled a team including the industry lead, Ability Composites, NREL and Colorado State University (CSU). Ability Composites had originally expressed interest in alternate methods of producing tooling for composite parts. In follow-up discussions, it became clear that one of the bigger tooling challenges revolved around small production volume composite parts that were tooled on washout material due to the complex geometry. To build an understanding of the potential, both from a technology and a cost perspective, for replacing conventional washout tooling with 3D printed thermoplastic tooling, a number of commercially available dissolvable FDM printing materials were evaluated, leading to tooling representative of commercial articles of interest to Ability Composites. Ultimately, Ability Composites was able to directly compare autoclave processed prepreg composite parts produced on conventional washout tooling to composite parts molded on 3D printed dissolvable tooling produced at CSU.

Small, laboratory test specimens were developed to investigate the structural performance of the candidate materials under autoclave processing conditions, which were nominally 121 °C (250 °F) and 345 kPa (50 psi). In addition, several internal structural configurations (infills) were evaluated under autoclave conditions using model materials. The results of these tests indicated that two materials, Stratasys ST-130 and Infinite Materials Solutions Aquasys 180 (AQ-180), were the best candidates, given the specified autoclave processing conditions. ST-130 was slightly more robust than AQ-180; however, the AQ-180 was carried forward as it was dissolvable in water, not requiring the basic solution needed to dissolve ST-130. Based on the preliminary material and 3D printed structures evaluations, larger tools with a truncated square pyramid geometry were created to produce prepreg composite test articles for 3D printed dissolvable tool evaluation under standard autoclave fabrication conditions. Two tools were manufactured using ST-130 and one tool using traditional ceramic washout tooling media. The tools were evaluated for geometric fidelity and surface roughness changes before and after carbon fiber/epoxy prepreg composites were manufactured on the tooling. The autoclave processing did not impact the geometry significantly and was completed at 121 °C and 345 kPa, indicating satisfactory tool performance. The results from surface roughness testing of both the resulting composite and the associated tooling indicated that an adequate surface resulted without the need for a surface sealing step, as was required for the conventional washout tooling.

Based on results of the truncated pyramid tests as a basis, ST-130, AQ-120 and AQ-180 materials were carried forward to the tool geometry of interest to Ability Composites. These hollow rectangular bent ducts, which were complex in nature and not extractable after cure, were used to understand the impacts of tool material and thickness. One ST-130 tool was produced as a partially solid part, with an enclosed 40% dense infill region to reduce weight and material use. This was the same approach evaluated in the truncated pyramid portion of the study. This tool was to be envelope vacuum bagged and directly compared to a monolithic tool of conventional washout material. The traditional monolithic ceramic tool was manufactured by Ability composites using CNC-based subtractive methods. An additional five dissolvable polymer tools, manufactured from ST-130, AQ-120, and AQ-180, using a hollow design were 3D printed and used to produce carbon fiber/epoxy composite evaluation articles. These hollow dissolvable tools were expected to be less influenced by the autoclave conditions as the wall was solid and vacuum bagging was inside and outside the tool. This alternative geometry was also evaluated as an option in techno-economic modeling. Print times were reduced from in excess of 3 days to under 30 hours, while surface quality and and tool integrity were substantially improved in the transition from the partially solid tool to the hollow tooling concept.

Ability Composites produced autoclave-cured prepreg ducts on each of these tools. The autoclave conditions utilized were more severe than those of the initial trials, reaching temperatures of 160 °C and a

pressure of 414 kPa. Under these conditions, the partially solid 3D printed tool with skin and 40% dense infill crushed significantly; however, the thicker ST-130 hollow tool showed good promise, deforming only slightly. The thinner hollow tool walls were unsuccessful as were the other materials. Overall, the hollow tool manufacturing process saved significant amounts of time and material in manufacturing as compared to the solid ducts and produced composite surface quality improvements compared to the traditional washout tooling.

The TEM was developed to allow direct comparisons between conventional washout tool manufacturing processes and those developed at CSU. It also allowed for two separate 3D printed tool geometries to be analyzed and compared. In this case, the square bent duct tool geometry was determined to be representative of common washout tools. This geometry was compared with a scaled-up version of it to assess differences in the two manufacturing processes based on tool size. The model was developed to make use of user input in the form of geometry details, process steps, manufacturing parameters, bulk material costs, capital equipment costs, and general costs to calculate overall labor, material, capital equipment, and energy costs per manufactured tool for the conventional and additive manufacturing processes for the two representative geometries. It was also able to estimate step-by-step process times for the manufacturing process and geometries.

Based on significant input from Ability Composites and CSU from their knowledge gained from hands-on manufacturing of the 3D printed bent duct tool geometry, costs and process times were calculated for the two manufacturing processes. Results showed that the additive manufacturing techniques developed at CSU can substantially reduce the costs of tool manufacturing by reducing labor times and material usage. This is because additive manufacturing is a relatively hands-off process and allows for the tool design to be optimized to reduce material usage. The disadvantage, however, is that process times for additive manufacturing are significantly longer. The three-dimensional (3D) printing process is slow if tight tolerances are required, but the analysis did show that print times could be reduced with the hollow tool geometry. Also, further advances in additive manufacturing could expedite the process. Costs and process times for the tool washout process were calculated separately. They showed that costs are relatively insignificant when compared to the overall tool manufacturing processes, but with increases in tool size, costs for the conventional manufacturing approach are larger than for additive manufacturing. Again, the washout process for conventional tools is very hands-on, whereas for additively manufactured tools the print medium is dissolved in an automated detergent bath at the sacrifice of process time. The analysis showed that optimizing the additively manufactured tools may also reduce washout times.

Overall, Project 4.9 demonstrated that commercially available dissolvable 3D printing materials exist that can be used to produce dissolvable tooling capable of surviving prepreg composites fabrication under autoclave conditions of 121 °C (250 °F) and 345 kPa (50 psi). An alternative hollow dissolvable tool design was developed which was structurally superior to the initial concept and was cost and time effective versus conventional washout tooling. The 3D printed sacrificial tool required no added surface sealing steps prior to composite part layup and cure, offering a significant advantage over the porous conventional washout tooling.

1 INTRODUCTION

In the manufacture of advanced fiber reinforced composite parts, a mold or tool is required to define the shape of the final part. A high-quality mold or tool should develop good surface finishes, maintain its form during processing, and be removable from the completed part. Most composites utilize a contact molding process to reduce cost and complexity. With contact molds, only one surface of the part is in contact with the tool resulting in a single high-quality and reproducible surface. In thermoset based composites, the part shape needs to be maintained by the tool until the composite processing is complete and the composite part becomes rigid. The processing of these composites commonly occurs in an autoclave where the temperatures and pressures are elevated to both advance the degree of cure of the thermoset and to consolidate the composite. The elevated temperatures and pressures mean that considerations of the tool's thermal and structural stability, and the tool's coefficient of thermal expansion (CTE) are important to success.

For a single-piece contact mold, the contour of the surface has to be relatively simple, with positive draft angle, so that no portion of the geometry is trapped, thus ensuring consistent part removal. If the component design requires a more complex part geometry, then the mold is commonly produced in multiple segments such that the simpler mold subsections can be disassembled from around the completed composite part. While the multisegmented mold approach is acceptable in many cases, some components are too complex even for this approach. These components are generally in the form of complex ducts for aerospace applications, where internal surface finish is of great importance. In such cases, the alternative is to create all, or at least a portion, of the mold, or tool, from a material that can be readily broken up and removed from the final composite part. This trapped, or negative draft, portion of the mold, or tool, is either washed out or dissolved out and thus must be remanufactured for each composite part produced. Conventional approaches to wash-out tooling are to machine, cast, or mold the tool from a bonded ceramic sand or other material that can be readily dissolved. This added step can lead to substantial cost increases of the final composite part. Further, the integrity and surface finish of these wash-out tools can limit the application of such technology and thus limit the acceptable shape of the composite product.

With advances in additive manufacturing technology, 3-dimensional (3D) printed tooling has recently been investigated as an alternative to conventionally produced tooling for composites, because of its potential to reduce costs and lead times [1]. Recent efforts have involved developing materials and processes that result in molds acceptable for many composite-processing operations, including elevated temperature autoclave cures of composites [2]. In these studies, the expectation was that the molds, or mold segments, have positive draft to enable removal of the composite component. Rather than focusing on 3D-printed permanent tooling as has been recently popular, the current effort focuses on investigating the printing of sacrificial washout tooling [3].

The overall goal of this collaborative research project was to develop manufacturing processes for 3D printing of washout tools and assess their viability, both from a technical and from a techno-economic perspective. The work detailed in this report was undertaken to demonstrate the potential for 3D printed dissolvable thermoplastic tools to be used for composite manufacturing, allowing more complex, low-volume composite structures with trapped tooling. Experiments ranging from those developed to down select dissolvable candidate materials to autoclave processing trials on full-scale trapped tooling are described. A techno-economic model (TEM) to compare the cost and process time impacts of the conventional, subtractive manufacturing of washout tools with dissolvable tools additively manufactured within this project is discussed. A brief scaling study was also conducted to assess the effects of tool size on cost and lead time for each respective manufacturing technique.

2 BACKGROUND

2.1 Technology Review

The purpose of this work was to investigate the applicability of melt-extrusion type 3D printers as an option to rapidly manufacture complex, robust, soluble, and geometrically accurate composite tooling. AM has recently been demonstrated as a potential solution for rapidly manufacturing composite tooling [4,5,6]. As composite geometries become more complex, melt extrusion type AM becomes a tempting option for generating the tooling. As compared to subtractive methods, melt extrusion typically requires fewer process steps to manufacture complex geometries.

Many complex composite structures are prone to mechanical trapping of the tool. Some of these include ducts, cable tracks, and pressure vessels. A few options exist to address this issue. Often, the easiest solution is to leave the tool within the part. This is an appropriate option if the tool can be multipurposed to act as either a diffusion barrier or a structural component; however, this negatively affects many of the benefits related to utilizing composites [3,7]. A reusable and removable tool is an appropriate approach for larger production volumes. Some of these tooling options include multi-part hard tooling, shape-memory flexible bladders, or collapsible tooling. Each of these techniques provides their own issues. Shape-memory bladders require a mold made from hard tooling to define the shape of the tool. The shape memory tool requires molding after every composite part, increasing the cost and adding manufacturing steps [8]. Multi-part hard tooling creates high quality and repeatable composite parts, but is typically complex in both design and implementation. Multi-part hard tooling typically requires large production volumes to amortize the cost [9]. Finally, as an alternative, sacrificial tooling is an appropriate solution for low volume manufacturing runs or geometries that prevent the use of reusable tooling [8].

The most common sacrificial tools are made from either plaster, ceramics with a soluble binder, expandable self-pressurizing tools, or eutectic salts [8,10]. Plaster based tools are widely used because of their water solubility and relative ease to cast. However, they have a downside of requiring a geometrically accurate mold to cast them in and a heat cycle prior to manufacturing to remove any trapped water. If the water is not removed it can affect the quality of the final composite. Tools utilizing ceramic media with soluble binders are common as well and can be machined or cast to yield high quality washout tools. Self-pressurizing mandrels utilize a powder made from a soluble polymer component and a microsphere-based blowing agent to provide predictable internal pressure for hollow geometries [10]. Eutectic salts are also used to create complex geometries but require casting at high temperatures, have slow washout times, and result in corrosive waste [8]. Further complicating matters is the fact that plaster, ceramic-based, and self-pressurizing washout tools tend to have porous surfaces that must be sealed to prevent resin infiltration during the cure of the composite part [8,10].

While there has been strong interest in using AM for conventional tooling for composite structures, there has been only limited discussions of in the application of AM to the manufacture of sacrificial tooling for trapped tool applications. Since a new sacrificial tool must be manufactured for each composite part, even at low production volumes, there is a need for a more automated approach to tool production. One AM approach is to use binder jetting to create ceramic-based tools with soluble binders [11]. Unfortunately, these tools, like the traditional washout tools, also require an additional step of sealing the surface, commonly with an overwrap of PTFE tape. Further, most traditional washout tools, independent of the manufacturing approach, are monolithic in nature. This leads to slow heat up rates and the implementation of small intricate features is limited by the brittle nature of the tooling material.

As an alternative to binder jet printing of sacrificial ceramic tooling, there have recently been attempts to utilize dissolvable thermoplastics that can be 3D printed using melt extrusion [12,13]. Melt extrusion is a type of AM that can be used to create complex geometries without significant impact on manufacturing

cost, making it an obvious option for low production volumes and parts of complex geometry. Melt extrusion, when utilizing a continuous thermoplastic filament as feedstock is also known as fused filament fabrication (FFF) or the trademarked name, fused deposition modeling (FDM). It is common within melt extrusion AM of complex geometries to incorporate 3D printed scaffold materials to support overhangs in a model during the printing process. These can be break-away or dissolvable substructures [14]. Dissolvable polymers are often chosen for these scaffold materials and while many are based on PVA as a water-soluble polymer, there have been commercial modifications to the polymer to adjust the temperature stability of these dissolvable scaffold materials to improve compatibility with a variety of 3D printed thermoplastic structural materials. However, even common thermoplastics used in melt extrusion additive manufacturing may lose their rigidity at the elevated temperatures encountered during the processing of composite materials. This loss of rigidity with temperature is even more of a challenge when considering 3D printed dissolvable tooling candidate materials. Further complicating matters, materials suitable for AM can have large anisotropic coefficients of thermal expansion (CTE) due to differences in properties introduced at the fusion boundaries, both side-to-side, between the individual printed beads (roads) and between layers [15]. For tooling manufacture, the CTE needs to be accounted for in the design if acceptable dimensional fidelity of the final composite part is to be achieved [1]. The CTE effect can lead to non-uniform shrinkage during the AM processing, but it can also make dimensional control during elevated temperature composites processing difficult. Additionally, the CTE and the shrinkage of extruded and cooling thermoplastics can result in high thermal stresses, warping, and cracking, necessitating the use of a heated print chamber or enclosure. Finally, the surface finish resulting from melt extrusion is typically poor compared to the tool surfaces achieved by subtractive manufacturing. While not necessary, a surface treatment like sanding, filling, or sealing may be desirable to improve the surface finish of the 3D printed tool, but if such procedures are applied, care must be taken to not alter the geometry.

This current research effort is focused on using dissolvable additively manufactured polymer tooling as an alternative to traditional removable or sacrificial tooling media. Specifically, this study was conducted to address the limited information available related to the use of AM dissolvable polymer tools in the processing of autoclave cured prepregs. The study considers the material and structural stability at temperature and pressure, by considering different hollow tooling concepts. Hollow or partially hollow tooling is investigated rather than 3D printed dissolvable monolithic polymer tooling to not only reduce the manufacturing time and amount of material used, but also in consideration of the dissolution time required. In conjunction with the tooling design variations, several commercially available dissolvable polymers were included to study the stability under autoclave processing conditions, and to investigate the dimensional fidelity and surface finish of composites produced on these dissolvable tools.

2.2 Project Goals and Objectives

A set of tooling geometries were decided upon that would represent commonly encountered geometries in composite manufacturing, increasing in complexity and size, and all manufacturable by either subtractive or additive approaches. One of the geometries represented a trapped tool, exemplifying the use case for dissolvable tooling. The geometries would help to understand if the production of certain geometries using 3D printing was made easier than the alternative subtractive approaches. It was desired to compare the commercially available dissolvable thermoplastic materials and their approximate upper use temperatures to fully understand their benefits, drawbacks, and practicality for composite tooling. Additionally, for each 3D printed geometry, a conventional washout tool would be manufactured to directly compare the performance between the conventional technique and the additive technique.

Most of the conventional washout tooling that is commercially available has a porous surface that requires a sealing process to prevent resin infiltration during cure. The surface of 3D printed thermoplastic tooling may not require a sealing step and is characterized by a texture caused by printing parts in discreet layers. Therefore, an additional goal of this study was to assess the need to seal the surface of the printed tool, and

to focus on the surface texture on 3D printed parts and approaches to improve them, as well as compare them to a conventionally tooled composite part.

One of the important considerations of sacrificial tooling is the ease of tool removal. Many conventional tooling options still require additional labor to remove a component of the material from the tool. This process can be a time-consuming step in the manufacturing process, and so the washout process of dissolvable thermoplastic materials is an important consideration. Certain soluble thermoplastics dissolve entirely in their respective solvents. Others leave behind a component of the material, so these may still require some degree of manual material removal.

2.3 Approach to Meet Project Goals and Objectives

Additively manufactured, dissolvable tools for autoclave cured composites were developed and tested to meet the objectives of this project. The final tooling geometry was developed to be large enough to represent a commercially manufactured component. This required the development of an understanding of the tooling materials and structural configurations that could survive autoclave processing conditions. The approach was separated into three parts as described in Sections 3.1, 3.2 and 3.3.

The first physical investigation, Section 3.1, identified 3 basic tool geometries of increasing complexity and dissolvable candidate materials for the study. The three tool geometries were for (a) tooling material autoclave process condition compatibility evaluation, (b) composite laminate preparation and surface fidelity and roughness study, and (c) a trapped tool, of geometry and size representative of an actual industry component, for autoclave processing studies.

Section 3.2 describes the investigation of the interaction of the prepreg composite part with the 3D printed tool. This section includes results related to the surface finish of printed tools, the surface finish of the resulting composite, and the effects of a surface smoothing routine on surface finish. Slightly larger tool geometries were used that were more compatible with prepreg layup for this processing component investigating the effects of composite cure on the printed tooling. This allowed comparison of the printed geometry and surface characteristics of the printed tools and the resulting composite specimens. A monolithic tool of the same geometry, was manufactured from conventional washout tooling material and used as a baseline for comparison with the printed tools. The conventional washout tooling manufacturing details also provided a direct comparison of the tooling manufacture that was necessary for the techno-economic modeling.

The final physical tooling is detailed in Section 3.3. This bent duct tool geometry provided a real-world example that aided in the understanding of the tooling material degradation at autoclave processing parameters and yielded improvements in the techno-economic model predictions. Several iterations on this tool geometry were created to better understand effects of vacuum, cure temperature and pressure on the success of the 3D printed dissolvable tooling. A matching monolithic tool, of the same bent duct geometry was again manufactured for comparison. I washout characteristics of the final tooling materials utilized, including the commercial washout tooling, were evaluated. This was performed on a reduced scale by manufacturing small cubes of the washout materials, and then dissolving or breaking them down to observe the associated characteristics.

2.4 Qualifications and Experience

CSU has a number of 3-axis gantry style printers, with capabilities including a build volume of up to 600 mm x 600 mm x 300 mm (2 ft x 2 ft x 1 ft), a max nozzle temperature of up to 500 °C, a maximum build chamber temperature of 100 °C, and experience printing numerous challenging materials. In addition, the composites laboratory at CSU houses an autoclave capable of performing the preliminary studies, as well as appropriate materials testing capabilities. 3D printing of the majority of the dissolvable tooling

candidates required a heated enclosure and thus a highly modified commercial Ender 5 Plus printer, shown in Figure 1, was used for the majority of this effort.

Ability Composites currently produces tooling, molds, and wash-out tooling, in-house, using conventional approaches. In addition, Ability Composites has the equipment to perform many common composites manufacturing procedures, including autoclave and oven cures, filament winding and resin transfer molding. The capabilities of Ability Composites enabled direct comparisons of the time, effort and quality of tooling produced in an industrial setting, versus those produced by 3D printing.

2.5 Equipment

The samples and tooling were printed on commercial filament extrusion printers including a Prusa i3 MK2, a Creality Ender 3 Pro, a Lulzbot Mini 1.04, and a modified Creality Ender 5 Plus. Substantial modifications were made to the Ender 5 Plus, shown in Figure 1, including upgrading to an all-metal hotend, to allow increased extruder temperatures and the addition of a heated enclosure (build chamber). The heated build chamber was added to the Ender 5 Plus to successfully print the ST-130 and AQ-180 samples without defects such as warping or cracking. The enclosure used an Omega temperature controller with a Type K thermocouple as a sensor. The heating element was a 750-1500 W heat gun, connected to the control system via a relay. The heat gun nozzle was connected to a flexible aluminum duct running to the inside of the enclosure. The enclosure temperature was limited to 105 °C due to the characteristics of some of the commercial Ender 5 hardware. Since one of the stepper motors of the 3D printer had to remain inside the enclosure for functionality, it was attached to a water-cooling system to successfully function at 105 °C. An image of the heat gun, printer enclosure, and water-cooling system are shown in figure 1.
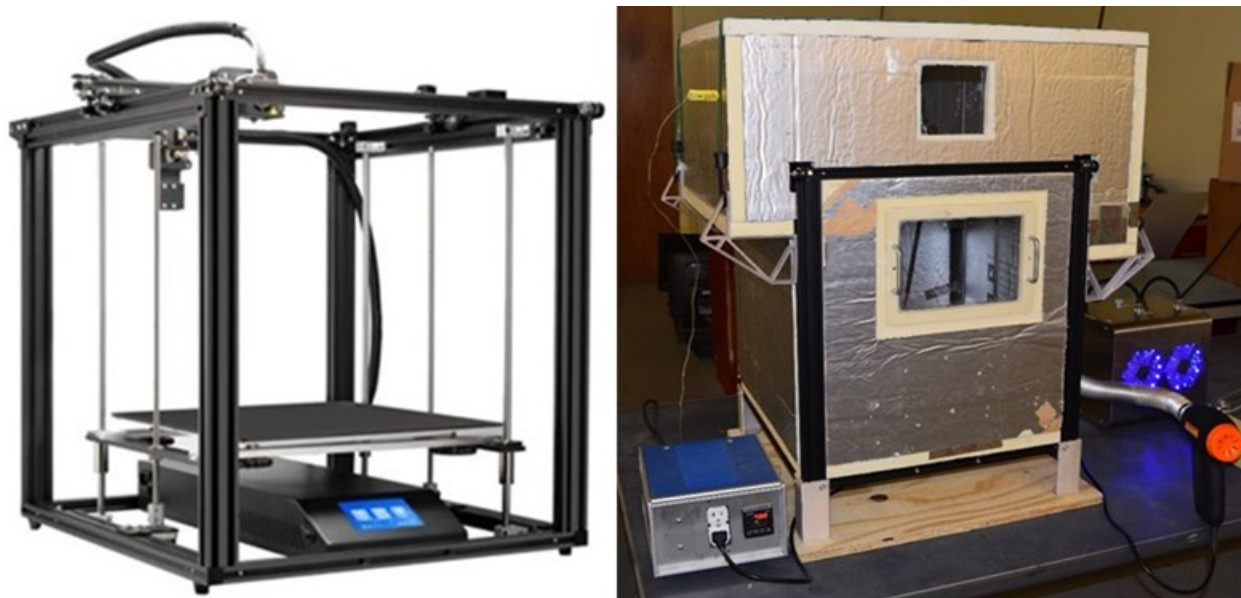
Figure 1 The stock Ender 5 Plus and the heated enclosure built for the printer.

Temperature at pressure tooling stability testing was performed in an autoclave capable of 200 °C (400 °F) and 690 kPa (100 psi). This same autoclave was used during the proof-of-concept manufacture of the prepreg composite specimens on the truncated, square pyramid tooling. The autoclave processing of the composite on the complex tooling was completed by Ability Composites. Additionally, the dimensional fidelity of the manufactured tools was documented by Ability Composites using a FaroArm to create 3D point cloud data that was compared to the original CAD models. Surface roughness evaluations were completed using a Surtronic S-Series profilometer. Dissolution of the various materials was completed

using a Corning Hot Plate Stirrer model PC-351. Additionally, a type K thermocouple was used to maintain the solution temperature during dissolution.

3 RESULTS AND DISCUSSION

3.1 DISSOLVABLE TOOLING MATERIAL ASSESSMENT

Subtask 4.–.2 - Identify tool geometries to be evaluated, in increasing order of complexity and tabulate compatible reusable tooling materials and associated use conditions.

3.1.1   Materials Selected

One objective was to identify and evaluate commercially available dissolvable plastic feedstock (1.75 mm diameter filament) and the stability of 3D printed tool structures under autoclave processing conditions. The materials considered were: Verbatim Butenediol Vinyl Alcohol (BVOH), LAY-Filaments Chamberlay 130 (CL-130), Infinite Material Solutions Aquasys 120 (AQ-120) and Aquasys 180 (AQ-180), and Stratasys ST-130 (ST-130). BVOH is included as a baseline material as it is commonly used as a dissolvable scaffold material that is considered to perform better that common Polyvinyl Alcohol (PVA). The ST-130 filament is marketed as a soluble composite tooling material, so it was expected to perform well. However, its dissolution involves a basic solution with 11.5-12.6 pH. Water soluble tooling is highly desired to avoid safety, disposal, and regulatory challenges of using caustic solutions, making AQ-120 and AQ-180 more desirable, if robust enough for autoclave processing. Both CL-130 and AQ-120 are marketed as soluble support materials for high temperature 3D printing applications, where typical supports may be unstable due to elevated build chamber temperatures. Aquasys 180 became available later in this study, but is marketed as a high temperature support material, and as a potential tooling option for composites processing. Table 1 lists the material properties that were available from the material suppliers, including the maximum build chamber temperatures,. The coefficients of thermal expansion (CTE) and heat deflection temperatures (HDT) are important properties to consider for tool fidelity. The glass transition temperature (T_g) is important for determining the nominal extrusion parameters for the material. All 3D printing filaments were dried in advance of 3D printing and stored in a desiccated enclosure until used, with a relative humidity of 10-15% or less.

Table 1 A summary of the relevant feedstock material properties and characteristics from manufacturer information.

Material	Supplier	Maximum build chamber temperature (°C)	CTE (μm/m/°C)	HDT (°C at 461.9 kPa)	T_g (°C)	Solvent	Density (g/cm³)	Cost ($/kg)
BVOH	Verbatim	90	NQ	NQ	68	Water	1.14	160
CL-130	LAY-Filaments	130	NQ	NQ	NQ	Water	1.19	250
AQ-120	Infinite Material Solutions	120	NQ	NQ	NQ	Water	1.32	180
AQ-180	Infinite Material Solutions	180	42	70	90	Water	1.26	400
ST-130	Stratasys	130	107 (T<100 °C) 177 (T>100 °C)	121	132	Basic Solution	1.19	150
PETG	Overture	80	51-68	68	80	Not dissolvable	1.38	22

* NQ: Not quoted by the manufacturer.

The optimal nozzle size, print speed, and nozzle temperature are interdependent. In the studies conducted, these parameters varied slightly due to changing nozzle size. This is due to the heat transfer from the nozzle to the filament, where more heat flow is required if the material volumetric flow rate is increased, as in the case with a larger nozzle or faster print speeds. Thus, any changes to the nominal manufacturing parameters listed in Table 2 are reported in the results section.

Table 2 Parameters used for manufacturing.

Material	Extruder Temperature (°C)	Print Bed Temperature (°C)	Enclosure Temperature (°C)	Hot-End/ Filament Drive	Printer Used
BVOH	210	60	Ambient	Stock/ Direct Drive	Lulzbot Mini 1.04, Prusa i3 MK2
CL-130	240	90	Ambient	Stock/ Direct Drive, Bowden	Prusa i3 MK2, Ender 3 Pro
AQ-120	235	100	Ambient	Stock, Direct Drive	Prusa i3 MK2, Ender 3 Pro, Ender 5 Plus
AQ-180	275	90	80	All-metal hot end, Bowden	Ender 5 Plus
ST-130	285	126	105	All-metal hot end, Bowden	Ender 5 Plus
PETG	240	90	Ambient	Stock, Direct Drive	Prusa MK2

Challenges were encountered when manufacturing the AQ-120 using the commercial printers in the as-received condition, as the filament would jam in the nozzle. This became a problem on longer prints, so it

was possible to create small samples using standard hardware with no faults. The solution used was to increase the nozzle temperature and use a direct filament drive extruder setup. The Ender 5 Plus was converted to a direct drive extruder for printing AQ-120.

Another challenge was related to moisture uptake in the raw filament. This often results in expanding moisture inside the extruder and then in processing defects and reduced properties in many polymer feedstocks. The problem was compounded by the fact that the dissolvable filaments are even more sensitive to moisture uptake. To avoid this issue, the raw filament was dried in a laboratory oven and stored inside a desiccated dry box. The filament was fed through tubing, directly from rolls which remained in the dry box, to the extruder during printing of the specimens, to ensure that moisture uptake did not occur during the 3D printing process.

A Toray F2673C-07M plain weave carbon fiber/epoxy prepreg was utilized for the fiber reinforced composite articles made by Ability Composites. This material has a typical process temperature window up to approximately 135 °C and can be consolidated with vacuum pressure alone. The ability to process at slightly lower temperatures matching expectations of the tooling materials and availability were the primary determining factors for choosing this carbon fiber reinforced epoxy material.

3.1.2 Technical Approach

To evaluate the stability of the various candidate tooling materials and structural configurations, tool stability testing was performed in the autoclave under increasing temperature and pressure conditions. This approach was undertaken, rather than mechanical testing at temperature, under compression, as it more closely mimics the processing conditions required for prepreg composite materials. The objective conditions were 121 °C (250 °F) at 345 kPa (50 psi) to 690 kPa (100 psi) under vacuum bag conditions. The samples were designed to test tooling robustness under autoclave conditions and used a truncated conical geometry. The samples were visually evaluated for deformation. Thus, the tooling stability testing is based only on qualitative evaluation of deformation at each temperature/pressure step.

A summary of the tests performed is shown in Table 3. These tests were performed to determine suitable manufacturing parameters and processing steps for each material as well as to gain information on material selection, processing conditions, infill structure, infill type, nozzle size, short carbon fiber loading, and exterior thickness.

Table 3 The test matrix used to investigate material and structural autoclave robustness.

Test	Description
1	This tested each material type (except AQ-180) with varying top surface thicknesses
2	The effects of drying the AQ-120 filament for 12+ hours were tested, as well as CL-130 and ST-130 with improved printing parameters
3	ST-130 samples printed in an enclosure were tested against AQ-120 filament dried for 72+ hours, and against AQ-180
4	PETG samples were tested to understand the effects of top surface thickness; wall thickness; nozzle size; short carbon fiber loading; infill density; and added solid secondary support regions.
5	ST-130 samples were printed with varying infill densities and top surface thicknesses prior to printing the complex tooling, to understand if a decision to scale up nozzle size would have detrimental impacts on tool robustness.

3.1.3 Specimen Preparation, Test Procedures, and Characterization Methods

The specimens were printed with a 30% infill density, which was arbitrarily chosen for testing, to represent the potential for tooling which would be more readily dissolved, and more rapidly manufactured, than a monolithic tool. The complete test specimen was 3D printed in a continuous fashion, incorporating both the solid and infill, from a given material. A cross-section of the axisymmetric tool geometry is shown in

figure 2, with the solid outer surfaces indicated by the shaded region and the unshaded region representing the 30% dense infill region which also saves a substantial amount of material.
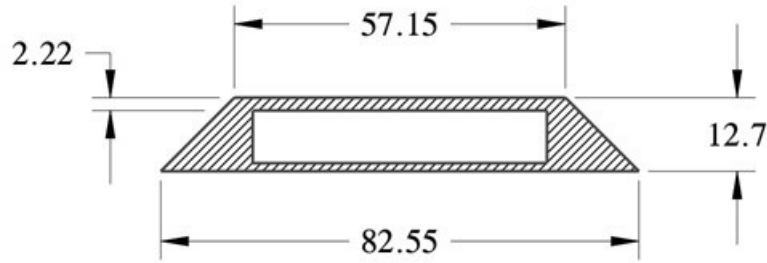
Figure 2 Crush Test Sample geometry for the 2.2mm top surface thickness sample. (All dimensions in mm.)

The geometry for these specimens was also chosen to simplify vacuum bagging and minimize pressure variations, as well as to leave a large flat surface that would be prone to deformation, as compared to the sloped sides. The samples were printed from each candidate material with nominal top thicknesses of 3.3 mm (0.125"), 2.2 mm (0.0875"), and 1.2 mm (0.050") which resulted from 11, 7, and 4 top printed layers, respectively, with a 0.2mm layer height. These varying thicknesses were used to verify the effects of differing outer surface thickness versus resistance to deformation during autoclave evaluation. The specimens were printed at a speed of 30 mm/s, using a 0.6 mm nozzle orifice diameter, and a bottom surface thickness, against the build plate, of 1.6 mm.

The samples were manufactured then stored in a desiccated environment to maintain a low, consistent moisture content prior to testing. Preparing for testing was done by placing a batch of samples on a flat aluminum tooling plate. Then, standard breather/bleeder material was used to ensure a vacuum path would reach each sample, as seen in figure 3. IThe breather/bleeder did not extend far up the sample sides to allow photographic documentation of the surfaces. The relative roughness of the surface of each sample was assumed to allow enough air flow to expose the sample surfaces to vacuum. After vacuum bagging, a 10-minute drop test was performed to observe any loss of vacuum gauge pressure prior to test initiation as an assessment of vacuum quality. With vacuum still applied the samples were placed into the CSU autoclave and exposed to the prescribed temperature and pressure cycle.
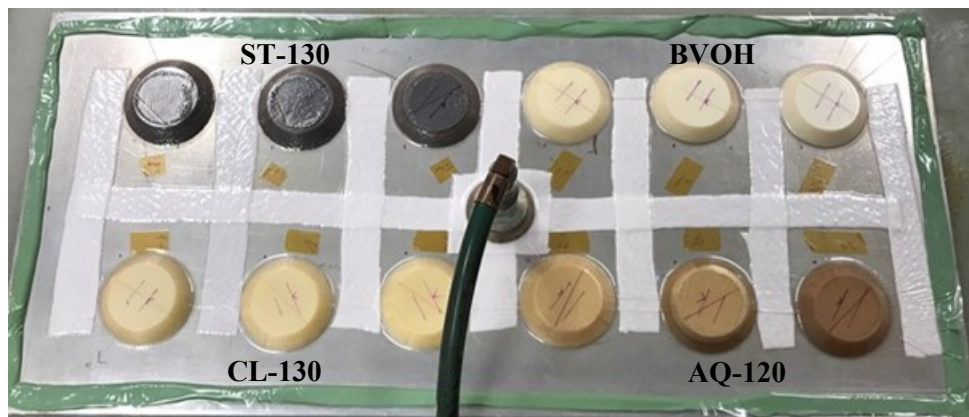
Figure 3 Tooling Stability Specimens configured for Autoclave Temperature/Pressure study.

3.1.3.1 Test Procedure

The tooling stability samples were tested at temperatures of 65 °C (150 °F), 93 °C (200 °F), 107 °C (225 °F), and 121 °C (250 °F), in a stepwise fashion, to observe deformation at increasing temperatures.

The samples, under vacuum on the tooling plate, were placed into the autoclave and heated, first to a temperature of 65°C (150 °F), for a 30-minute dwell, during which time the pressure was increased to 345 kPa (50 psi). Once the dwell was complete and the temperature and pressure were returned to ambient, the autoclave was opened and the tooling plate with the specimens was removed allowing the specimens to be visually evaluated for deformation and photographed. This process was repeated at 93 °C, 107 °C, and 121 °C. The rate used for heating and cooling was approximately 2.8 °C/minute (5 °F/minute) and the pressure ramp was initiated once the hold temperature was reached. The pressure ramp rate was at a maximum for the equipment used which was approximately 43 kPa/minute (6.25 psi/minute). For context, the samples used a ramp from 0 to 345 kPa (50 psi) that lasted approximately 8 minutes. The hold temperature duration was 30 minutes and, thus, the specimens were at the temperature and pressure of the test for approximately 22 minutes. The temperature/pressure cycle for the 121 °C (250 °F) process step is shown in figure 4.
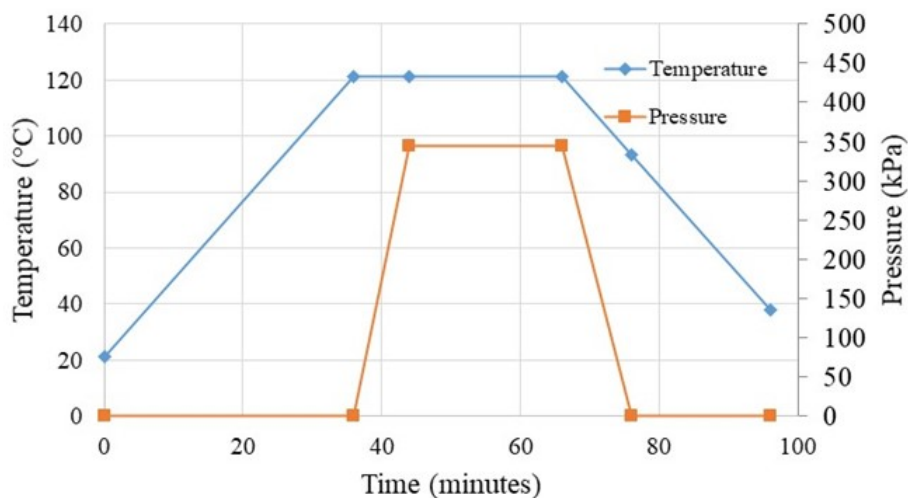
Figure 4 The nominal temperature and pressure cycles applied to the crush samples during cure.

After a completed cycle, the samples were removed from the autoclave to capture photographs of any deformation and to qualitatively assess deformation without removing the vacuum bagging film.. Additionally, a straight line was drawn across the vacuum bag film, on top of each specimen, to better visualize deformation. Samples were then retested, at pressure, at an increased autoclave hold temperature. Any noticeable deformation indicated failure of that specimen, resulting in its rejection from use at the tested temperature and pressure.

3.1.4   *Presentation and Discussion of Results*

3.1.4.1 *Preliminary Temperature/ Pressure/Vacuum Test*

Preliminary testing involved three samples of each material printed with nominal top surfaces that were 3.2 mm (0.125"), 2.2 mm (0.0875"), and 1.2 mm (0.050") thick. This test was meant only to verify the experimental approach as specimens were printed without consistent environment control. The materials were BVOH, CL-130, AQ-120, and ST-130. The ST-130 samples had defects coming from incorrect extrusion temperatures and the AQ-120 likely had moisture absorption issues prior to printing. The ST-130 printing temperature was originally set too high, resulting in foaming as material degradation occurred. The AQ-120 likely absorbed atmospheric moisture resulting in samples with excess porosity due to moisture vaporization in the extruder, as well as under-extrusion issues related to an inability to extrude the material with a Bowden drive setup. The ST-130 and AQ-120 samples that most clearly showed these problems are a lighter color. The 12 samples, as well as close ups of the ST-130 and AQ-180 samples showing their processing defects, are presented in figure 5.
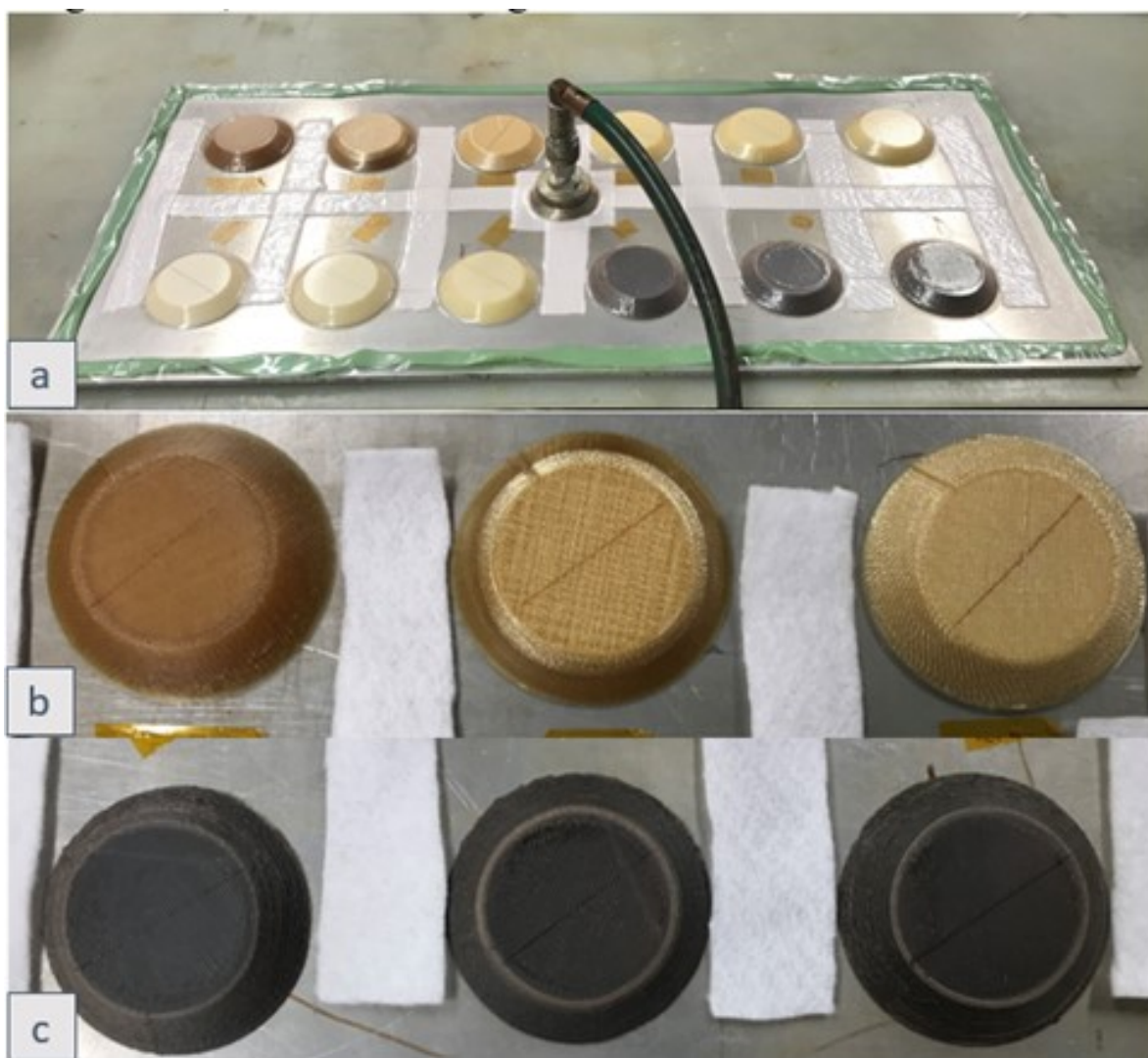
Figure 5 The crush test configuration (a) including both AQ-120 (b) and ST-130 (c).

The varying color of the AQ-120 samples is caused by under extrusion. Initially it was thought that this lighter color was due to moisture trapped in the filament; however, the results were unchanged after drying the filament and controlling the moisture content. The increased opacity is indicative of reduced interlayer fusion (poor layer-to-layer adhesion) and with moisture ruled out as the cause, it followed that under extrusion was causing the problem. Under extrusion is related to lower than desired extruder flow rates which result in a smaller than desired bead (road) cross section. This allows voids to be introduced between adjacent roads and layers, resulting in the opaque and lighter color. The specimens that were translucent and darker in color are higher quality, with low void content. The lighter color samples had a rough surface texture and were completely opaque, as compared to the dark colored sample that was translucent. The ST-130 samples had a light-colored ring on the outside of the top surface that is assumed to be from incorrect extrusion temperatures, causing material degradation and discoloration/foaming. The ring along the edges is likely the only discolored region because that is where the extruder is decelerating as the turn is made and thus, in contact with the material for a longer time. These preliminary ST-130 samples were printed at a nozzle temperature of 320 °C, but with further process optimization it was determined that a temperature between 270 and 285 °C was more appropriate. The surface finish on the sloped walls of the ST-130 was also poor. The custom machine that was originally used to print the ST-130 samples had vibration and resonance issues leading to poor surface finish.

These samples were tested at 65 °C (150 °F), 93 °C (200 °F), 107 °C (225 °F), and 121 °C (250 °F) at 345 kPa (50 psi), except for the 121 °C run, which was tested at 552 kPa (80 psi). The photographed samples shown in Tables 4 and 5 have the thinnest of the three top surfaces tested, at 1.3mm thick, to better highlight the deformation.

Table 4 Photographs of the 1.3 mm thick ST-130 and AQ-120 samples during testing up to 121 °C (250 °F) and 552 kPa (80 psi).
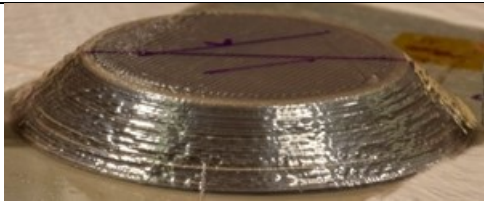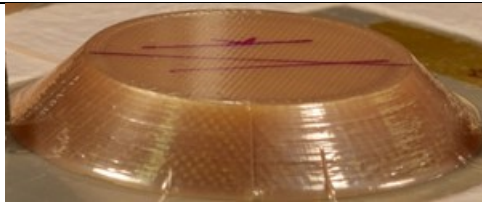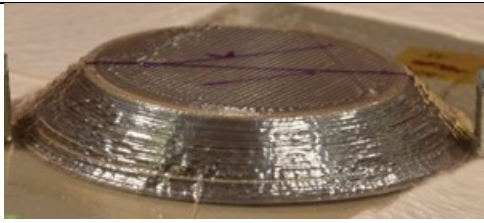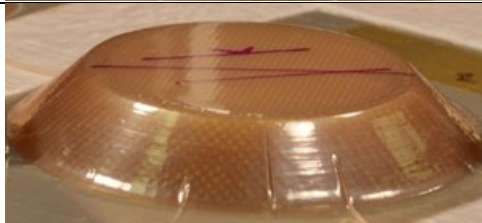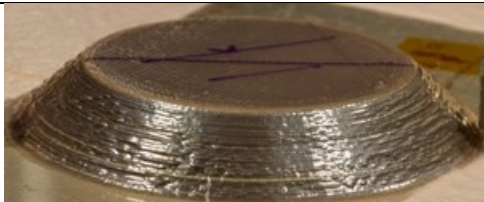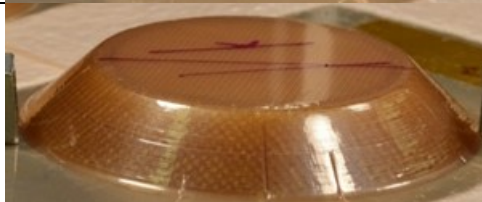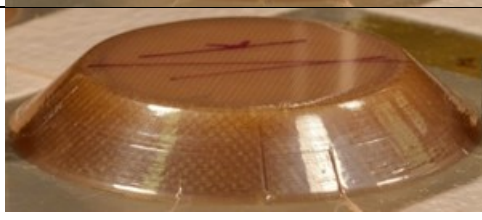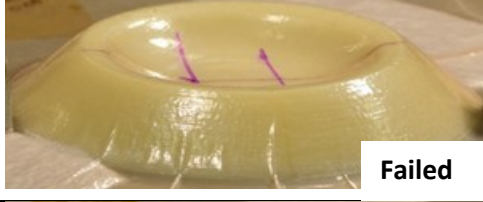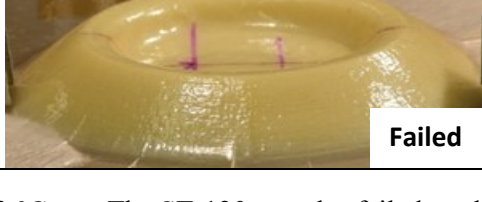
Temperature (°C)/ Pressure (kPa)	ST-130	AQ-120
65/345		
93/345		
107/345		
121/552	**Failed**	

Table 5 Photographs of the1.3 mm thick CL-130 and BVOH samples during testing up to 121 °C (250 °F) and 552 kPa.

Temperature (°C)/ Pressure (kPa)	CL-130	BVOH
65/345		**Failed**
93/345	**Failed**	**Failed**
107/345	**Failed**	**Failed**
121/552	**Failed**	**Failed**

The BVOH failed on the 65 °C run. The CL-130 failed on the 93 °C run. The ST-130 samples failed on the 121 °C and 552 kPa run. The AQ-120 specimen (only the 1.2mm thick sample) did not exhibit failure; however, this result was not reproducible in following tests. A significant effort was undertaken to determine printing parameters that could produce an AQ-120 specimen that could repeat this performance, but no follow-on AQ-120 specimens resisted this temperature and pressure. Additionally, the two thicker specimens of AQ-120 tested during preliminary trials (that also showed obvious visual defects) performed poorly and failed at 93 °C at 345 kPa. The three AQ-120 specimens are shown in figure 6 after the 93 °C cycle.
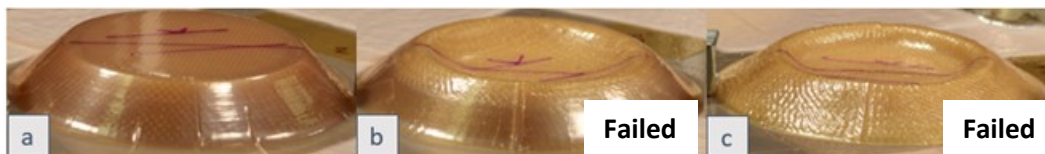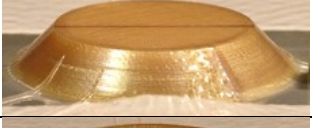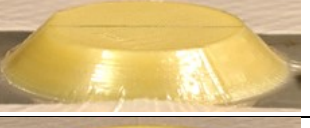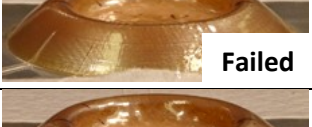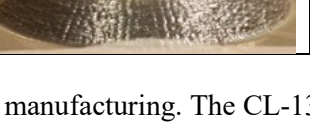
Figure 6 - The samples with nominal top surface thicknesses of 1.3 mm (a), 2.2 mm (b), and 3.2 mm thick.

The success of the 1.2 mm thick AQ-120 sample was assumed to be caused by processing defects during vacuum bagging. Additionally, AQ-120 presented significant challenges with print consistency, related to both moisture absorption and under-extrusion. After noticing this, the filament was dried and stored in a desiccated environment both before and during printing. BVOH was eliminated from further testing due to poor performance in this test, as well as its lower thermal properties indicating poor suitability as autoclave processable tooling.

3.1.4.2 Temperature/ Pressure/ Vacuum Test – Verified Printing Conditions

This test was conducted after a more detailed study and careful control of processing conditions. The ST-130 samples still showed similar problems from too high of material extrusion temperatures and machine vibration issues using the custom-built printer. In this test, the AQ-120 was kept in a desiccated environment while in storage and while printing. The AQ-120 was dried at 70°C for at least 12 hours prior to each print. CL-130 samples were manufactured with slightly adjusted parameters. The results are shown in Table 6.

Table 6 Photographs of the 1.3 mm thick AQ-120, CL-130, and ST-130 samples during testing up to 121 °C (250 °F) and 621 kPa (90 psi).

Temperature/ Pressure (°C/kPa)	AQ-120	CL-130	ST-130
Pre-testing			
Pre-testing, bagged			
93/345	Failed	Failed	
107/345	Failed	Failed	
121/345	Failed	Failed	
121/621	Failed	Failed	
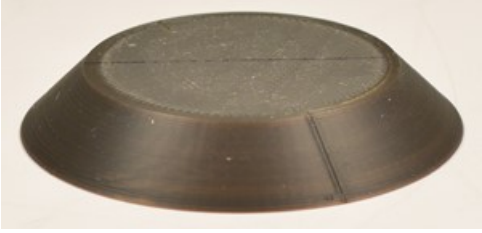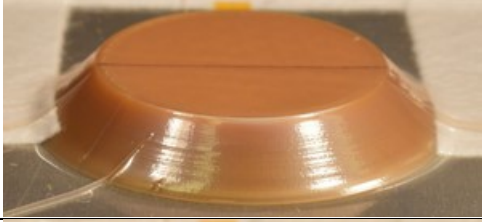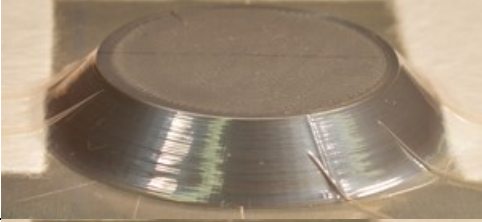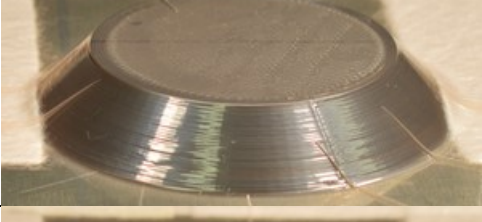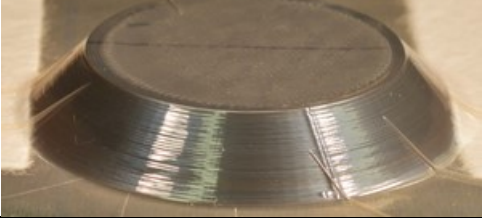
The results suggested that ST-130 would be the final candidate for future tool manufacturing. The CL-130 and AQ-120 samples, even after being printed in a fully desiccated environment and lacking any visual defects which could cause failure, still failed at 93 °C at 345 kPa. While the ST-130 samples were still being printed at too high of a print temperature, they all survived the 121 °C test at 345 kPa with no deformation and survived the 121 °C/ 621 kPa test with only minor deformation. It was necessary to further test ST-130 with improved manufacturing parameters, in order to determine if the performance changed. The Aquasys 120 and Chamberlay 130 were carried this far into the study in hopes that adjustments in print parameters would enable use, as both were soluble in water. Solubility in water was considered very desirable compared to the high pH solution necessary to dissolve ST-130. However, none of the adjustments were successful and thus the Chamberlay 130 was removed from further processing trials. Aquasys 120 was still pursued in hope of adjusted processing conditions allowing use and to recreate the results from test 1.

3.1.4.3 Temperature/ Pressure/ Vacuum Test - New Candidate Material – AQ-180

A final set of temperature/pressure/vacuum tests was performed to evaluate effects of 3D printer modifications that enabled additional print parameter optimization. In addition, a new version of Aquasys, AQ-180, was released, which promised higher temperature stability than AQ-120 while retaining the ability to be dissolved in water. For this set of trials ST-130 specimens were printed in a heated enclosure, at 105 °C, with a nozzle temperature of 280 °C. AQ-120 filament underwent additional drying at 70 °C for > 72 hours before each sample was printed. The AQ-180 was manufactured with a nozzle temperature of 275 °C and an enclosure temperature of 80 °C, which was found to be sufficient to prevent warping.

This test was completed in two parts. The first compared the ST-130 specimens to AQ-180 specimens while the second reused the ST-130 specimens and compared them against the remaining AQ-120 specimens printed for the project, as well as the specimens with additional drying time. The results comparing the AQ-180 and ST-130 are shown in Table 7.

Table 7 Photographs of the 1.3 mm thick AQ-180 and ST-130 samples during testing up to 121 °C (250 °F) and 621 kPa).

Temperature/ Pressure (°C)/(kPa)	AQ-180	ST-130
Pre-test		
93/345		
107/345		
121/345		

It was noticed that during the 121 °C/ 345 kPa run, and slightly on the 107 °C/ 345 kPa run, that the surface on ST-130 and AQ-180 samples deformed slightly so that the infill pattern could be seen through the part, although the top surface remained flatter for the ST-130 than the AQ-180 specimen. This test indicated that

AQ-180 is an excellent choice in situations where water solubility is required, however the performance of ST-130 was still better. Infinite Materials, the manufacturer of AQ-180, indicated during a public webinar that due to the make-up of the material and the associated fillers, the solubility should be expected to decrease with extended time at elevated temperatures.

The second part of this test included dried AQ-120 and ST-130. The ST-130 specimens were the same specimens used in comparison with the AQ-180. This test also included every AQ-120 specimen that had been printed, but not previously tested, to determine if one of the early samples of AQ-120 matched the performance of the single AQ-120 specimen that survived to 121 °C (250 °F) at 345 kPa (50 psi) in the preliminary temperature/pressure/vacuum test. Additionally, three AQ-120 specimens were printed and tested with filament drying conditions of 72+ hours at 70 °C. This test was completed at 121 °C at 345 kPa, to see if any individual specimen could match the performance of ST-130. An image of the tooling plate after processing is shown in figure 7.
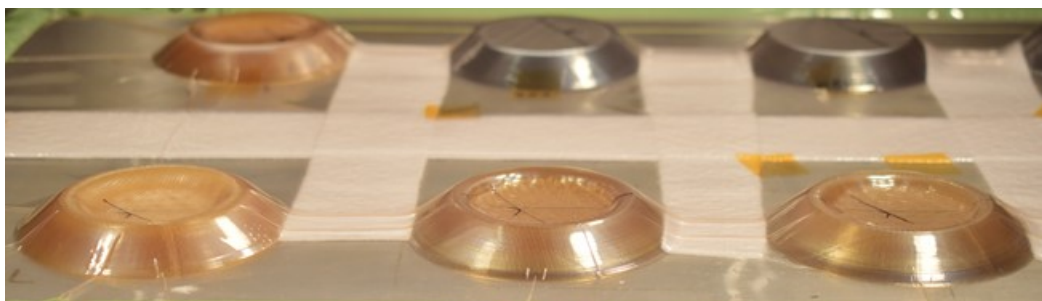
Figure 7 Various tested specimens after the 121 °C at 345 kPa test run.

This test verified that independent of the printing conditions, none of the AQ-120 survived under these pressure/temperature/vacuum conditions. IThe ST-130 specimens once again were undeformed after retesting at 121 °C and 345 kPa. By not having any of the AQ-120 specimens match the performance of the single 1.3 mm thick sample from Temperature/Pressure/ Vacuum Preliminary test, it can be assumed that the single surviving sample was an outlier, most likely due to inadequate vacuum distribution.

3.1.4.4 –Temperature/ Pressure/ Vacuum Test - Structural Configuration

This test utilized 13 samples made from PETG. PETG is not one of the dissolvable candidate materials, but rather was used as a model material to investigate the effects of structural configuration, including: infill type, infill percentage, short carbon fiber loading, wall thickness, top surface thickness, nozzle size, and the effect of secondary infills on the overall structural performance.

These samples were evaluated under autoclave conditions, in a similar manner to the previous temperature/ pressure/ vacuum samples; however, being a lower-temperature material than the dissolvable specimens tested, the PETG specimens were tested at lower temperatures. Test conditions were, 60, 70, and 80 °C and 345 kPa. The sample matrix is shown in Table 8. Samples 1-9 used a truncated square pyramid geometry, nominally 76.2mm x 76.2mm x 12.7mm high with 45-degree inclined sides, as shown in figure 8. [See Appendix B for detailed dimensions of specimen geometry.] Eight of the nine of these specimens included a Gyroid infill pattern, which is an infinitely connected triply periodic minimal surface discovered by Alan Schoem in 1970. It is pertinent to the dissolvable tooling effort since the connected nature offers the potential for enhanced distribution of the dissolution media. This size was utilized so that samples 1-9 could all fit onto the print bed of the Prusa i3 MK2 printer and be printed simultaneously. Printing all samples at one time was desirable to eliminate any external variables, such as filament moisture absorption between prints.

Samples 10-13 were printed separately and were of the same round geometry as the

temperature/pressure/vacuum tests of the dissolvable candidate materials. The infill for this group of specimens was cubic as had previously been used. These samples required changing the installed nozzle and the filament used during manufacturing, so they were not printed at one time.

Table 8 Test matrix for Temperature/ Pressure/ Vacuum Test 4 of PETG specimens.

Test		Infill Type (30% unless stated otherwise)	Perimeter Count	Top Layer Count	Solid Regions
1	Control	Gyroid	3	3	None
2	Compression Specific Infill	Stars (quarter isogrid)	3	3	None
3	Thick walls	Gyroid	6	3	None
4	Thick top layer	Gyroid	3	6	None
5	Thick top layer/ walls	Gyroid	6	6	None
6	Solid under angled surfaces	Gyroid	3	3	Under angled surfaces
7	Solid Ribs	Gyroid	3	3	Cross pattern through center of part
8	Low Infill Density	Gyroid 20%	3	3	None
9	High Infill Density	Gyroid 40%	3	3	None
10	Carbon Fiber Loading	Cubic	3	3	Under angled surfaces
11	No Carbon Fiber Loading	Cubic	3	3	Under angled surfaces
12	0.6mm nozzle	Cubic	3	3	Under angled surfaces
13	0.8mm nozzle	Cubic	3	3	Under angled surfaces

The first 9 samples were made during the same print to maintain consistent printing conditions, with a rendering of the organization of the specimens on the build plate shown in figure 8.
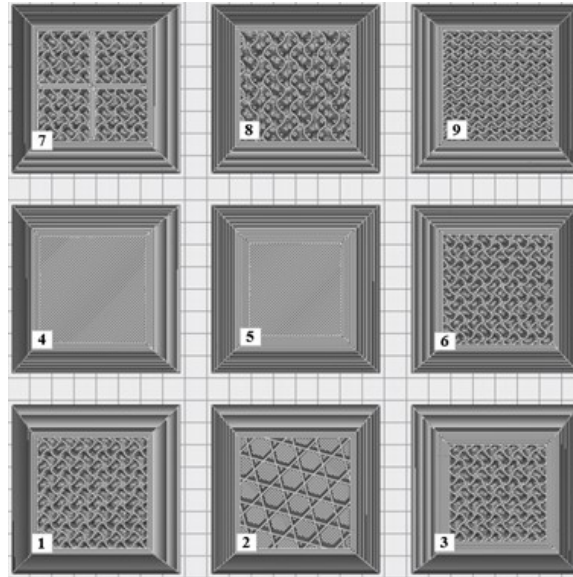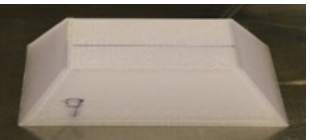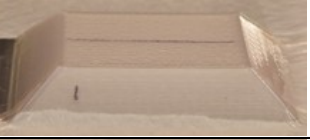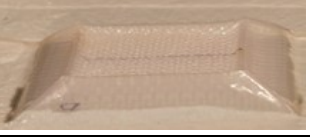
Figure 8 Plav View Rendering of samples 1-9 at stages in the manufacturing process, showing infill patterns
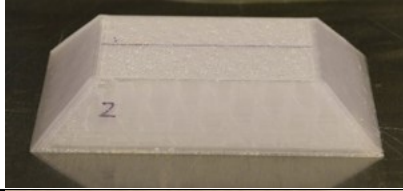
Gyroid infill densities of 20%, 30%, and 40%., specimens 8, 1, and 9, respectively, are compared in Table 9.

Table 9 Infill density test samples 8, 1, and 9.

Temperature/ Pressure (°C)/(kPa)	20% infill density	30% infill density	40% infill density
Pre-test			
70/345			
80/345			
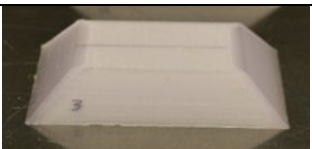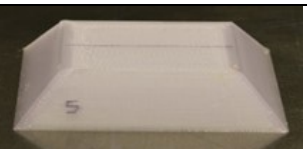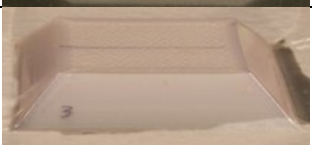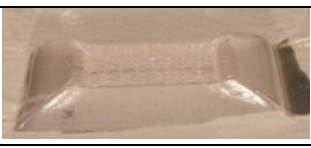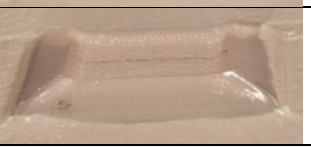
The higher infill density samples performed the best. Infill density was determined to be the most influential parameter for autoclave robustness of all the parameters tested with these PETG samples. Table 10 shows a comparison of the gyroid infill pattern and the quarter-isogrid pattern called Stars. The gyroid infill was chosen for evaluation as it provides a quasi-isotropic infill structure, and it also would provide continuous channels to improve tooling washout. This test was chosen to evaluate the gyroid infill versus a more conventional infill to evaluate the resistance to applied pressure. The results are shown in Table 10.

Table 10 Infill pattern test samples 2 and 1.

Temperature/ Pressure (°C)/(kPa)	Stars (quarter-isogrid)	Gyroid
Pre-test		
70/345		
80/345		
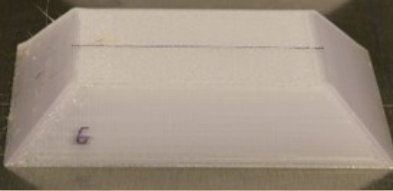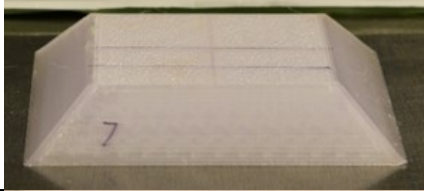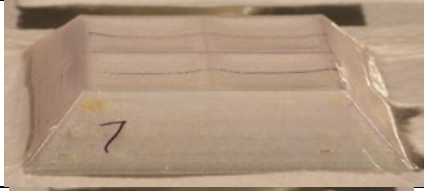
The results of the infill comparison test showed that the gyroid infill maintained dimensional fidelity at 70 °C, while the Stars infill failed. Another comparison can be made between samples with varying outer surface thicknesses. The three samples in Table 11 show a sample with thick walls, one with a thick top surface, and one with both thick walls and a thick top surface. It was expected that the sample with thicker outer surfaces would perform the best.

Table 11 Outer skin thickness test samples 3, 4, and 5.

Temperature/ Pressure (°C)/(kPa)	Thick Walls	Thick Top Surface	Thick Walls & Top Surface
Pre-test			
70/345			
80/345			
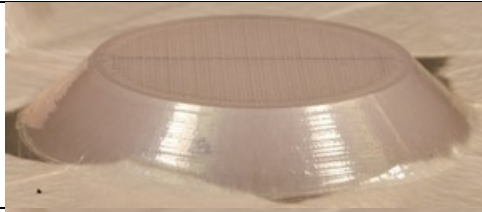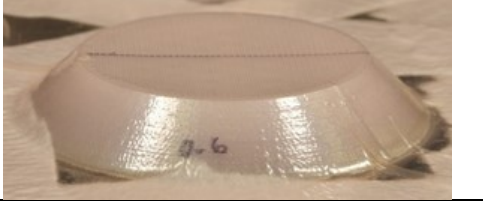
The outer skin thickness test showed that thicker walls and top surfaces are useful in increasing robustness. Another consideration was the addition of secondary support structures within the infill structure. These included solid regions under the walls and central solid supports in the part. The comparison of these samples is shown in Table 12.

Table 12 The secondary support structure test samples 6 and 7.

Temperature/ Pressure (°C)/(kPa)	Solid Under Sloped Walls	Solid Cross
Pre-test		
70/345		
80/345		

The results of this test showed that the additional structures tested did not provide the desired reinforcing performance. While they locally provided significant reinforcement, the structures would need to be placed closer together to be effective, resulting in a heavy part approximating solid infill. The next test was to understand the impact of a different nozzle size on performance. Both 0.6 mm and 0.8 mm nozzle sizes were used to create samples with similar structures. Both samples used 30% infill but the 0.8 mm nozzle roads were larger and therefore farther apart to provide the same infill density. The results of this are in Table 13.
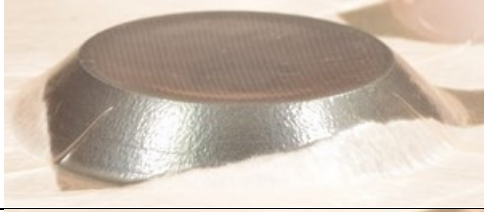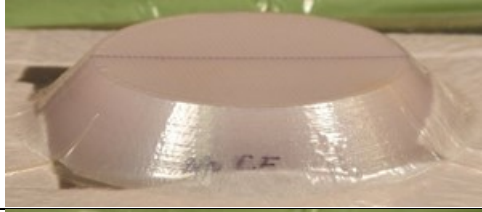
Table 13 Nozzle size test samples 12 and 13.

Temperature/ Pressure (°C)/(kPa)	0.6 mm nozzle	0.8 mm nozzle
Pre-test		
60/345		
70/345		

The nozzle size test showed that the infill printed with the thicker nozzle resulted in more deformation at 70 °C. This can be explained by the spacing between infill roads being greater for the 0.8 mm nozzle than for the 0.6 mm nozzle to maintain the same infill density. For a simply supported beam, the span is an important factor in bending stiffness. There was poorer performance for the 0.8 mm nozzle due to increased spans between supporting infill structures.

The final test compared a carbon fiber filled PETG and a neat PETG specimen. This test was designed to investigate the impact of carbon fiber filler on performance in autoclave conditions. The hypothesis was that adding carbon fiber would increase the HDT of the material, resulting in improved performance. Table 14 shows the short carbon fiber filled PETG and neat PETG samples tested up to 80 °C and 345 kPa.

Table 14 Carbon fiber loading test samples.

Temperature/ Pressure (°C)/(kPa)	Carbon Fiber PETG	Neat PETG
Pre-test		
70/345		
80/345		

This test showed that the neat PETG performed better than the carbon fiber loaded PETG, which can be seen in the 70 °C test where measurable distortion is noted for the carbon filled specimen and not for the neat PETG specimen. The cause of this was assumed, after an analysis of the raw filament densities, to be due to an increased void content in the carbon fiber loaded filament. The carbon fiber loaded filament had a lower-than-expected density, most likely due to poor fiber wetting during manufacturing and a high void content at the surface of the carbon fibers. This seemed to reduce the load transfer between the carbon fiber and the PETG resulting in poorer performance.

In summary, the parameter which made the greatest impact on the performance of the samples was the infill density. Following this, by using gyroid infill the sample performance was improved over stars. Carbon fiber loading in PETG was damaging to the structure's crush resistance. Finally, additional internal solid structures were deemed unnecessary for improved performance. The time savings available using larger nozzles are significant, so the results suggest that future prints should focus on increased infill percentage density and nozzle size.

3.1.4.5 Temperature/ Pressure/ Vacuum Test – ST-130 Deposition Rate Study

The tooling following these tests would be larger, and thus have longer print times with the 0.6 mm nozzle used in the temperature/ pressure/ vacuum test samples. This test used ST-130, as it was chosen as the tooling material for future tooling study. For example, the first complex bent duct tool was estimated to use over 3 kg of ST-130 and require multi-day print times. To reduce print time, the decision was made to move from a 0.6 mm nozzle to a 0.8 mm nozzle. The increase in nozzle size, as was seen in the PETG infill test prints tests with 0.6 vs. 0.8 mm nozzles, showed a widening of infill road spacing to maintain the same infill density. To further the understanding of this impact, four crush test specimens were printed, with the characteristics shown in Table 15, and tested to finalize infill settings before manufacturing the larger complex tooling.

Table 15 *Sample matrix for infill parameter testing.*

Sample	Infill (%)	Infill Road Width (mm)	Infill Road Spacing (mm)	Top Surface Thickness (mm)
1	40	0.8	2	3.2
2	~53	0.8	1.5	3.2
3	40	0.6	1.5	3.2
4	40	0.8	2	4.6

The results of the ST-130 infill settings test showed that all four samples performed well enough to meet project requirements. These samples were tested up to 121 °C (250 °F) at 621 kPa (90 psi). At 345 kPa (50 psi), the deformation was minimal. At 621 kPa, the deformation was slight, and could be seen by holding a straightedge across the sample. These results are shown in figure 9. The sample numbers in figure 9 correspond to those listed in Table 15.
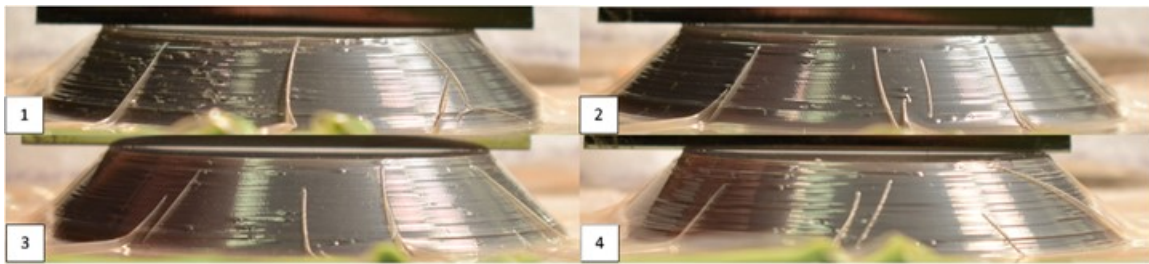
Figure 9 *ST-130 specimens after testing.*

The four infill parameter samples tested showed that, like the PETG sample tests, the infill density had the greatest impact on the performance of the specimen. The samples showed good fidelity at 345 kPa and additionally would only be tested to this value for the square pyramids. It is seen that sample 2 (~53% infill) performed the best, although marginally. This sample was the only sample with increased infill density. However, based on the marginal improvement and to conserve material and time, the default infill parameters (2 mm road spacing) for a 0.8 mm nozzle with 40% infill (sample 1) were utilized for Future specimen manufacture.

3.2 PRELIMINARY COMPOSITES MANUFACTURING TRIAL

Subtask 4.9.4 - 3D print and test "reusable" tooling, based on current documented efforts and 3D print preliminary wash-out tooling for comparison with conventionally manufactured washouts to serve as baseline and to inform the techno-economic model.

3.2.1   Technical Approach

The purpose of these tests was to evaluate the processing of prepreg composites on printed dissolvable tooling. This involved a small scale up of part sizes using the knowledge gained from the autoclave robustness testing to begin to understand the geometric challenges of using 3D printed tooling as they relate to CTE and autoclave integrity. Also, it was important to understand composite manufacturing related challenges such as the need to seal the tool surface, mold release reactivity, part release, and surface finish.

As an investigation into tool surface roughness, one specimen used a surface smoothing routine to modify the surface finish. The routine is called ironing and is an available option in the slicing software, Cura Ultimaker 4.6. Ironing makes many passes over a completed surface with very small stepovers and a small amount of material extrusion. The purpose of ironing is to improve the surface finish of the final part. The

surface finish was evaluated and compared with the printed tool that did not utilize ironing. The ironing parameters utilized in CURA were: ironing line spacing = 0.1 mm, ironing flow = 10 %, and ironing speed = 16.667 mm/s. These parameters produced a specimen with an improved surface finish (visually and tactilely). The ironing parameters were developed by printing many small test samples and measuring their surface roughness as well as by visual inspection.

3.2.2 Specimen Preparation, Test Procedures, and Characterization Methods

Three tools, two that were 3D printed from the dissolvable material candidate, ST-130, and one that was CNC machined from traditional washout ceramic tooling material by Ability Composites, were created. The two 3D printed tools used a truncated square pyramid geometry. The shaded regions of the geometry, as shown in figure 10, represent the solid outer surfaces of the tool. The enclosed region without any shading represents the infill region.
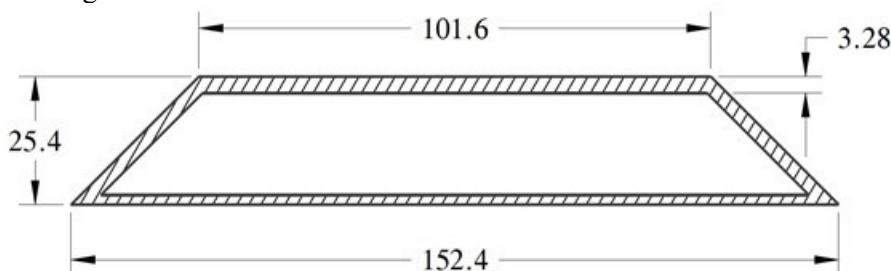
Figure 10 Truncated Square Pyramid tooling geometry. Dimensions in millimeters. For detailed drawing, see Appendix C.

These parts were manufactured from ST-130 with an extruder temperature of 285 °C, a build plate temperature of 126 °C and an enclosure temperature of 105 °C. Additional print parameters included a 20 mm/s print speed, a 0.3 mm layer height, a 0.8 mm nozzle size, and a 40% density gyroid infill pattern. The higher 40% density infill was chosen based on the deformation and print-through noted during tooling stability trials to better support the larger top surface of the square truncated pyramid specimens. The gyroid infill pattern was chosen as it has continuous open spaces which were of interest in terms of introducing the dissolution fluid through the tool to ultimately improve dissolution rates. One 3D printed tool was produced using an ironing routine to improve surface finish. The three pyramids are referred to as Tool/Composite A (printed, no ironing), Tool/Composite B (ironed) and Tool/Composite C (conventional ceramic washout).

While these dissolvable tools are only meant to be used once, it was advantageous to be able to release the composite from the tool and assess any geometric change after subsequent cycles. Therefore, two composite parts were manufactured on Tool A to determine changes in the tool between manufacturing runs. Only one composite was manufactured on each of Tool B and Tool C. Tool A was treated with Chemlease® 41-90 EZ Semi-Permanent Release Agent and Tool B used Stoner Molding Solutions G471 XK-22 LV.5 Mold Release, to ensure easy separation to allow for post-process measurements. The Stoner Mold Release is more commonly utilized at Ability Composites, so it was useful to verify material compatibility. No other form of surface sealing was required.

The composite prepreg material was processed on the tools using a typical autoclave cure cycle at CSU. The layup involved an aluminum tooling plate, a layer of peel ply, and a layer of breather/bleeder. The vacuum bag was pleated to prevent the bridging at the corners of the tool. The autoclave temperature was ramped to 121 °C (250 °F) at 2.77°C/minute (5°F/minute) and held for 150 minutes to complete the cure under full vacuum. The pressure was increased to 345 kPa (50 psi) once the cure temperature hold started. After the 150-minute cure temperature hold, the autoclave was cooled at a rate of approximately 2.77°C/minute (5°F/minute) and the composite part and tool were removed for evaluation.

FaroArm scans of the composite parts were completed before and after manufacturing to generate point cloud models of the tool that could then be compared to the CAD model to document any deformations. The surface roughness of the tools and parts were also measured to gain information on changes to the surfce before and after cure.

3.2.3   Presentation and Discussion of Results

3.2.3.1 Truncated Square Pyramid Tool and Composite A

The as-manufactured 3D printed Tool A is shown in figure 11. Tool A did not use an ironing procedure for the top surface. Also, the seam is seen as a diagonal line running across the front of Tool A in the figure 11 sample, caused by the start and stop point' of the 3D printer's path.
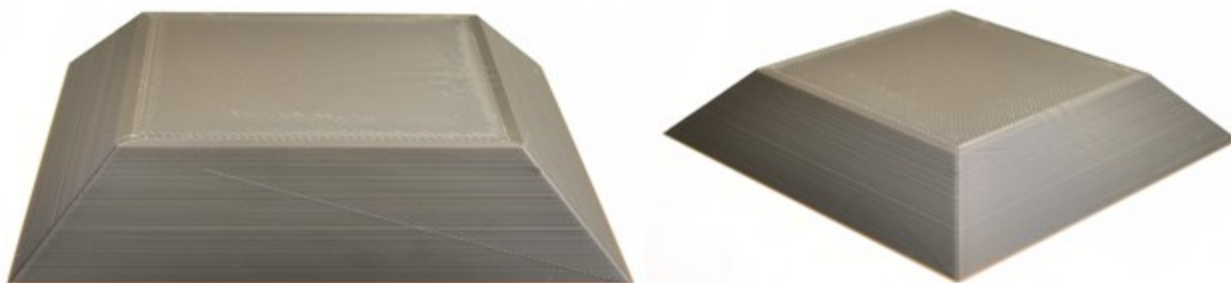
Figure 11 The as printed tool A used for composite manufacturing.

6 plies of prepreg were patterned and laid up on the tool . No debulking process was used during layup, but a debulk was completed prior to autoclave processing. Each ply is approximately 0.2 mm (0.008 in) thick, resulting in a laminate that was just over 1 mm thick. Photos of steps of the autoclave processing of this part are shown in figure 12.

Figure 12 Composite manufacturing process including: (a) the layup of prepreg on Pyramid A; (b) loading the vacuum bagged composite into the autoclave; and (c) removal of the consumable materials used during processing.

The composite cure was performed at 121 °C (250 °F) and 345 kPa (50 psi), similar to the conditions of the autoclave robustness and stability trials. The temperature was ramped to 121 °C at 2.8 °C/min (5 °F/min) then held at 121 °C for 150 minutes to complete the cure. The released composite and tool are shown in figure 14. It was noted that upon process completion and cooldown to ambient temperature the tool had already fully released from the composite laminate. This is assumed to be a result of the very high CTE of ST-130.
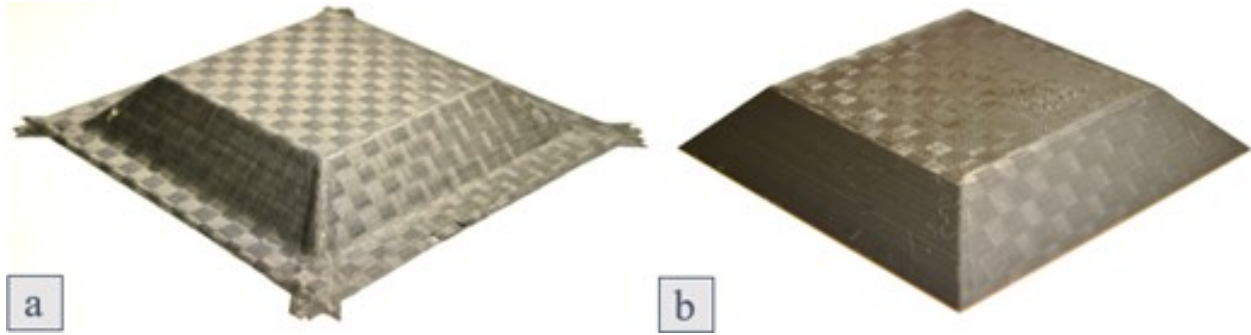
Figure 13 The completed composite for Pyramid A (a) and the tool used to manufacture the composite (b).

The inside surface finish of the composite specimen clearly replicated the surface features of the 3D printed tool. The curing process left a slight sheen on the surface of Tool A, that was undetectable to the touch. Also, undesirable surface features captured included the individual imprints of the roads on the top surface of the composite, as well as the layer lines created by the discreet layer heights, as seen in figure 14. It should also be noted that while there was a small amount of material transfer between the epoxy of the composite part and the 3D printed ST-130 tool, there was no indication of epoxy ingress into any unseen porosity of the tool surface. This suggests that the additional step of sealing a conventional washout tool is unnecessary with the 3D printed tooling, but the texture of the printed tool is transferred to the completed part. Additionally, the pattern of the prepreg weave is apparent on the 3D printed tool surface, yet the surface texture associated with this pattern was difficult to measure.
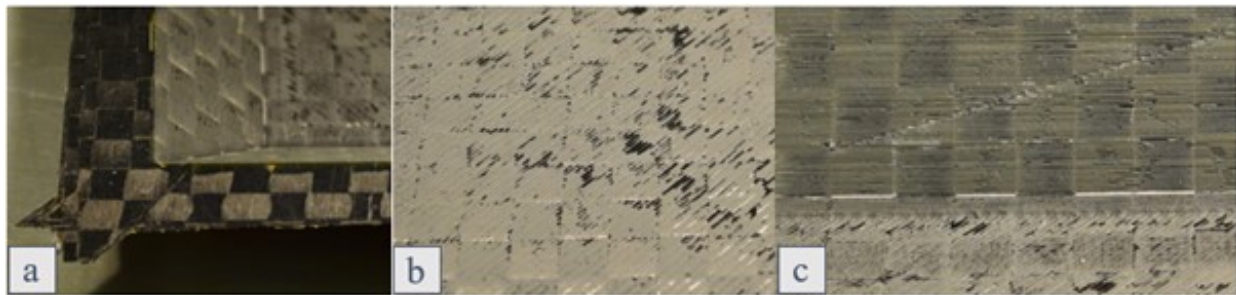
Figure 14 - The interior surface of Composite A including: (a) the interface between the aluminum tooling plate and the composite; (b) the interior of the top surface of the part; and (c) the side wall where the seam was located on the interior of the part.

Tool A was reused once, to manufacture an additional composite part. The purpose of this was to determine the effects of multiple manufacturing cycles on the tool and part geometry. The second composite was manufactured in the same fashion as previously described. A FaroArm was used to measure the tool and composite parts, after the first and second parts were manufactured. The geometry of the tool after one cure and after two cures, as well as each composite part geometry were recorded. Two FaroArm scans of the tool are shown in figure 15.
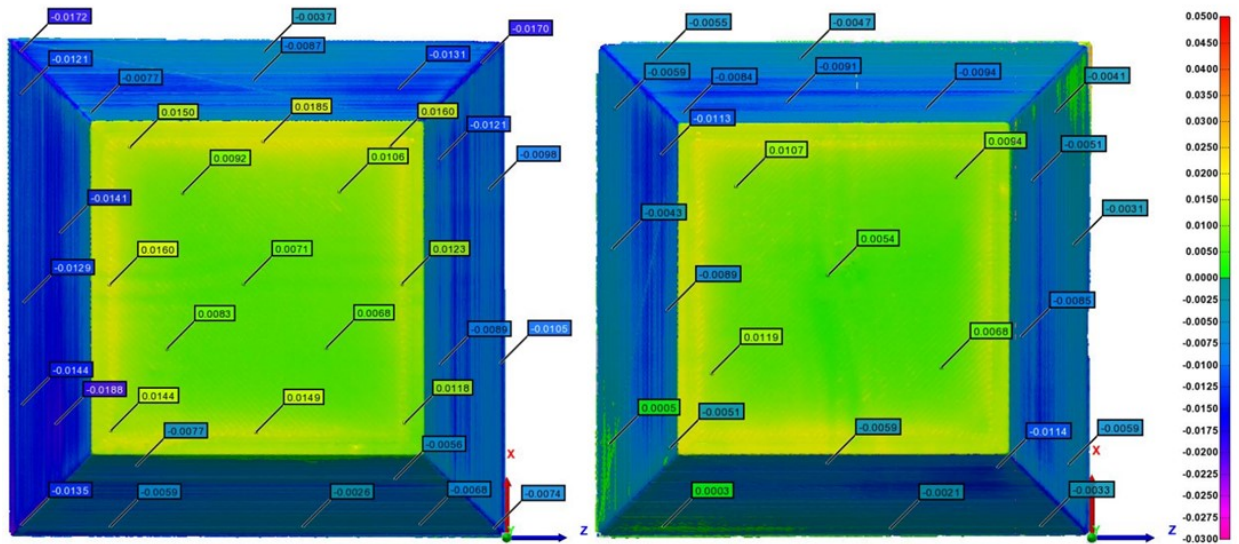
Figure 15 - The FaroArm scans show Tool A after manufacturing one composite part (left), and two composite parts (right).

The scans in figure 15 show relative inaccuracies between the CAD geometry and the manufactured tools. Also, it is important to note that the tool has been rotated counterclockwise by 90° between the first and second scans. The top surface is larger than nominal by approximately 0.25 mm (0.010 in) and the sides are smaller than nominal by around 0.25 mm Faro arm scans of the inner surfaces of the composite specimens manufactured from this tool are shown in figure 16.
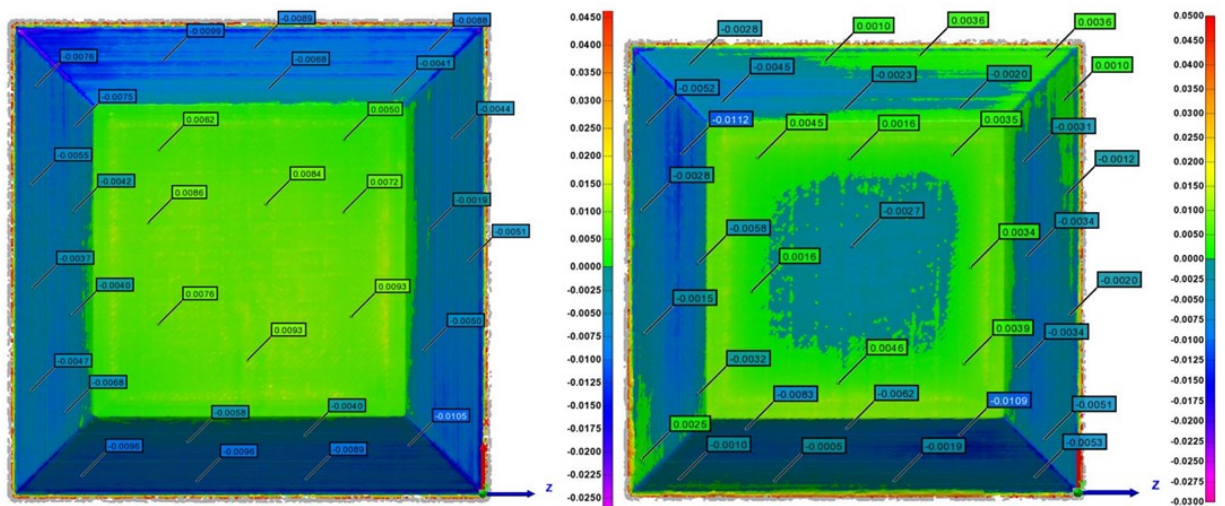
Figure 16 - FaroArm scans for the first (left) and second (right) composite parts manufactured from Pyramid A.

The scans of Tool A and the two completed parts have geometries that agree relatively well with one another. The first composite part showed larger deviations from the nominal geometry; however, these deviations were more consistent across the entire part for the first composite specimen than for the second composite specimen. The larger than nominal top surface was transferred over to the completed composite, with similar deviations from nominal. The scan of the composite created in the second manufacturing cycle shows some differences from the scan in the first manufacturing cycle, and additionally shows some depression occurring on the center region of the top surface. This indicates a small amount of deformation had occurred after the second processing cycle. However, the scan of the tool does not indicate this same deformation.

3.2.3.2 Truncated Square Pyramid Tool and Composite B

Tool B was manufactured to measure the effects one of the first cure cycle on the tool. The effects of a single cure cycle were not included in the study of Tool A, so it was important to revisit. This tool also utilized ironing to smooth the top surface of the tool, with the desire to improve top surface finish. Ironing requires the extruder to remain normal to the surface being smoothed and thus the angled surfaces were not able to be ironed due to the limitations imposed by the 3-axis automation system utilized. The composite cure cycle was the same as that used for Composite A. The completed part is shown in figure 17 with a view of the entire part and an inside view of the surface finish of the part created by the tool.
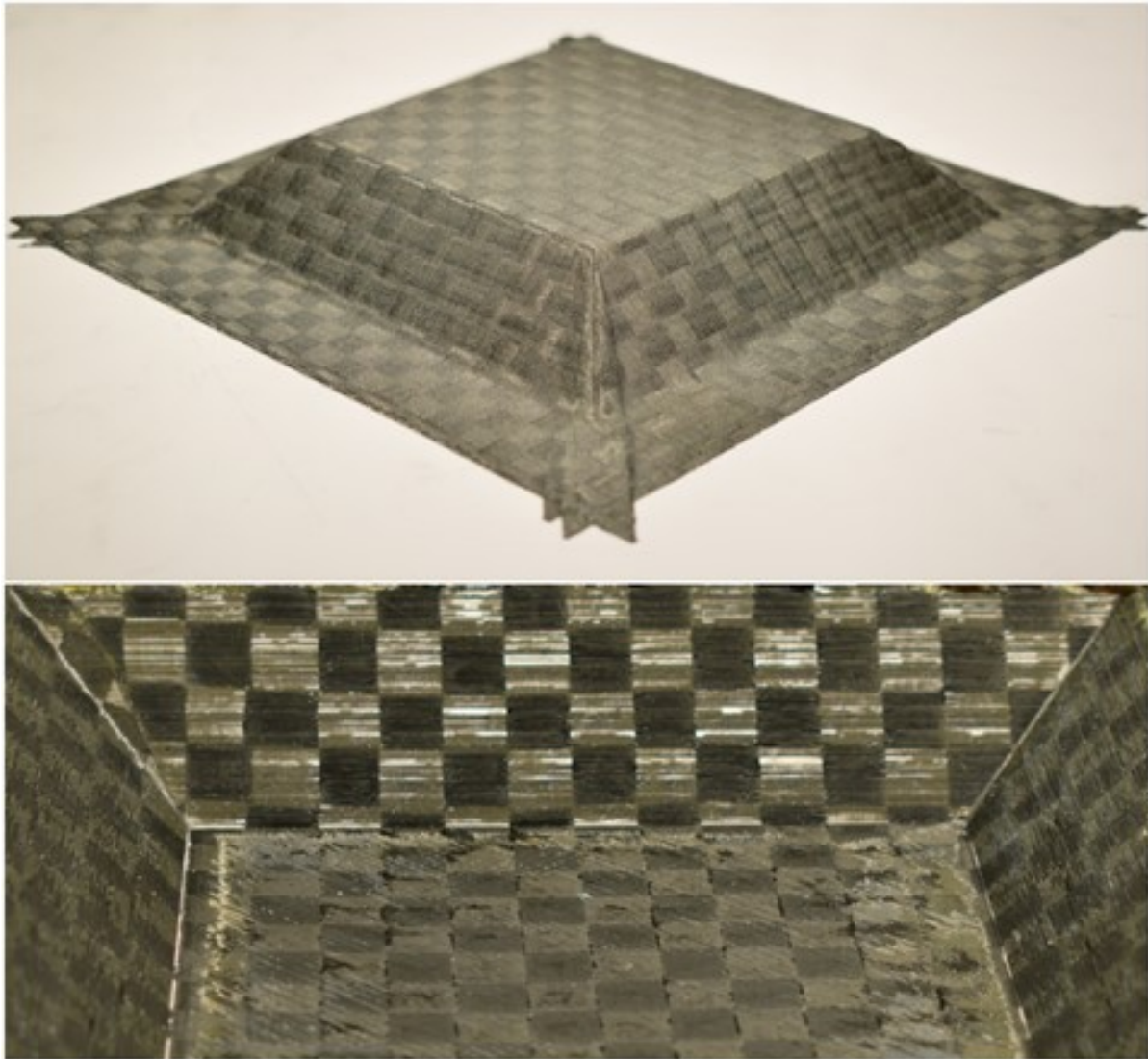
Figure 17 As manufactured Composite B.

A small portion of the tool did fracture on one edge. This could have been caused by the tool becoming mechanically trapped in this region by cured epoxy or by poor mold release coverage. The tool and the fractured area are shown in figure 18.
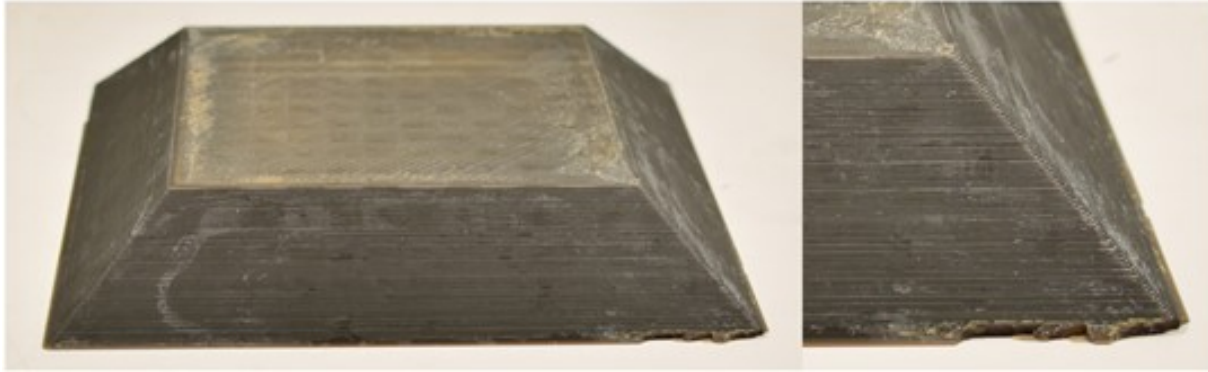
Figure 18 Tool B after composite processing.

Tool B was evaluated in the same manner as Tool A. Measurements were taken before and after manufacturing one part on the tool and the changes that occurred during cure are shown in figure 19.
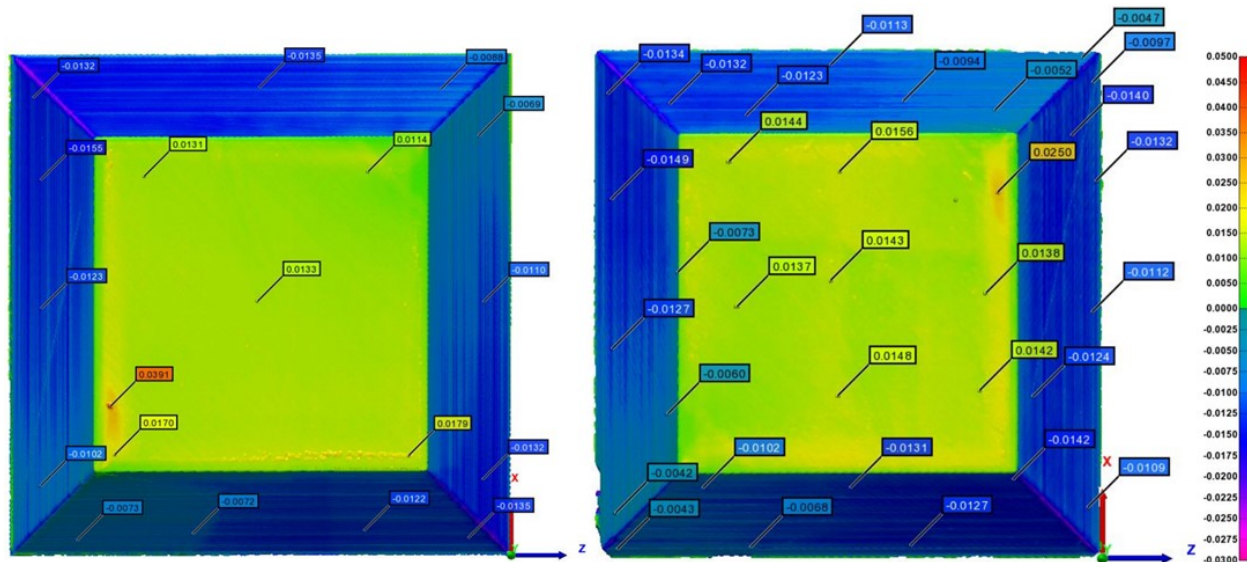
Figure 19 Tool B before and after being used to manufacture a composite part.

The results from the above scans show that the general shape and distortions present in the printed tool remained the same before and after curing. Note that the part has been rotated by 180° between scans. The top surface of the tool looks less smooth after having a part cured on it. However, some of the texture appears to have been removed or flattened during cure. The corresponding composite specimen was scanned to compare to the tooled part geometry, as seen in in figure 20.

Figure 20 The FaroArm scan of the part created on Tool B.

Composite B showed a slanted top surface that was not present on the tool. After examining the part, the exterior of the top surface was not flat, and could be rocked back and forth. While scanning the inside of the part, this surface was likely used as a datum, and could have been rocking back and forth during measurement resulting in this slanted scanned surface. There could have also been deformation of the part during cure.

3.2.3.3 Truncated Square Pyramid Tool and Composite C

The final truncated square pyramid geometry which was scanned on the FaroArm was the tool made from the traditional washout tooling. This tool was CNC machined, and then scanned. The results for that scan are shown in figure 21.

Figure 21 The scanned traditional washout tooling.

The Faroarm scan of figure 21 shows that most of the external sloped surfaces were too small by approximately 0.05 mm (0.002"). The top surface was too high by about 0.1 mm (0.004 in). This is improved accuracy compared to the 3D printed surface, which had an approximate top and side surface inaccuracy of +/- 0.25 mm (0.010 in). Additionally, the printed tooling material has a much higher CTE than the traditional washout tool, and thus, additional tuning of the CAD is needed to compensate for the increased tool size at the process temperature. There was no change of the tool geometry after a composite was cured upon the tool by Ability Composites. Additionally, the composite manufactured had excellent agreement with Tool C's geometry.

3.2.3.4 Surface Roughness Evaluation

The surface roughness of the tools and parts were measured to understand the effects of the cure. Table 16 indicates average surface roughness parameters determined for the top surfaces of the pyramids. The surface roughness of the conventional tool was not evaluated, as it depends on the surface roughness of the sealant used. The tool ironing data was collected over 9 points along the surface of the tool, with each point having surface roughness data collected in four orientations that were 45° apart. This resulted in one measurement direction aligned with the final printed roads.

Table 16 Surface roughness data for Tool A and B, as well as the Composite A and B.

Sample	Ra (μm)	Rz (μm)
Tool A tool after 1st cure	4.2	25.8
Tool A tool after 2nd cure	3.3	20
Composite A (1st cure)	4.7	29.3
Composite A (2nd cure)	4.9	27.8
Tool B tool pre-cure	7.5	35.2
Tool B tool post-cure	5.7	22.8
Composite B	4.7	24.7

The results shown in Table 16 show a decrease in roughness of the tool after curing. This result could be from residual epoxy or from local surface deformation occurring during cure. The composites manufactured from Tool A (without ironing) both had increased roughness compared to the tool. The composite manufactured from Pyramid B had reduced Ra, but a medial Rz value compared to the tools' pre and post cure values. This indicates that ironing results in a composite molded surface at least as smooth as the tool, while not ironing results in composite specimens that have greater roughness than the tool. Therefore, based on this preliminary assessment, a surface smoothing routine is beneficial.

3.3 DEVELOPMENT AND EVALUATION OF COMPLEX 3D PRINTED TOOLS

Subtask 4.9.5 - 3D print a second set of washout tooling and compare to conventionally manufactured washout.

3.3.1   Technical Approach

Often complicated internal tooling geometries will be trapped by a cured composite part. A rectangular 'bent duct' geometry was chosen to represent the trapped-tooling situation and 3D printed to provide an alternative approach to traditional ceramic washout tooling media. The part shape was complex and would result in a trapped tool. The ceramic tool and all the additively manufactured tools included fiduciary 12.7 mm (½ in) hemispherical impressions to locate ball bearings that would allow for easier locating of the part for trimming the composite duct later in the process. The length of the tool was nominally 317.5 mm (12.5 in), so that it could fit on the print bed of the Ender 5 Plus. The bent duct tool geometry is shown in figure 22.
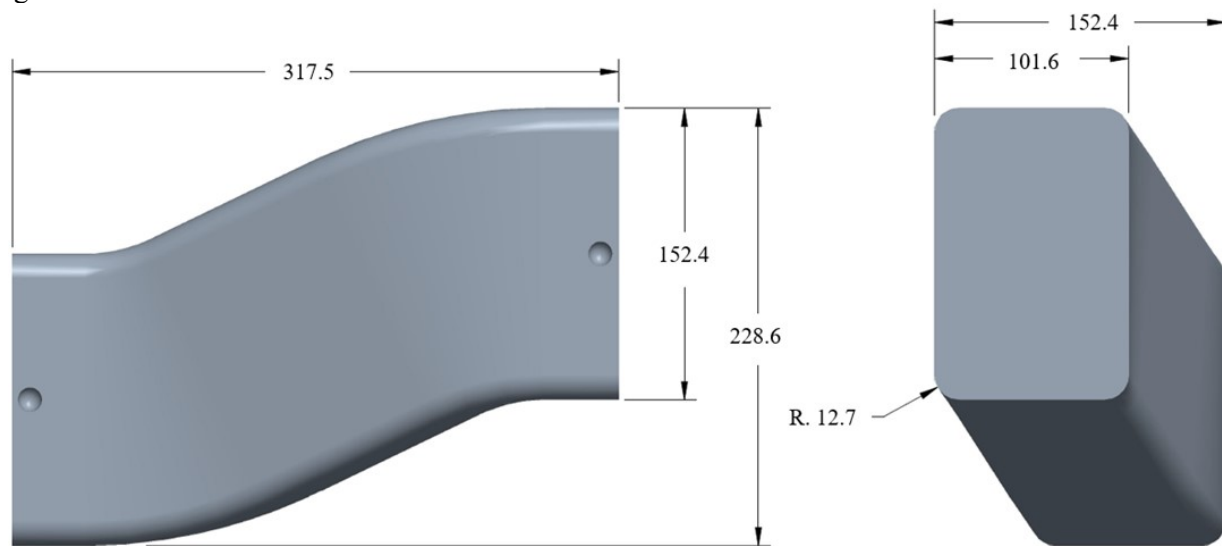
Figure 22 Geometry of the complex tooling.

The ducts were compared both before and after autoclave processing of prepreg composites to determine the geometric fidelity of the approach. An elevated autoclave temperature was chosen to accentuate the deformation. A total of six complex tools were 3D printed, and a seventh was manufactured using CNC methods and a traditional ceramic washout media. The materials used were Stratasys ST-130, Infinite Material Solutions Aquasys-120 (AQ-120), and Infinite Material Solutions Aquasys-180 (AQ-180).

The manufacturing parameters were largely nominal for the manufacturing of these ducts, except a 0.8 mm nozzle was utilized like in the truncated pyramid trials, but unlike the autoclave robustness trials that used a 0.6 mm nozzle. The larger nozzle size would help to reduce manufacturing time.

3.3.2   Specimen Preparation, Test Procedures, and Characterization Methods

A total of six tools were 3D printed, and one control sample was manufactured with traditional washout tooling media using a CNC approach by Ability Composites. Table 17 shows a summary of the ducts manufactured.

Duct	Material	Wall Thickness
0	Ceramic Washout Tooling	N/A – Control Duct
1	ST-130	N/A – Split Duct Approach
2	ST-130	6.35 mm (0.25 in)
3	ST-130	3.2 mm (0.125 in)
4	AQ-120	6.35 mm (0.25 in)
5	AQ-120	3.2 mm (0.125 in)
6	AQ-180	3.2 mm (0.125 in)

The bent duct tool geometry is shown in figure 23 and involved a 101.6 mm x 152.4 mm (4 in x 6 in) cross section that was swept in two directions, resulting in a complex tool geometry that would be trapped within any manufactured composite part, requiring either a very complex multi-part tool, or washout tooling.
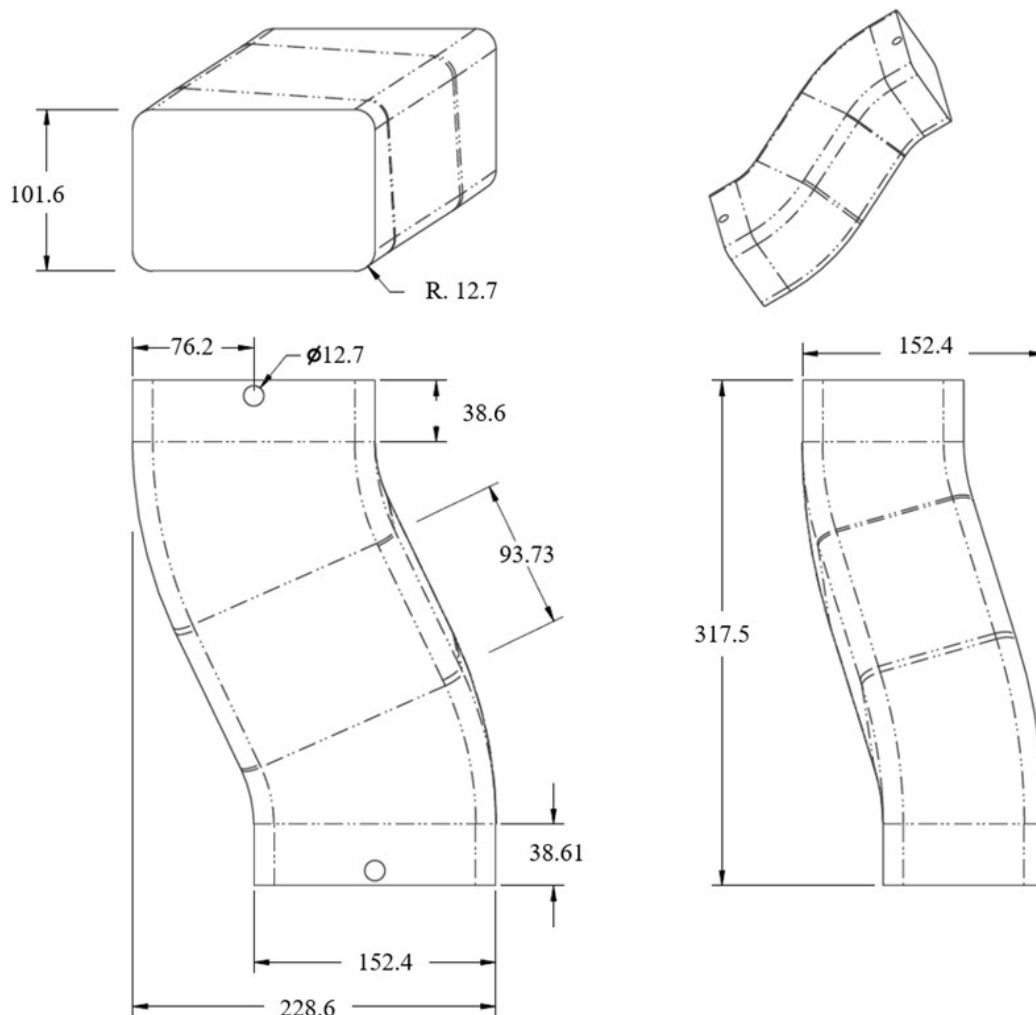
Figure 23 The complex tooling geometry of the bent duct. See Appendix D.

Duct 0, the traditional washout duct, was manufactured using subtractive CNC techniques, creating two halves that were then bonded together and wrapped with Teflon tape to seal the surface. Duct 1, dubbed the split duct' used a similar two-half approach but was produced using additive processes from the dissolvable

candidate materials. It was printed in a horizontal orientation using a longitudinal parting plane that would allow it to be printed in two halves. The two halves were then bonded together and wrapped with Teflon tape to mimic the procedure used on duct 0. Duct 1 was 3D printed with a 40% gyroid infill and a 3.2 mm (0.125 in) shell thickness as determined from prior studies of autoclave robustness. Figure 24 shows the configuration for both the control duct, duct 0, and the split duct, duct 1.

Figure 24 The printing configuration for ducts 0 and 1.

The horizontal printing configuration used for the split bent duct (duct 1) is shown during manufacturing of one half of the tool on the Ender 5 Plus in figure 25.
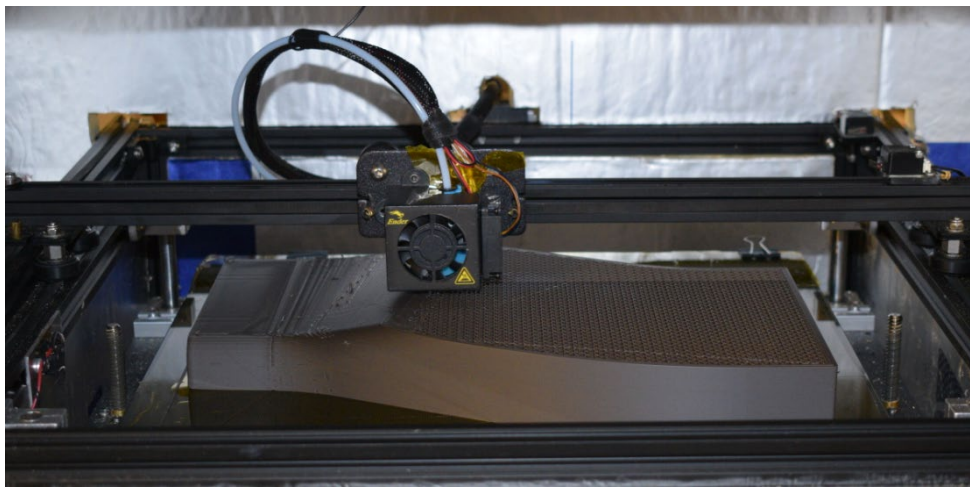
Figure 25 Printing the split bent duct (duct 1).

Based on challenges encountered in the manufacture of the split duct (duct 1) and on discussions related to the techno-economic modeling, the remaining five ducts were printed in a vertical orientation using solid walls, as seen in figure 26. These ducts were printed using either 3.2 mm (0.125 in) or 6.4 mm (0.25 in) wall thicknesses. The benefits of this approach included: (i) a reduction of the visibility of 'stair stepping' caused by discreet layer heights over the gradually sloped surface of the split duct geometry; (ii) the elimination of the need to bond two halves of the duct together; and (iii) the reduction in print time and weight. Additionally, it was proposed that by removing the infill regions, there would be less tendency to collapse assuming that the tool was either vacuum tight to allow bagging to the surface, or that vacuum bagging material could be applied on the inside and outside of the hollow tool surface. In either case, this allows equal pressure to be applied to all surfaces of the tool, reducing the amount of pressure applied to the tool and thus reducing the likelihood of crushing. This is especially beneficial when processing near the upper limit of the tooling material stability, such as in the case of the materials in this study at 121 °C

(250 °F) and 345 kPa (50 psi).
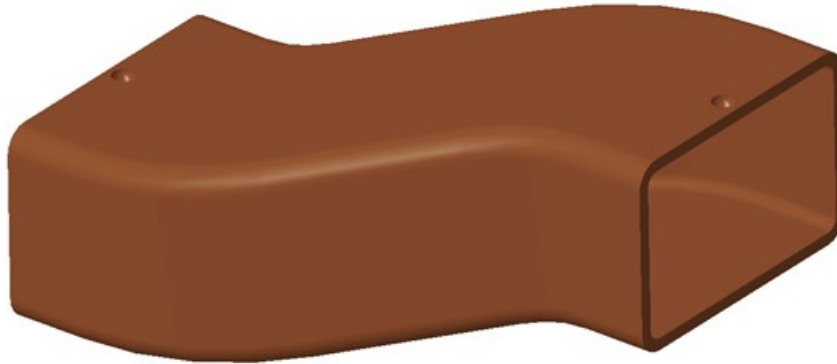
Figure 26 The printing configuration for Ducts 2-6.

The manufacturing process of each of the hollow ducts (ducts 2-6) was completed in a single step, unlike the process used for the split bent duct (duct 1). The printing process for the 6.4 mm wall thickness ST-130 duct (duct 2) is shown in figure 27.

Figure 27 Hollow bent duct printing process for Tool 2.

The hollow geometry was initially considered because of the reduced print time and material required. However, since the manufacturing time, using the prior parameters, was so significantly reduced, this approach offered the opportunity to further refine the printing parameters to improve the overall tool surface

quality. For example, the layer height was reduced from 0.3mm to 0.17mm when moving from the, horizontal configuration with a longitudinal split, to the vertically oriented duct with a hollow geometry Which substantially improves the as-printed surface finish. The associated print time and material usage for a vertically oriented hollow geometry duct made from ST-130, using 6.35 mm thick walls, were 2 days, 17 hours, and 45 minutes and 1.17 kg (2.59 lb). This is compared to the horizontally oriented solid duct (with 40% infill) geometry, which had an associated print time and material usage (for the complete duct) of 4 days, 17 hours, and 46 minutes and 3.08 kg (6.8 lb) of material. Additionally, the hollow geometry was predicted to allow improved tool performance in the autoclave if vacuum bagged appropriately. The thickness of the tool was ensured by printing an extra road on the regions of the tool that were sloped. Ironing was not implemented because of the vertical build orientation; however, the smaller layer heights reduced the stair-stepping effect between layers.

The tools were delivered to Ability Composites for composite specimen manufacture. The ducts were photographed both before and after processing. Additionally, Ability Composites used a FaroArm to create scans of the completed parts, accounting for ply count and thickness so that the tool and CAD data could be accurately compared.

Ducts 0, 1, and 2 used 12 plies of carbon fiber/epoxy prepreg, while ducts 3-6 used 6 plies to save time on layup. The layup procedure involved debulking after the first ply, and then again after every 3-4 plies. The plies used 13-25 mm ply overlaps in the corners, resulting in more prepreg material in the corner regions. The composite manufacturing process is shown in figure 28, with the only changes between duct manufacturing runs being that duct 0 and 1 were wrapped with Teflon tape, duct 2 used mold release, and ducts 3-6 did not use either.
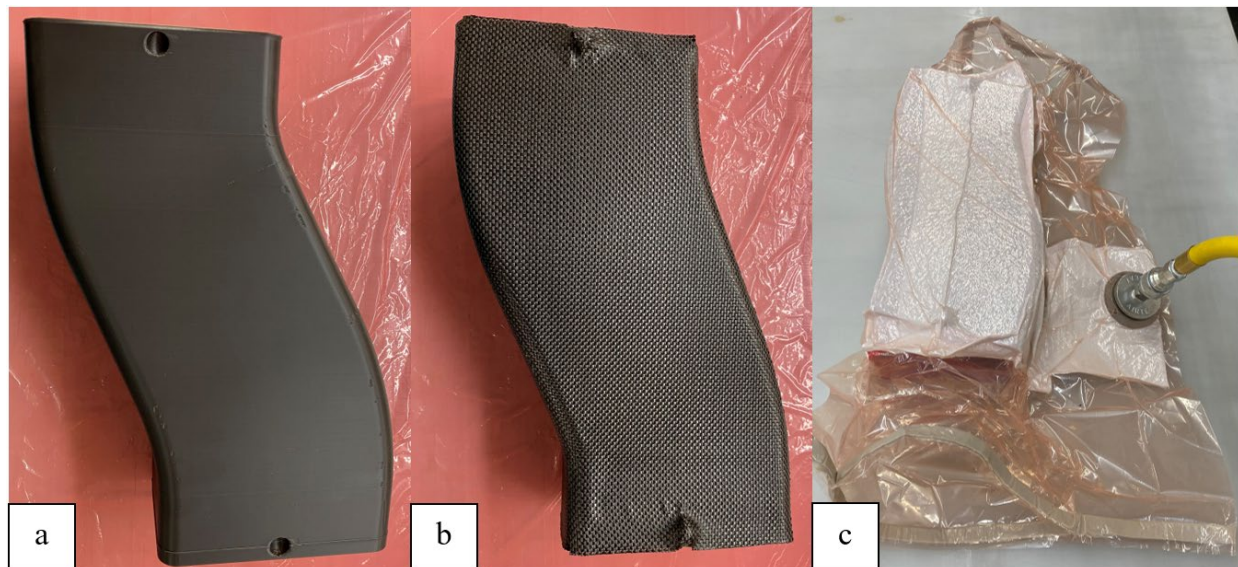
Figure 28 A representative composite manufacturing process of one of the hollow ducts at steps: bare tool (a), during layup (b), and during debulk (c).

Notice in figure 28-c that the bagging material is on both the inside and outside of the tool. The nominal cure cycle for all of the ducts included a 2-stage temperature and pressure cycle while maintaining full vacuum throughout the cure. The initial hold temperature was 82 °C (180 °F), at a pressure of 207 kPa (30 psi), followed by a second hold at160 °C (320 °F). This programmed cure cycle is shown schematically in figure 29.
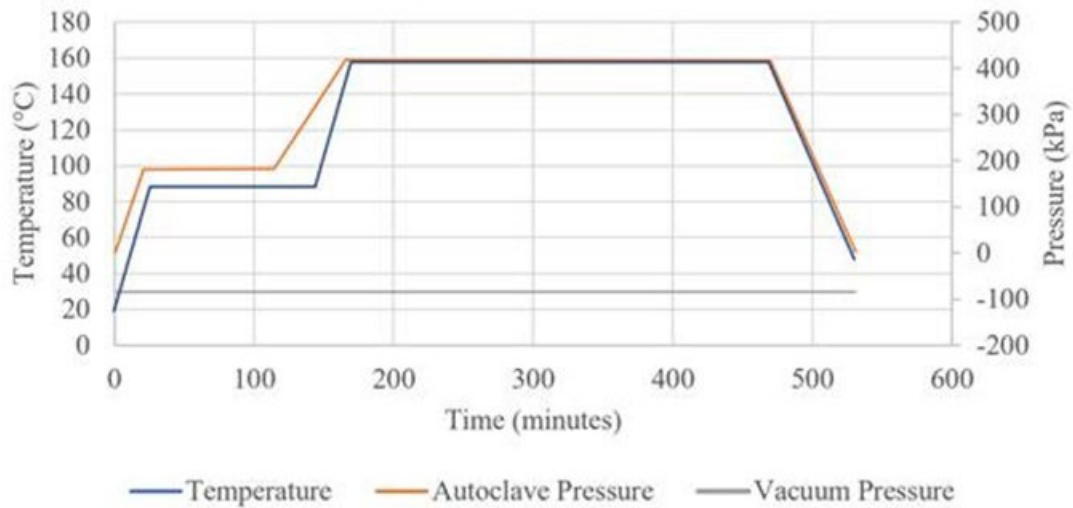
Figure 29 *The nominal autoclave conditions programmed for each of the ducts manufactured*

3.3.3 Presentation and Discussion of Results

3.3.3.1 Duct 0 – Baseline CNC Machined Monolithic Washout Tool

A control sample was manufactured using traditional ceramic washout tooling media. The tool was CNC machined from a billet of flat material. The duct was made in two halves, then bonded together and wrapped in Teflon tape due to the inherent porosity of the washout tooling material. The FaroArm scan for the ceramic washout tool, before and after autoclave processing, is shown in figure 30.
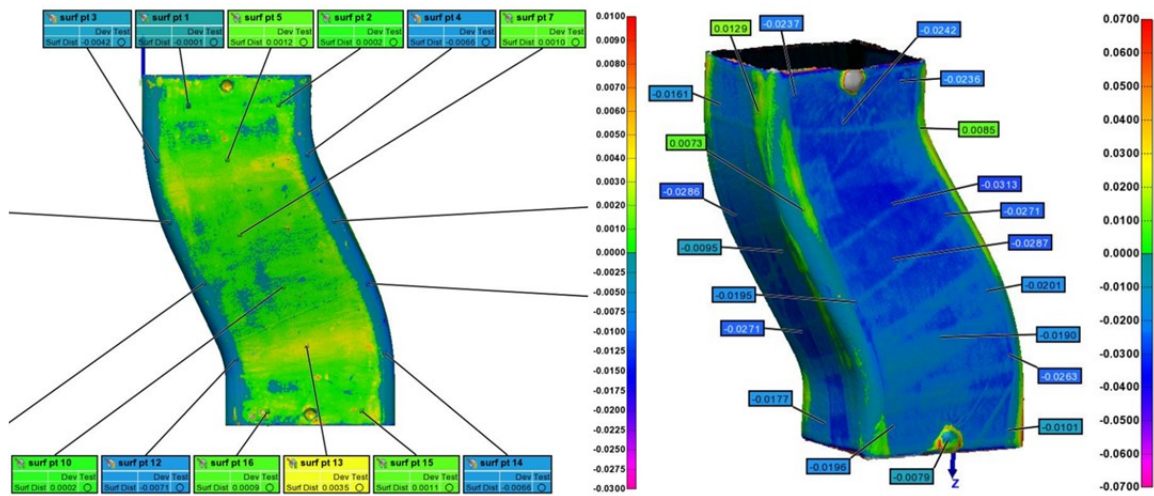
Figure 30 *The FaroArm scan of the top half of the CNC machined control sample duct (left) and the resulting composite part (right).*

The ceramic washout control sample was manufactured to within approximately +0.13/-0.26 mm (+0.005/-0.010 in) of nominal. The scan on the left was performed prior to the Teflon tape wrap. Since the Teflon tape needed to seal the surface was applied after this scan its impression is present in the scan of the composite part. The Teflon tape is 0.13 mm (0.005 in) thick, so the tool should, if high accuracy is required, account for the extra thickness. In this case, it was not considered. The duct showed overall good consistency after autoclave processing. There were some regions in the corners of the tool where the prepreg

wrinkled during cure, creating high spots. The tool was soaked in water for 6 hours allowing it to soften, then removed manually. The tool was easily removed, but in the future a pressurized water jet would make removal much easier. Figure 31 shows duct 0 before and after tool removal.
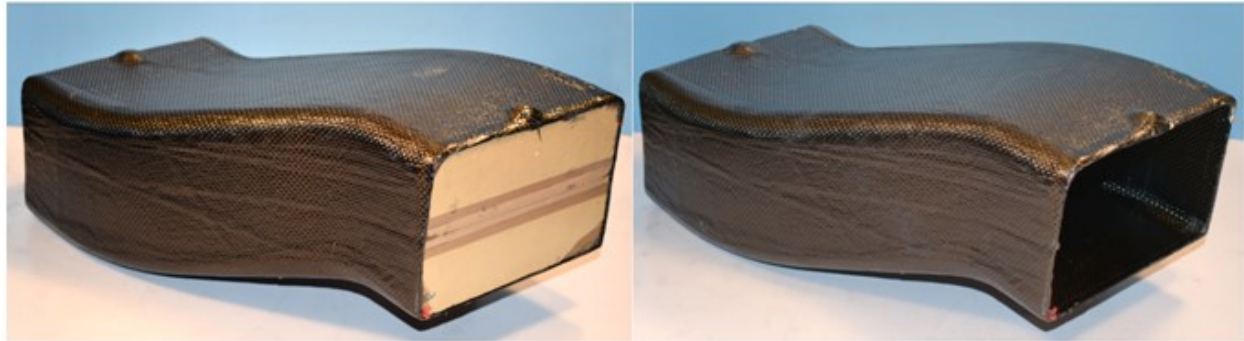
Figure 31 The completed duct before and after washout tooling material removal

3.3.3.2 Duct 1 - 3D Printed – ST-130 2 Part Tool with Solid Surface and 40% In-fill

The first 3D printed tool, the split duct, was printed in two halves. Significant issues with warping were encountered during manufacturing due to the large footprint. ST-130 has a relatively high coefficient of thermal expansion, making the environment temperature an important parameter to prevent thermal stresses, warping, and cracking. The enclosure temperature was at 105 °C for the split duct, which was deemed the limit for avoiding excessive damage to the plastic components of the printer within the heated chamber. However, had higher temperatures been feasible for the enclosure, the warping and thermal stresses may have been reduced.

The split duct was printed with a layer height of 0.3mm, 40% dense gyroid infill, 3.2mm wall thickness, 3.3mm top thickness, and 1.3mm thickness on the bottom print surface (which would become the bonding plane). These settings were determined from the crush test samples. The estimated material usage and print time for the whole duct (including the two equal length prints, one for each half of the tool) was: 3.1 kg and 4 days, 17 hours, and 46 minutes, respectively. The horizontal regions of the duct used surface smoothing to produce an improved surface finish. The prints had matched holes drilled into the bottom surfaces to allow fluid flow between halves for washout. The two halves were bonded together using an adhesive made up of 2 parts Epon 828 epoxy resin and 1 part Epikure 3140 hardener. The manufactured duct halves, as well as the bonding process, are shown in figure 32.

Figure 32 Duct 1 was printed as two halves and experienced ironing on the surfaces indicated by the red arrows (a, b), had holes drilled in the bottom bonding surface (c), was bonded together (d) and clamped to cure (e).

The warping created a 1-3 mm gap at the bonding plane that did not completely fill with the first application of epoxy. It required additional epoxy thickened with glass microspheres to completely fill the bond line. The thickened epoxy was applied and allowed to cure at room temperature, then sanded to be flush with the tool surface. The room temperature cured epoxy was post-cured at 100 °C for 1 hour after a 2.8 °C/minute ramp up.

The tool, upon cooldown from bonding, fractured along layer lines. The crack opened along one end of the duct. A combination of thermal stresses from printing, stresses introduced from the clamps during bonding, and thermal loading during the post-cure likely caused this failure. The developed crack was filled using the same thickened epoxy. The result of post-curing the filled crack was another small fracture that appeared in the part. Instead of attempting to repair the second smaller crack, the part was wrapped with Teflon tape to seal the surface, and a composite was manufactured on the cracked tool with minimal impact from the crack. The filling and heat treatment cycles were used to save the split tool and the amount of time and material required to print it. The completed tool (without Teflon tape) is shown in figure 33.
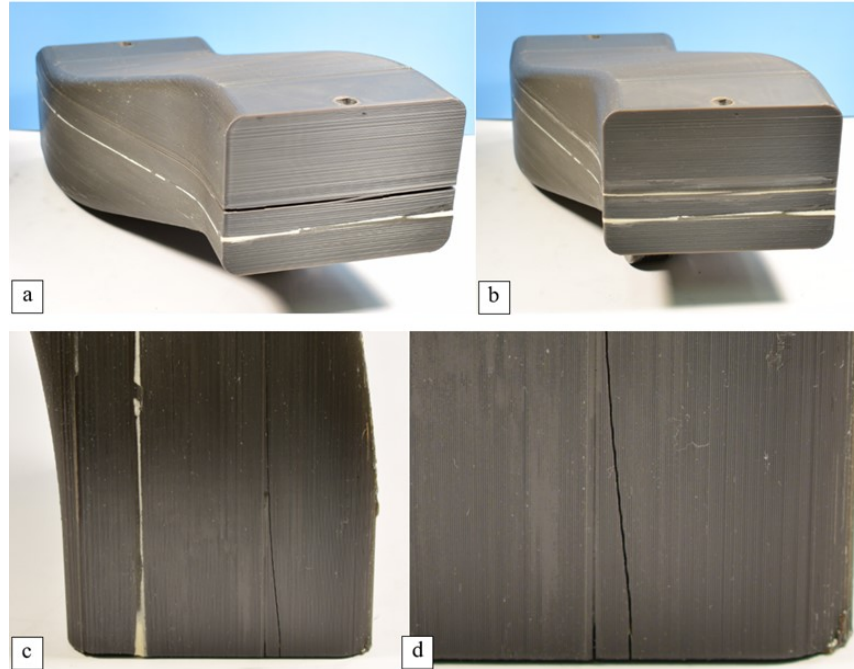
Figure 33 The tool had a significant crack form during the post cure of the epoxy used to bond the two halves together (a). This crack was then filled, and post cured again (b). During the second post cure, a new crack formed (c) and can be seen traversing multiple layers (d).

A composite was manufactured on this tool by using an envelope bag around the whole part and curing in the autoclave. This vacuum bagging approach is consistent with the temperature/pressure/vacuum tests previously performed. The completed duct with the tool trapped inside is shown in figure 34.
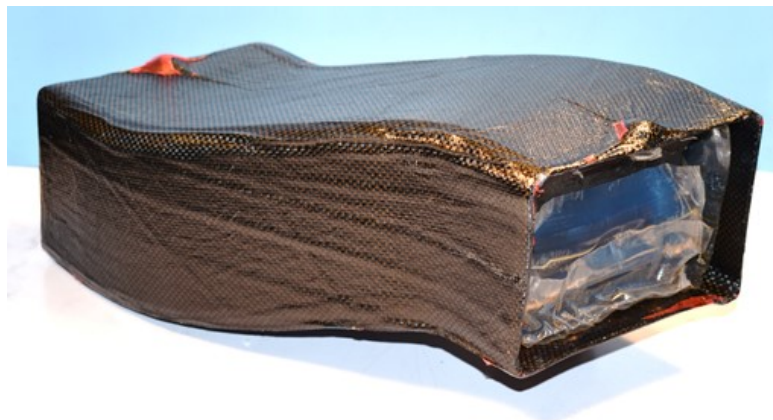
Figure 34 The cured part and tool used for duct 1.

The split duct tool and composite collapsed during processing. A vacuum bag leak was recorded during the cure that can be seen developing at around the 290-minute mark in the vacuum trace shown in the autoclave data in figure 35. Figure 34 shows the cured part surrounding a collapsed tool, covered in Teflon tape. The tool collapsed in all directions. The loss of vacuum is assumed to be associated with tool collapse. It is believed that the sharp corners of the partially cured composite could have compromised the vacuum bag on the ends as tool collapse began. Interestingly, the composite part maintained its form after the cure completion. It is assumed that the initial 1 hour hold at 82 °C (180 °F) and 207 kPa (30 psi), plus over 1 hour at 160 °C (320 °F) and 414 kPa (60 psi) prior to the loss of vacuum, resulted in a sufficient degree of

cure to maintain rigidity. The tool was likely stable during the first hold but began to collapse once the 160 °C (320 °F) hold was achieved. It is assumed that the tool collapse caused the loss of vacuum integrity, so the tool structure was compromised by the 290-minute mark. The temperature of 160 °C (320 °F) and pressure of 414 kPa (60 psi), were notably higher than the values used in the preliminary laboratory trials.
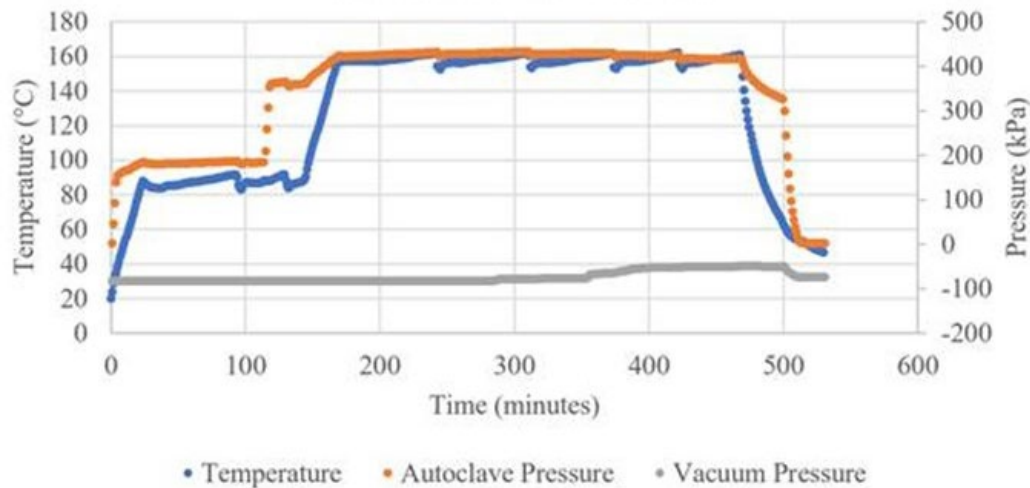
Figure 35 Cure cycle used to manufacture duct 1 showing a loss of vacuum.

3D scans were completed using a FaroArm before and after manufacturing the part. These are shown side-by-side in figure 36. The FaroArm scans of the composite duct are of the outer surface and then a subtraction of the composite thickness is performed, resulting in a geometry to compare to the tool surface scan.
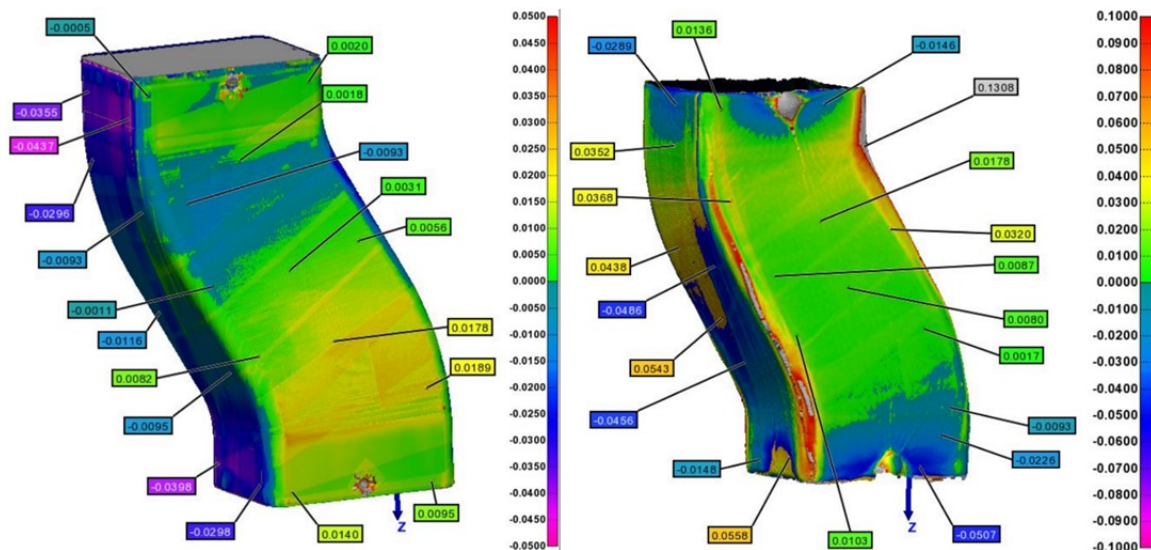
Figure 36 Scans of the tool (left) and part (right) were made using a FaroArm by Ability Composites.

The composite deformation was minimal over large regions of the duct. The corners had high spots, which can be attributed to the overlaps of plies at the corners and resulting wrinkling. The Teflon tape is clearly visible in the scan of the tool. Also, the Teflon tape is 0.13 mm (0.005 in) thick, and this was not accounted for in the scan so its thickness should also be considered. The split tool had significant challenges associated with warping, bonding, material usage, print time, and stair-stepping along the shallow sloped regions.

The second 3D printed tool was made from ST-130 and was manufactured using a hollow geometry. This geometry was printed upright, and only required one print to complete rather than the two prints required for Duct 1. It had slight geometry deviations from filament changes during printing primarily related to pauses in the print and inadequate cooling on some of the overhanging edges. The tool and the composite manufactured on it are shown in figure 37.
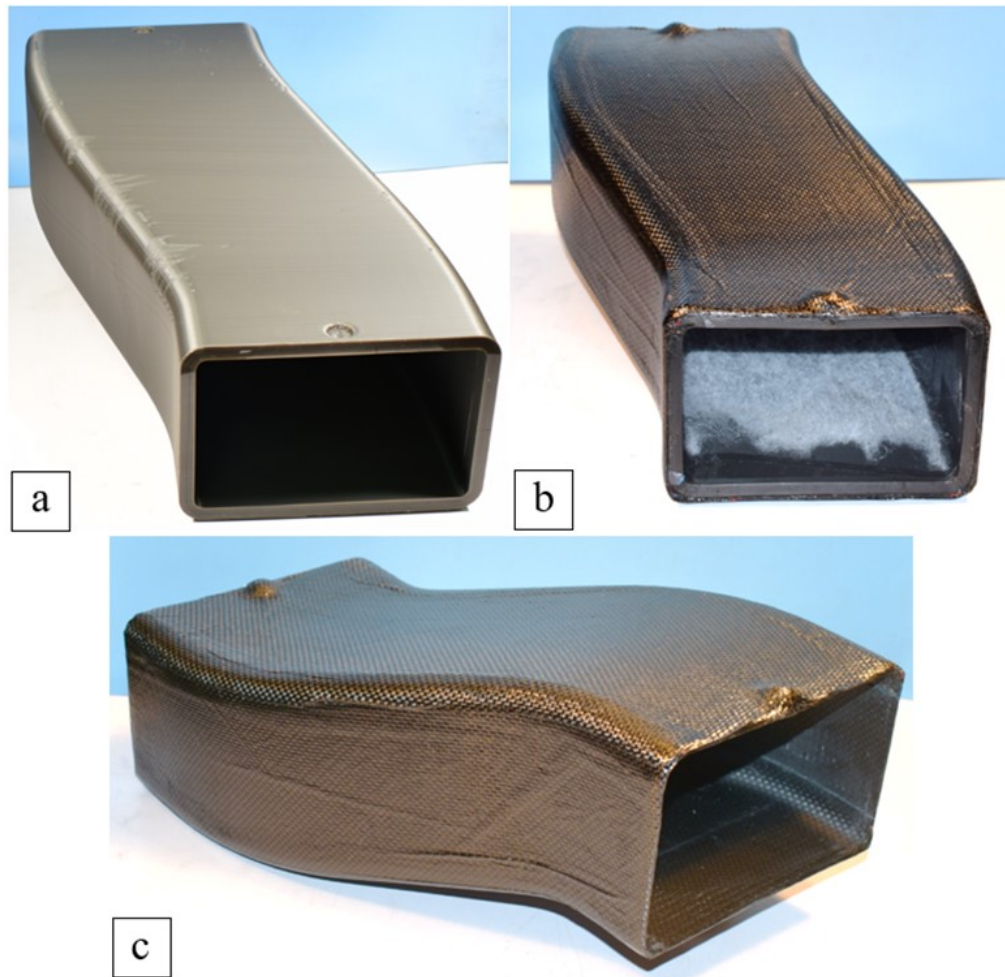
Figure 37 The printed tool (a), the composite manufactured on the tool (b), and the composite part after the tooling was removed (c).

The resulting composite had very slight deviations at the ends of the part. These deviations appeared to be concave along the long edges of the end profile. This duct used ST-130 and was the first sample article that was used to compare the solid duct approach to the hollow duct approach. The results using ST-130 and a 6.35 mm (0.25 in) wall thickness were promising. The tool was not dissolved out, but rather cut out into sections using a Dremel tool in an attempt to further inspect the printed tool post composite duct manufacture. Figure 38 shows the as-manufactured tool and the deformation of the duct in the FaroArm scan.
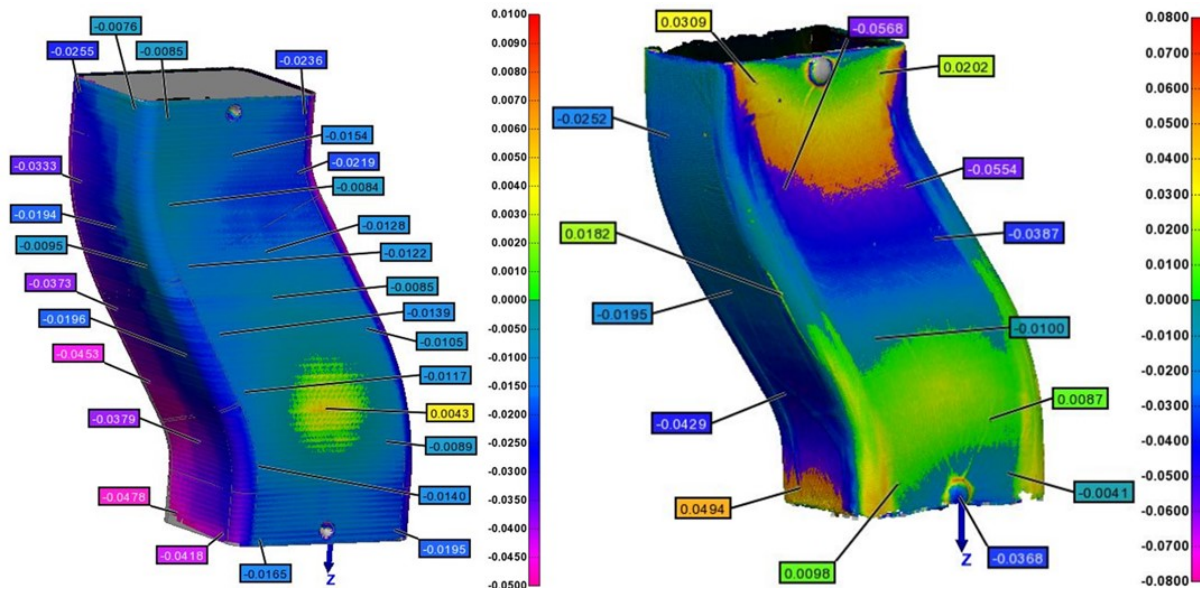
Figure 38 The FaroArm scans of the thick-walled ST-130 tool (duct 2) and the resulting composite.

The FaroArm scan indicated that the tool performed well, even at the elevated temperature of 160 °C (320 °F) and 414 kPa (60 psi). These conditions were much higher than tested during the temperature/pressure/vacuum trials. The promising outcome even at these extreme conditions can be related to of the hollow geometry and the vacuum bagging technique used. Had an alternative vacuum bagging technique been used, where the tool was enclosed in an envelope vacuum bag as used in duct 0 and 1 catastrophic tool failure surely would have occurred. The top-down view of this duct is shown in figure 39 and the slight deformation is clearly present. This lozenging is primarily apparent at the ends of the duct.

Figure 39 The top-down view of duct 2.

Figure 39 shows a slight concavity on the edges of the duct that was caused by either a manufacturing error or by another process occurring during cure that was causing deformation. The cause of this deformation is unknown and was originally assumed to be caused by bridging of the bagging material on the inside corners of the part, causing slight concavity of the long edges. The performance of this duct was promising, but left unanswered questions about minimum tool thickness, tool thermal properties, and the cause of the deformation. The positive outcome prompted the manufacturing of ducts 3-6. The assumption made at this point was that the hollow tool approach would allow equal loading from the vacuum bag on the inside and outside of the duct during cure. This would allow materials with reduced thermal properties to be used as

tooling, reducing the cost and printing conditions required to print. The hollow ducts three through six were 3D printed and tested to investigate these assumptions.

3.3.3.4 Duct 3 – ST-130 Hollow Tool – 3.2 mm Wall Thickness

Duct 3 was manufactured from ST-130 using 3.2 mm (0.125 in) thick walls. The thinner wall sections were utilized in an attempt to recreate the prior results, with a reduced stiffness tool. If the thin-walled tool performed as well as the thick-walled tool, then the vacuum bagging scheme could be assumed to provide no unequal loading to the part, allowing reduced thickness tools to be used. Figure 40 shows the manufactured tool which was printed in approximately 31 hours and required slightly less than 0.6 kg (1.3 lb) of ST-130.
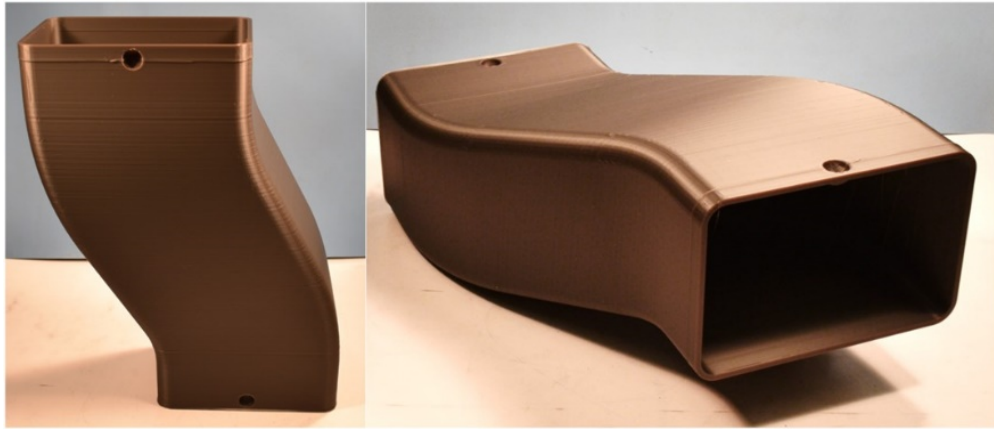
Figure 40 The manufactured thin-walled ST-130 tool.

The tool that was manufactured for the thin-walled ST-130 tool (duct 3) had one primary defect near the locating pocket for the ball bearing at the top of the tool. The filament ran out at this location in the print, resulting in the start of a filament run-out-routine where the printer pauses to allow the user to reload filament. At some point during this routine, one of the stepper motors must have skipped a step causing the inconsistency. The composite duct that was manufactured using duct 3 is shown in figure 41.
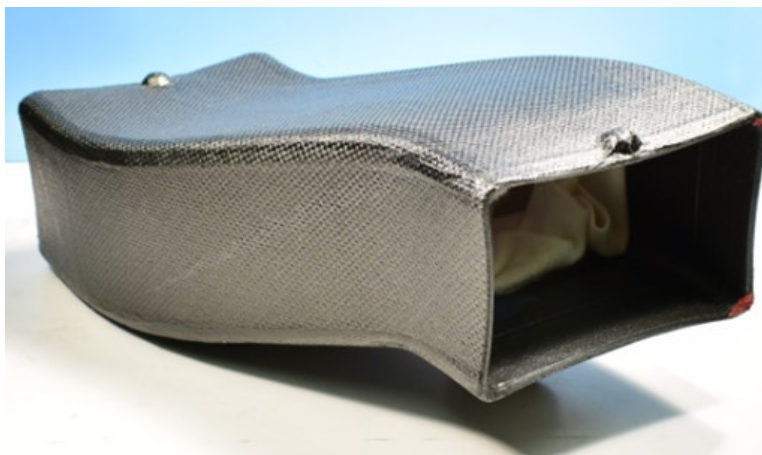
Figure 41 The cured composite and tool.

The manufactured composite showed significant deformation; however, the general form of the duct was still intact. The results seen in duct 3 were significantly worse than duct 2, indicating that the bagging scheme utilized does not eliminate tool stiffness requirements. However, this scheme largely resulted in a

duct that maintained its form throughout the cure. This is promising for future efforts at reduced temperatures because it may be possible to still create thin-walled low stiffness tooling that is stable at reduced autoclave temperatures using this vacuum bagging approach. The FaroArm scans of Tool 3 and Composite 3 are shown in figure 42.
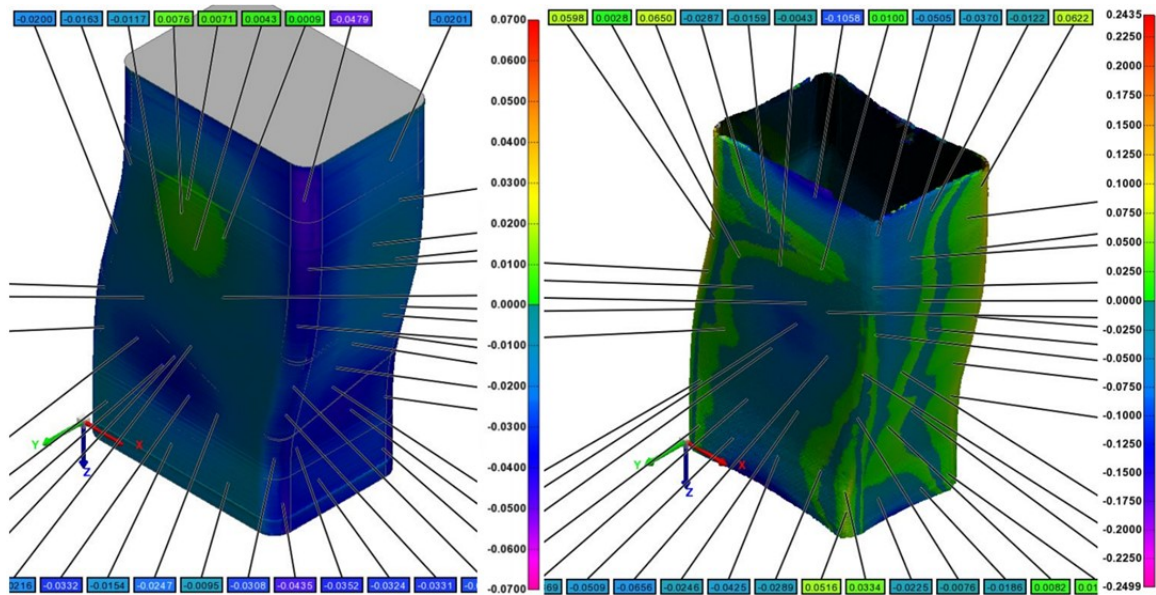
Figure 42 FaroArm scans of Tool 3 and Composite 3.

The FaroArm scans of the tool shows undersized geometry, especially on the corners, and a high spot on the front face. The composite shows high regions on the corners, and low regions on the face. The concave regions at the ends of the duct appear to be too small by up to 2.54 mm (0.1 in). The undersized geometry of the tool is consistent with the undersized geometry seen in the truncated square pyramid tools. The undersized geometry is likely due to the high CTE of the material and printer inaccuracy.

3.3.3.5 Duct 4 – AQ-120 Hollow Tool – 6.35 mm Wall Thickness

Duct 4 was 3D printed from AQ-120, considered to be a low temperature material, and used 6.35 mm thick walls. This thick-walled AQ-120 duct would indicate if the vacuum bagging scheme used would allow lower temperature materials to be used at elevated cure temperatures of 160 °C. The advantages of using AQ-120 if possible revolve around the ability to dissolve in water, not a caustic solution as required for ST-130, and reduced enclosure and print temperatures. The tool for duct 4 is shown in figure 43.
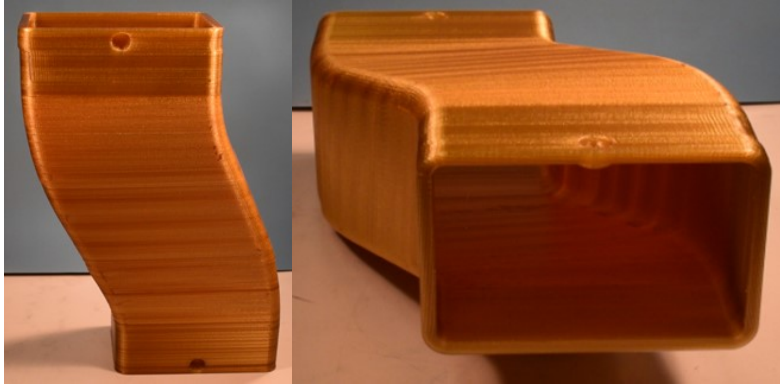
Figure 43 The manufactured tool for Duct 4.

Tool 4 had some slight printing defects, namely a layer shift near the top of the part. This was likely caused by the belt slipping. The belt was tightened, and the error was not seen again with other ducts. Additionally, there were some small regions where under extrusion caused voids in the part. The Aquasys tooling materials tend to create banding of color parallel to the build plate. The ducts 4, 5, and 6 all have horizontal banding occurring in the material. This color shift was discussed with technical support engineers at Infinite Material Solutions (the manufacturer of the Aquasys products) who indicated that the cause of the banding is unknown, but that the bands are typical and should not impact part performance. Figure 44 shows the composite manufactured on Tool 4.
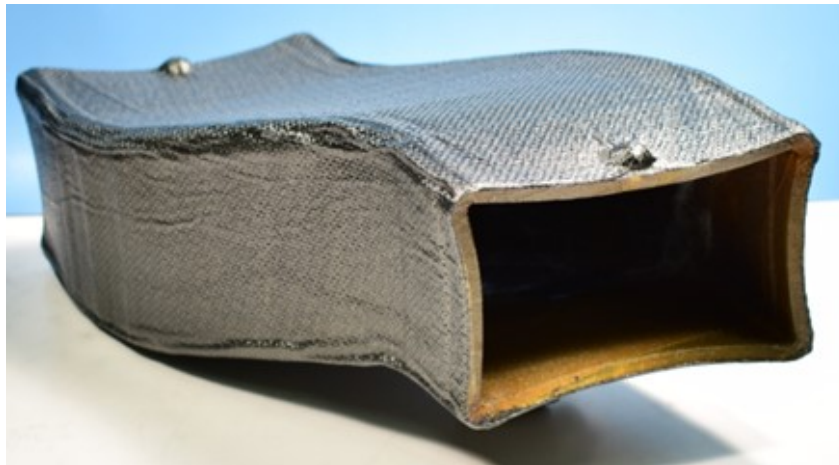
Figure 44 The completed part and tool used to manufacture Duct 4.

The results of the thick-walled AQ-120 duct showed similar results to the prior two ducts. Composite 4 had significant deformation, primarily located at the ends of the part, but this lozenging was also present down the length of the duct. There was more wrinkling in the corners on this duct, but that was decided to be caused by improper consolidation during layup. The concave deformation mode was seen in this duct and is depicted clearly in the FaroArm scan of the composite shown in figure 45. Figure 45 shows both the FaroArm scan of the tool prior to manufacturing and of the cured composite.
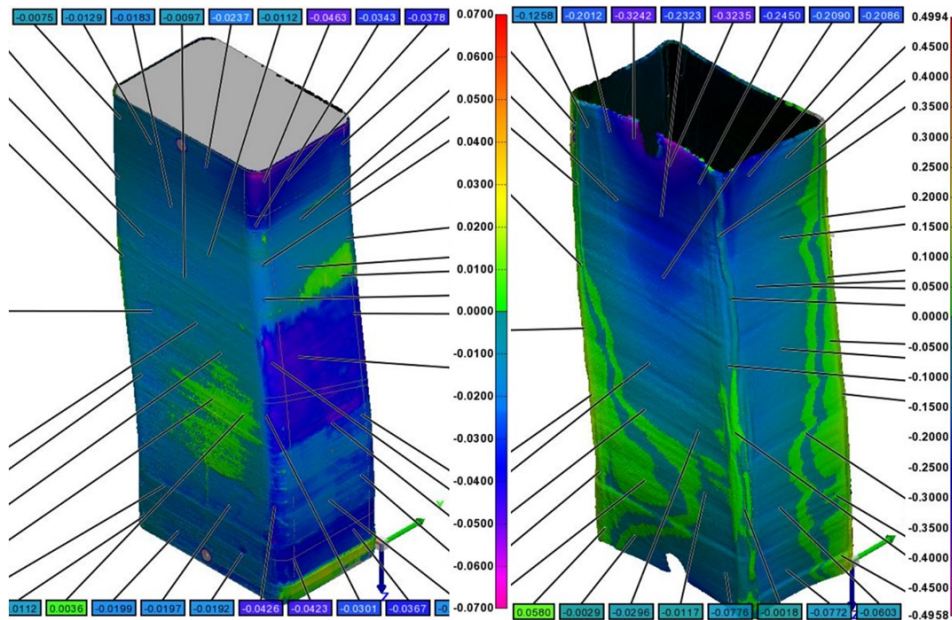
Figure 45 The FaroArm scans of Tool 4 and Composite 4.

The FaroArm scan of the Duct 4 tool shows similar characteristics to the previous ducts (2 and 3) with undersized geometry, except for a high spot on the front face. Composite 4 shows high corner regions, that are oversized by around 1.5 mm (0.06 in), and low face regions on the ends that are too small by up to 13 mm. Some of the regions in the center of the duct do not have as severe of deformation, but the entire duct would likely be too badly deformed to use. The deformation of this 6.35 mm thick AQ-120 tool was greater than that measured for the 3.2 mm thick ST-130 tool. The deformation of the low temperature tooling material, AQ-120, provided additional evidence that the vacuum bagging scheme used still requires a higher degree of tool stiffness than was provided at the autoclave process temperature.

3.3.3.6 Duct 5 – AQ-120 Hollow Tool – 3.2 mm Wall Thickness

Duct 5, like duct 4. was manufactured from AQ-120, just with a reduced 3.2 mm wall thickness. Therefore, it is not surprising that many of the results and discussion points for ducts 4 and 5 are similar, except with worse performance for duct 5. The 3D printed tool for duct 5 is shown in figure 46.
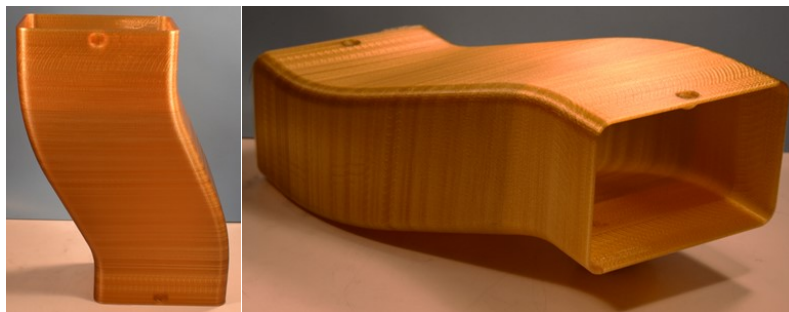
Figure 46 The manufactured tool 5.

Tool 5 did not have any large-scale printing defects. However, there were some regions where additional cooling could have been useful to prevent minor printing errors. Additionally, some errors from the machine vibration can be seen as slight surface irregularities towards the top end of the part. Figure 47 shows the composite manufactured using Tool 5.

Figure 47 The completed part and tool for Duct 5.

The thin-walled AQ-120 duct had the most severe deformation. This is consistent with the use of the low temperature material and the lowest wall thickness tested. This combination was the worst-case scenario for tool rigidity during cure. The associated FaroArm scan is shown in figure 48.
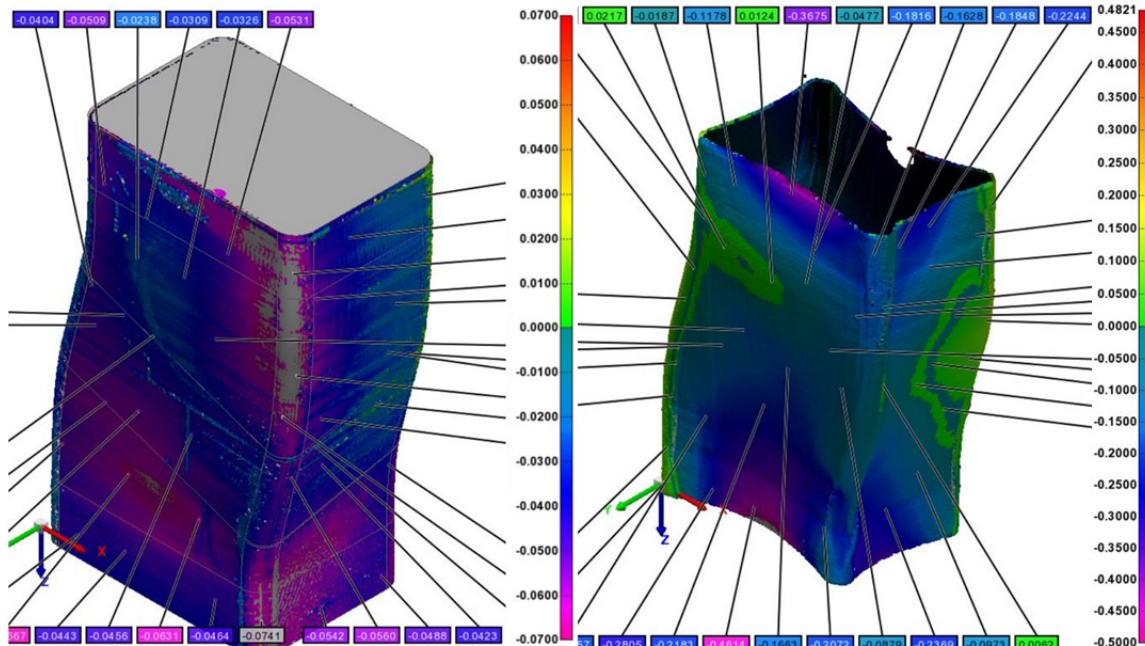
Figure 48 The FaroArm scans for Tool 5 and Composite 5.

The results from manufacturing duct 5 were more-or-less conclusive that the vacuum bagging technique does not provide sufficient support by itself, and rather the tool needs to maintain higher rigidity than what was used in these tests (especially at elevated temperatures). However, it has yet to be seen if the same tooling configurations would provide sufficient results at lower temperatures like the 121 °C (250 °F) conditions used in crush test and square pyramid trials.

3.3.3.7 Duct 6 – AQ-180 Hollow Tool – 3.2 mm Wall Thickness

Duct 6 was manufactured using a thin-walled AQ-180 configuration, with wall thicknesses of 3.2 mm thick. The manufactured tool can be seen in figure 49.
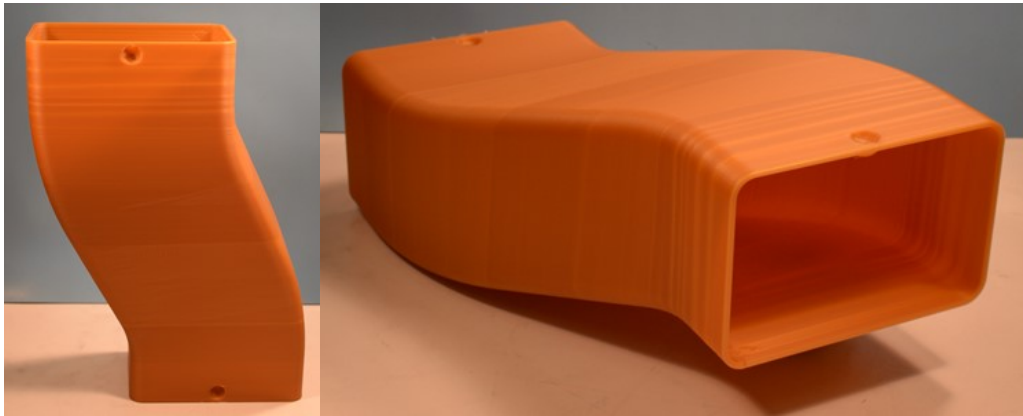
Figure 49 The manufactured tool for Duct 6.

Tool 6 was the only duct to use AQ-180, the second-best performing material to ST-130 in prior trials, and the best performing water-soluble printed material. Tool 6 had a rough surface texture on the overhanging region of the duct as seen above and in the close-up photos in figure 50. This was likely caused by insufficient cooling and deposition on material that was not yet fully rigid from the previous layer. A combination of printing with no part cooling fan (it would fail due to enclosure temperature), high enclosure temperature, and high print speeds caused this defect. After the rough surface finish was noticed, it was addressed by lowering the enclosure temperature from 90 °C to 75 °C and reducing the speed from 32 mm/s to 19 mm/s. It is likely that 32 mm/s would be sufficient for part manufacturing with adequate cooling, however the machine used did not have cooling available at the time this tool was manufactured. Additionally, while the manufacturer stated there would be no adverse effects from the banding on part quality, it was seen that the color banding observed was in regions of locally undersized geometry seen next to a straightedge in figure 50. So, it is assumed that the color banding does have some impact on tool performance, but it may be small enough in most applications to not have a notable impact.
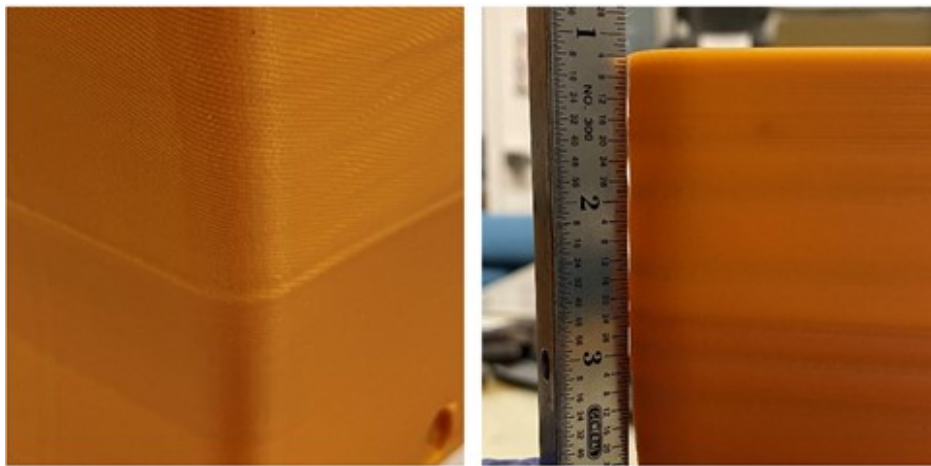
Figure 50 Duct 6 had a rough surface texture on overhanging regions (left) and a wavy surface located where the color banding occurred (right).

Composite 6 showed low deformation compared to the AQ-120 tools, and similar deformation to the ST-130 tool of the same thickness. Figure 51 shows the composite as manufactured using this tool.
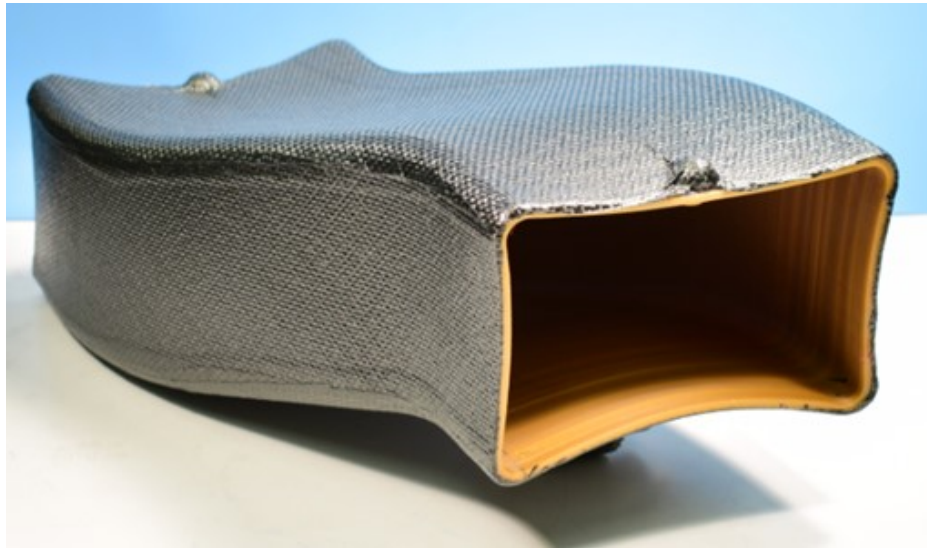
Figure 51 The cured composite and tool used to manufacture Duct 6.

The composite that resulted from Tool 6 performed similarly to the ST-130 duct with the same 3.2 mm thickness (duct 3). This agrees well with the previous conclusion that AQ-180 is a suitable alternative to ST-130 in scenarios where reduced cure temperatures and water solubility are necessary. The FaroArm scan of the tool and of the composite for Duct 6 are shown in figure 52.
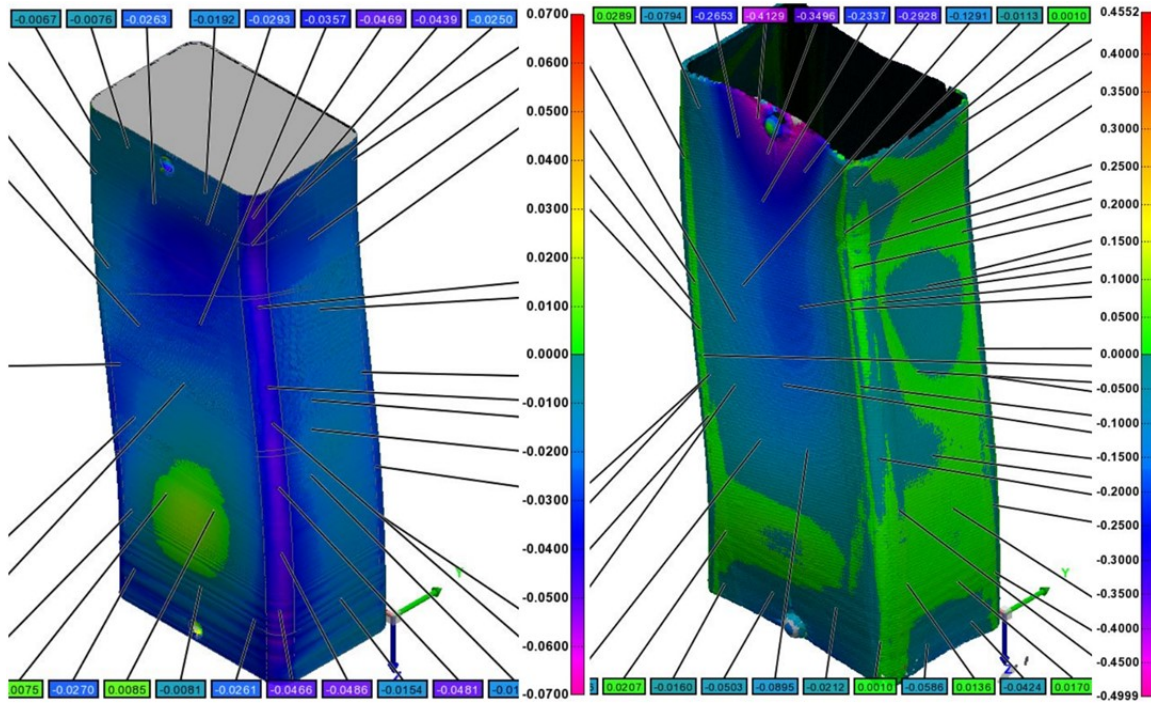
Figure 52 The FaroArm scans for the tool and composite for Duct 6.

The tool had uniform and undersized geometry by around 0.5 mm with a high spot located in a similar region to the prior ducts. The high spot was no more than 0.5 mm. The manufactured composite had local high regions near the corners. Additionally, one end of the duct performed much worse than the other, with one end deforming as much as 13 mm and the other deforming closer to 1.3 mm. The reason for this inconsistency is unknown.

3.3.3.8 Direct Comparison of Ducts and Additional Discussion

Each of the tools were manufactured with relatively repeatable geometry. Figure 53 shows the FaroArm scans of the tools after printing. It does appear that each duct was manufactured smaller than desired. This is important to note because uniform and consistent geometry deviations are easier to correct than local geometry deviations. The tools that were manufactured within the heated chamber likely changed size in part due to CTE as they cooled and shrank. The tools without a heated environment still appeared small in the FaroArm scan, so it is likely there is some amount of machine error as well, and this is most likely the dominant factor in part size deviation.
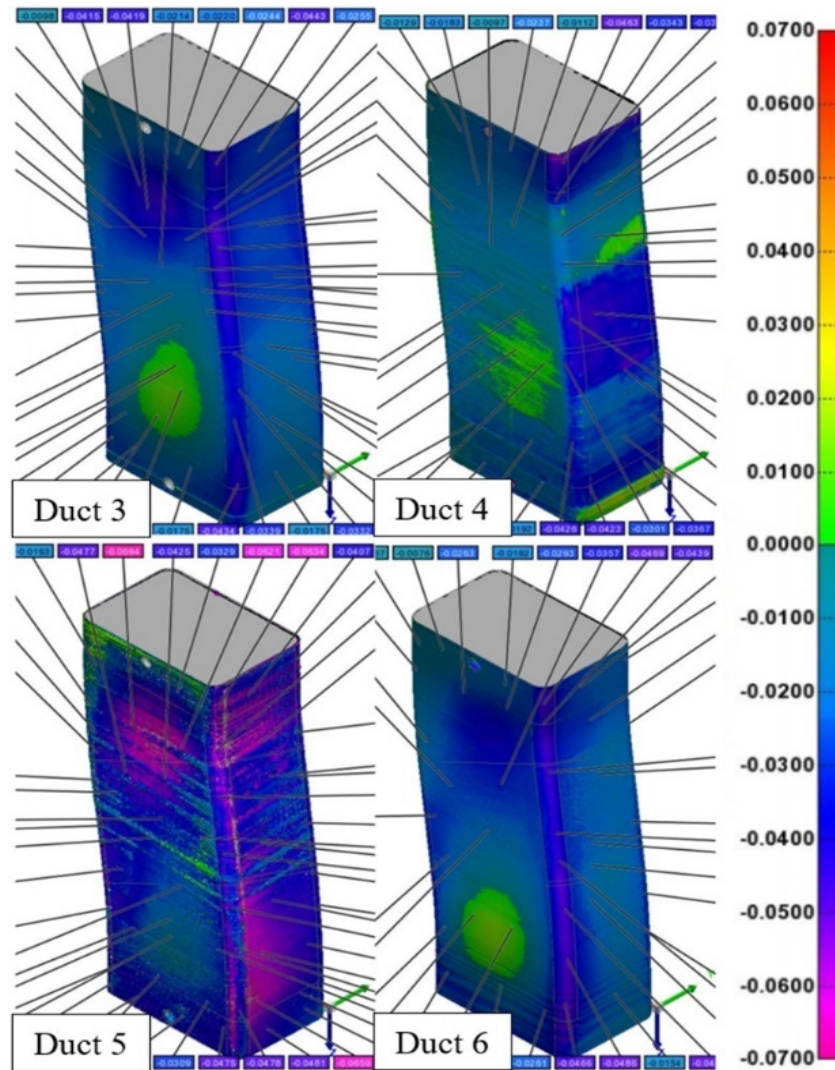
Figure 53 The FaroArm scans of the tools 3-6.

The most severely undersized tool was duct 5, the thin-walled AQ-120 duct. It did not have any significant printing defects; however, its geometry was the most undersized, which is likely due to improper printer calibration. It was also noted by Ability Composites, that during the scans, the semi-opaque surfaces of AQ-120 tools were difficult to scan with the FaroArm. This is likely a contributing factor to the quality of scans seen in ducts 4 and 5.

The tools did not fare well during the 160 °C cure. This temperature allowed each material to be pushed passed its glass transition temperature and deform relatively easily. Thus, the tools deformed significantly past what was expected based on the earlier temperature/pressure/vacuum trials. The assumption that the tools did not experience any unequal loading was likely incorrect. The cause of the deformation had previously been assumed to do with bridging on the internal vacuum bag, however no bridging was observed during the manufacturing of ducts 3-6, and excess bagging was left in the corners to prevent bridging. The observed deformation mechanism is still unknown. A comparison of the completed parts and their associated deformations is provided in figure 54.
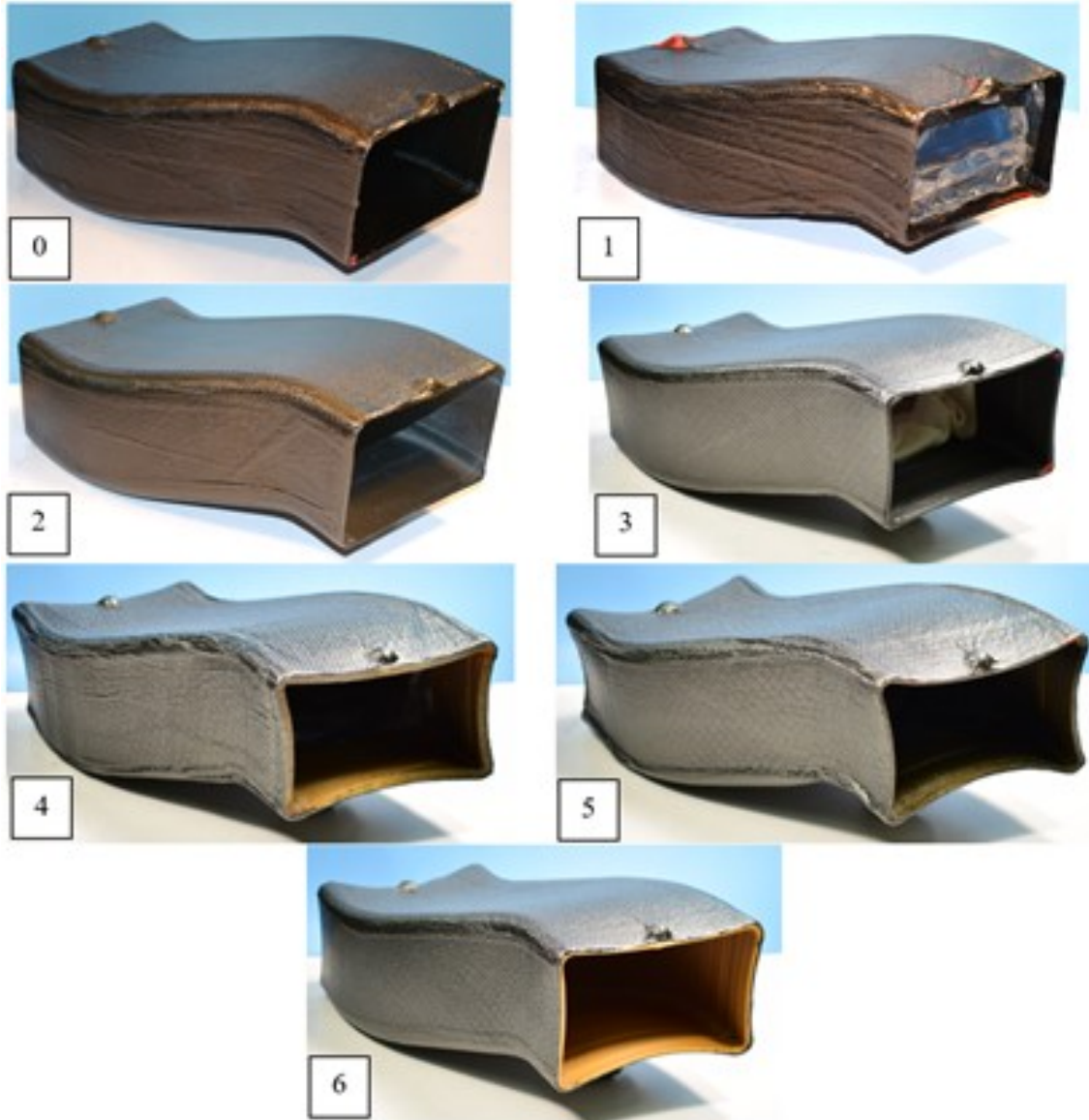
Figure 54 Comparison of ducts 0-6

The comparison of ducts 0-6 showed duct 0, the control duct using ceramic washout media, performed the best, followed by Duct 2, the 6.35 mm thick hollow ST-130 tool. The performance of the 3D printed ducts was not sufficient at the 160 °C cure temperature and 414 kPa (60 psi) pressure. The performance of duct 2 was the best of the 3D printed ducts, likely due to the increased tool wall thickness and the use of ST-130, the highest temperature material evaluated. In future endeavors, it would be wise to pursue a lower temperature curing composite system and utilize increased tool thickness. The performance of each duct was ranked (best to worst): duct 0 (control), duct 2 (thick ST-130), duct 1 (split duct ST-130), duct 3 (thin ST-130), duct 4 (thick AQ-120), duct 6 (thin AQ-180), and duct 5 (thin AQ-120). Another view of the ducts in figure 55 show the deformed cross-sections of the duct ends.

Figure 55 Views showing relative distortions of the manufactured ducts 0-6.

The results of this testing indicate that 3D printed tooling seems to be a reasonable approach for lower temperature and pressure curing prepreg material systems. To reduce deformation to a minimum, the cures should be limited to around 121 °C (250 °F) and 345 kPa (50 psi) for the dissolvable tooling materials evaluated, as indicated by the crush testing. However, it does seem that an increase in the tool wall thickness, and/or potentially a hollow design with more material in the corners could be sufficient to resist the 160 °C cures imposed. Additionally, ducts should be printed in a hollow configuration so that their print time and material usage is reduced, and the bagging material can be applied to both the inside and outside of the structure resulting in an improved loading condition. To reduce deformation for a similar geometry and vacuum bagging scheme, a hollow part may require 12.7 mm thick walls or greater if using ST-130 or AQ-180.

The internal surface of the composite ducts created with the washout tooling and the 3D printed tooling shows some differences. The inside surface of the composite duct made on the washout tooling replicates the surface of the Teflon tape that was used to wrap the tool. The inside surface of the duct made on the hollow 3D printed tool shows the tool's surface finish. Figure 56 captures the differences.
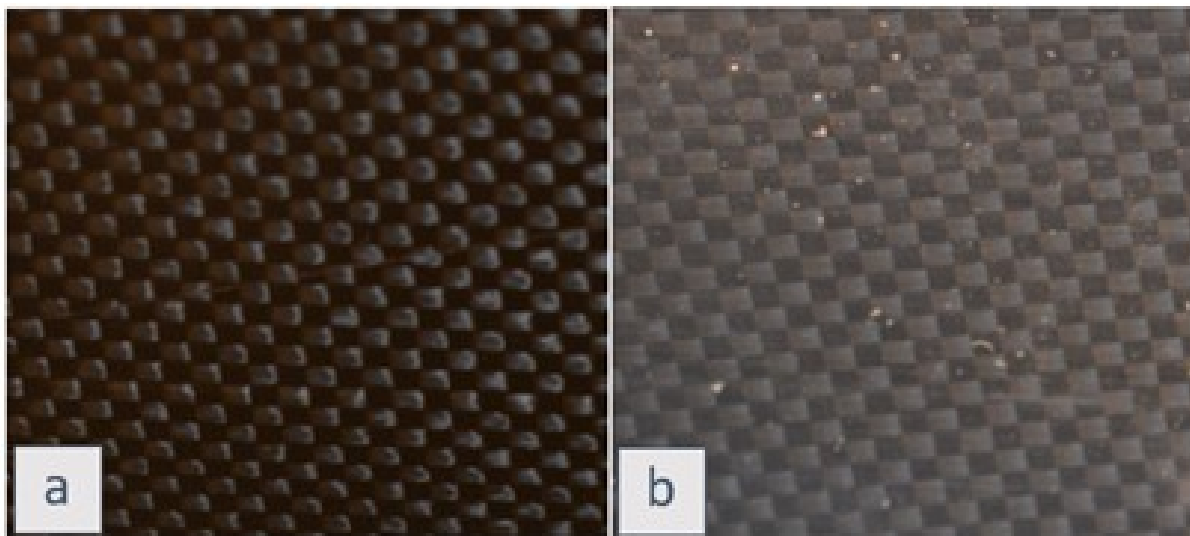
Figure 56 These images show the internal surface of the composites created by the washout tooling (a) and the hollow 3D printed tooling (b).

The glossy surface finish in figure 56(a) comes from the Teflon tape that was used to seal and provide a high gloss surface finish to the tool. It should be noted that the impressions left by the Teflon tape were visible and noticed as ridges on the surface. The matte surface finish seen in figure 56(b) comes from the as-printed tooling surface. The printed surface does not require mold release or Teflon tape to be used, because it is washed out from the part anyways. A benefit of using the printed surface is that the mold release/sealing step utilizing Teflon tape can be eliminated from the manufacturing process. While not a significant factor in accuracy, material, or time, the 3D printed tooling also promises to reduce geometry deviations caused by the Teflon tape and saves a small amount of material and time.

3.4 DISSOLUTION OF PRINTED AND CONVENTIONAL MATERIALS

> *Subtask 4.9.5 - 3D print a second set of washout tooling and compare to conventionally manufactured washout. The degree of tool removal and difficulty of tool removal will be documented.*

3.4.1 Technical Approach

A study of the washout characteristics of the ceramic tooling media, ST-130, AQ-120, and AQ-180 was undertaken. This required different dissolution media that matched the different dissolvable tooling materials. ST-130 is soluble in a heated, basic solution, while the other materials are soluble in water. Stratasys recommends WaterWorks or EcoWorks detergents, which provide a solution with 11-13 pH. The approach taken by CSU was to use an aqueous solution of trisodium phosphate (TSP) to result in a solution of at least 12 pH. Aqueous TSP solution is a commonly used as an industrial cleaning agent and was investigated as an industrially scalable, inexpensive alternative to the Stratasys solutions. Infinite Material Solutions recommends using water heated to 80°C for the dissolution of AQ-120 and AQ-180. Heated water decreases the washout time significantly. The ceramic washout tooling media can be left to soak in room

temperature water, where the binder is dissolved, and the tooling can then be physically removed rather than fully dissolving the tool.

3.4.2 Specimen Preparation, Test Procedures, and Characterization Methods

To compare the dissolution of the ceramic washout tooling material and the 3D printed filaments, the CMMS Lab manufactured 25.4 mm cubes of each material. The printed cubes had 4 perimeter roads, 11 top layers, and 6 bottom layers and the remainder was a 40% Gyroid infill.

A laboratory heated bath with magnetic stirrer was used for the dissolution trials. The washout time was recorded as the time at which the cube could be broken apart using tweezers. A ceramic cube, for example, was left in solution for 24 hours with little change to its shape. However, upon agitation it could be readily broken apart.

3.4.3 Presentation and Discussion of Results

The mass, solution conditions, and washout time of each material are shown in Table 18.

Table 18 The washout time and information for each sample cube.

Material	Mass [g]	Solution Temperature [°C]	Washout Time [hours]
Ceramic cube	11.3	18	1.0
ST-130	14.5	80	17.5
AQ-120	14.6	80	1.6
AQ-180	14.6	80	7.2
AQ-180, with holes	13.9	80	3.0

During a 6-hour span, the control sample (duct 0) was soaked in a bucket, and the tooling material was easily removed using a pry bar. This was the technique that Ability Composites uses on a routine basis. It is likely more practical to physically remove the washout material after some time soaking in water using pressurized water or tools, rather than waiting for complete breakdown of the washout media. Figure 57 shows the 2 mm laboratory test cube of ceramic washout tooling material prior to attempting dissolution, and after being submerged in the agitated water bath for a period of time. The geometry of the test cube changed very little prior to being physically broken up after 1 hour.
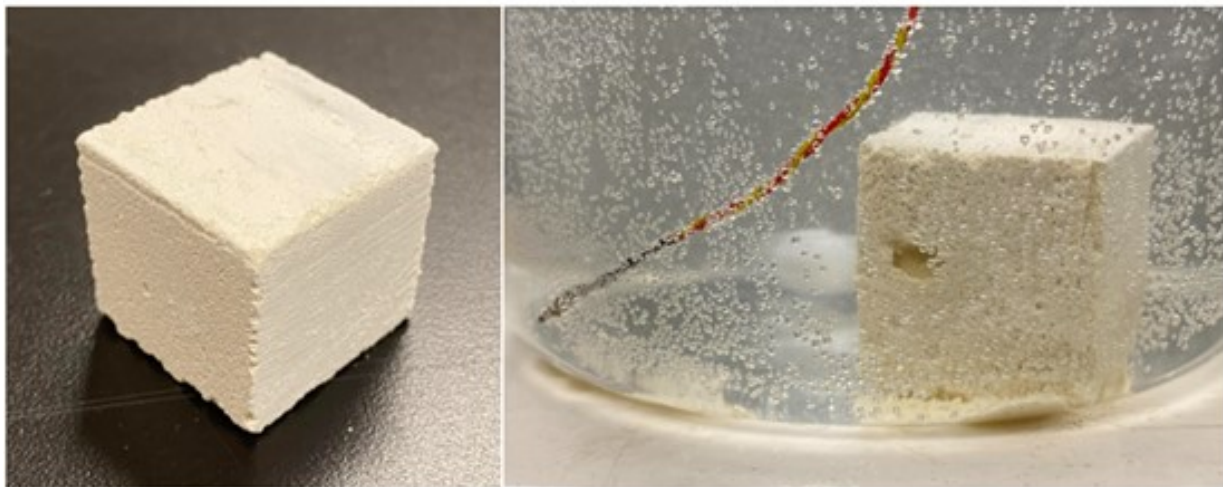
Figure 57 The ceramic washout tooling sample prior to dissolution (left) and during dissolution.

The ST-130 cube was placed in a solution composited of 200 g trisodium phosphate (TSP) dissolved in 750 mL of water (~26% solution). The manufacturer specifies that a 1% solution of TSP in water has 12 pH. The higher concentration solution was used in an attempt to offset any contamination issues related to the dissolving tooling material. Additionally, every 1-2 hours when the solution would become cloudy, 250 mL of the solution was removed and replaced with an equal amount of a fresh 40% TSP solution. The dissolved material would create a gel-like substance as it was dissolved. This was removed from the test cube whenever the solution was changed. The gel-like material is shown in figure 58. After about 12 hours, a hole was noticed on the external corner meaning solution could flood the interior of the infill region. At the 17.5-hour mark, the part was removed from the solution and easily broken into two pieces. The infill region had coalesced into solid gel-like material. It was at this point that the test was stopped because, in practice, the tooling material could be physically broken up and removed.
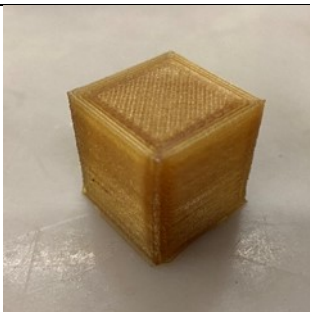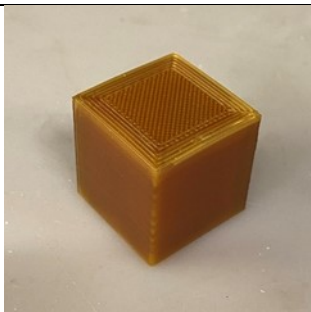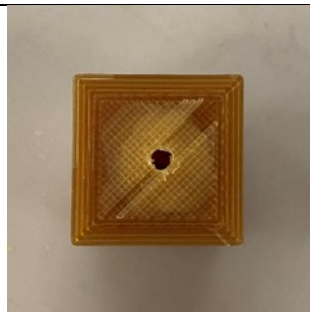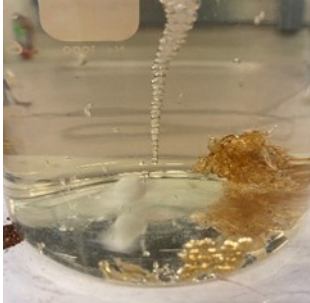
Figure 58 The ST-130 sample during dissolution trials.

Stratasys reports a dissolution rate for ST-130 of 12 g/minute using WaterWorks detergent, and 6 g/minute using EcoWorks. The washout rate using the TSP solution was much slower than the values reported by Stratasys, indicating that an improved approach would be to use either WaterWorks detergent or EcoWorks detergent. The AQ-120 and AQ-180 required less preparation of the solution used for dissolution because they both used tap water. During dissolution, these materials also developed a gel residue on the surface, which unlike the ST-130 cube, was not removed systematically during the test. The AQ-120 and AQ-180 cubes are seen in Table 19 at various stages during their dissolution.

Holes were drilled on top and bottom of a second AQ-180 cube. This allowed the water to enter the infill and reduced the washout time significantly. The AQ-180 cube with drilled holes had completely softened, including the infill, after 3 hours, while the cube without drilled holes had intact infill after 7.2 hours when it was physically broken apart. The introduction of the drilled holes is consistent with the original plan to use the Gyroid infill to allow the dissolution fluid to contact a greater surface area, which would be very effective.

Table 19 The dissolution process is shown below for the AQ-120, AQ-180, and drilled AQ-180 samples.

Dissolution Stage	AQ-120	AQ-180	AQ-180 with hole
Pre-Test			
During Dissolution			
After Dissolution			

3.5 TECHNO-ECONOMIC MODELING

Subtasks 4.9.3 and 4.9.6 - The techno-economic model outcomes comparing conventional tooling approaches and materials to potential advanced additive tooling, including washout features

The TEM for this project was developed to allow for direct comparisons between the conventionally manufactured washout tools and the 3D-printed ones being developed by CSU. It assumes that the manufacturing of the tool does not affect the composite component manufacturing process. Because of this, the TEM focuses only on the tool manufacturing and the final washout procedure after the composite processing and curing is complete. The manufacturing processes and materials defined in the TEM are specifically to produce tools that can be used to produce carbon fiber reinforced epoxy components in an autoclave with curing temperatures of up to 250°F and external pressures of up to 50 psi. This section details the construction of the TEM and all the underlying equations and assumptions. It also provides the values of specific parameters used to conduct the cost and process analysis, based on the research performed by Ability Composites and CSU.

3.5.1 Model Workflow and Process Steps

Advanced composite manufacturers, like Ability Composites, who regularly manufacture components that require sacrificial tools, often use a combination of in-house manufacturing and outsourcing for such tools. This TEM concentrates only on the in-house manufacturing of washout tools. Also, the composite manufacturing facilities and their capital equipment are not solely dedicated to manufacturing washout tools. Because of this, a full plant-scale techno-economic assessment was not required for the TEM. Only the most pertinent details needed to be accounted for. Figure 59 shows the general workflow and individual modules of the TEM that were developed. Parameters for the manufacturing were defined in terms of materials (both direct and consumable), required capital equipment, and manufacturing specifications (geometry, tooling, and general cost and time parameters) modules. All of the parameters from these modules were then directed into four main cost categories or modules:

Material costs
Labor costs and process times
Energy costs
Capital equipment costs.

We then used each cost module to calculate and analyze the final results in terms of cost and process time breakdowns and comparisons.
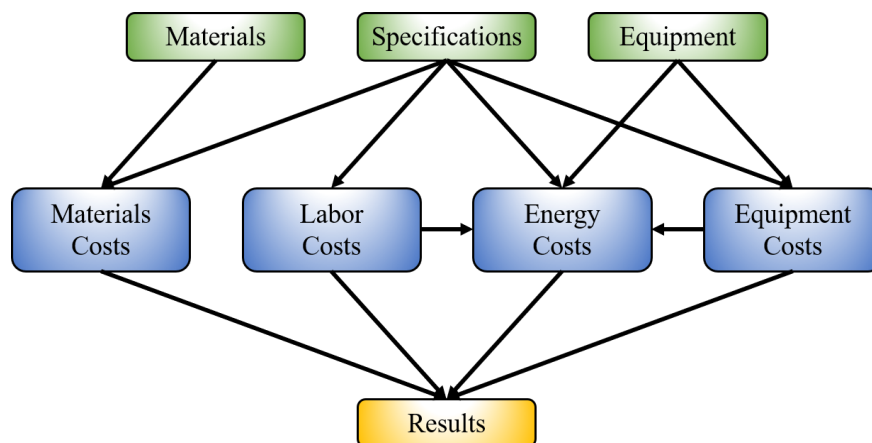
Figure 59. General workflow for the TEM and how each module is linked

Properly defining the parameters and equations needed for each model first required an in-depth understanding of the manufacturing processes. Figure 60 shows the main processing steps for both the conventional tool manufacturing and the 3D-printed tool manufacturing being developed by CSU. The conventional manufacturing of washout tools uses several common techniques, such as ceramic sand casting and subtractive machining of solid ceramic sand blocks. Casting is most often used when many units need to be produced, and subtractive machining is more typically used for prototyping and limited production runs. Because the purpose of the TEM was to compare conventional washout tools with 3D printing, subtractive machining was deemed the most appropriate for comparison.

Conventionally Manufactured Tools

| Ceramic block preparation | → | Ceramic block bonding | → | CNC setup & pre-processing | → | CNC machining |

| Final finishing | → | Sealing | → | Quality inspection | ····· | Tool washout |

Additively Manufactured Tools

| Print pre-processing | → | Printing | → | Cleaning support material | → | Secondary bonding and final finishing |

| Sealing | → | Quality inspection | ··········· | Tool washout |
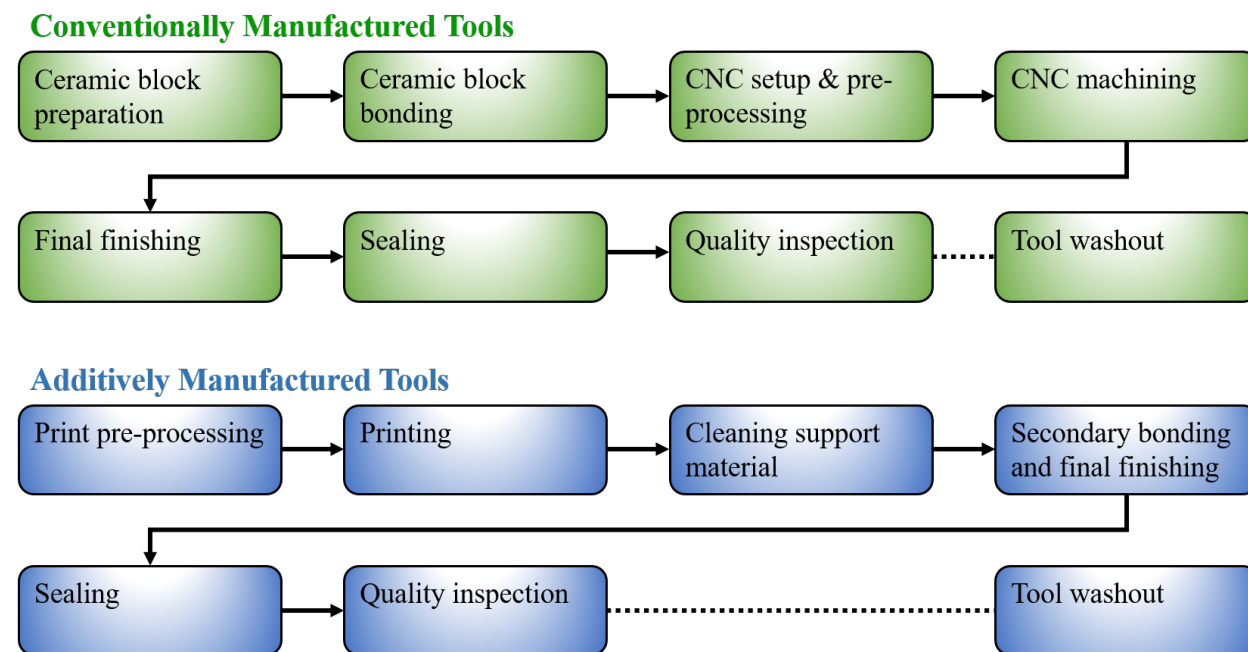
Figure 60. Main process steps for conventional washout tool manufacturing and the newly developed additive manufacturing approach

To manufacture ceramic washout tools through subtractive machining, arbitrarily sized cast ceramic sand blocks are typically bonded together to produce a preform larger than the desired tool geometry. The original blocks typically require some preparation, such as milling flat, before bonding. The bonded preform is then loaded into a computer numerical control (CNC) mill for machining to the net shape of the tool. Sometimes secondary finishing operations are required both on the mill and by hand to prepare the tool surface for composite processing. The tool then requires sealing to promote vacuum integrity and prevent epoxy from leaching into the porous ceramic sand. This is typically done by hand with adhesive-backed polytetrafluoroethylene (PTFE) tape. Finally, the tool undergoes a quality inspection to ensure dimensional conformity. After the carbon fiber composite is manufactured and cured on the tool, the tool is washed out with water pressure in a stock tank. The broken-down ceramic medium is skimmed off the surface of the water and disposed of with other general waste.

Naturally, additive manufacturing of washout tools requires a significantly different approach, but with some similarities. 3D printers typically need some preprocessing time to slice computer-aided design (CAD) files and convert them to Geometric Code (G-code) before printing. Depending on the material being printed, 3D printers generally need some time to heat up the nozzles, chamber, and print bed before printing can begin. Also, 3D printers are limited to a specific build volume. If the intended components are larger than the bounding box, they must be printed in multiple pieces. Depending on the complexity of the geometry being printed, the tool may require that a sacrificial support structure be printed to support

overhangs and other steep changes in angle. This is then typically broken away and dissolved in a mildly basic detergent solution afterwards. After cleaning, prints may require some degree of surface finishing to smooth filament lines and meet dimensional requirements. In some cases, this may be as simple as hand sanding, but larger components may require a final machining step. Like ceramic sand tools, 3D prints often need sealing to prevent leaching of epoxy. This can also be done with adhesive-backed PTFE tapes, but other novel techniques, such as ironing, allow for surface smoothing and sealing during the printing process itself [16]. Finally, additively manufactured tools are quality inspected in the same manner as conventional tools. The washout process is a little different and generally dependent on the polymer filament used to print the tool. Some filaments require only water to dissolve; others, such as ST-130 from Stratasys, require a basic detergent solution at an elevated temperature to dissolve. This step is a little more time-consuming than for conventional tools, but dedicated cleaning baths are available for an automated process.

3.5.2   Specifications

The specifications module was intended to be the primary module for user inputs, although other modules still required a small degree of user input. It is where the user can provide pertinent details on the tool geometry to be manufactured, rates of varying manufacturing processes for the two manufacturing techniques, and general labor rates and other costs.

3.5.2.1 Geometries

The TEM developed in this study was constructed in such a way that two different geometries can be analyzed simultaneously. This was done to allow for scaling studies, as demonstrated in this research, and other comparisons that might be required in the future. In this case, a bent rectangular duct was used as a representative geometry for the washout tool manufacturing process (see Figure 61). The cross section was 4 in. by 6 in., and the overall length was 12 in. (Geometry #1). This was determined and defined by CSU and Ability Composites. A scaling study was deemed to be of most interest to assess the advantages and disadvantages of the two tool manufacturing processes. Therefore, a second geometry was defined to be double in width, height, and length. Geometry #2 had a cross section of 8 in. by 12 in. and a length of 24 in.
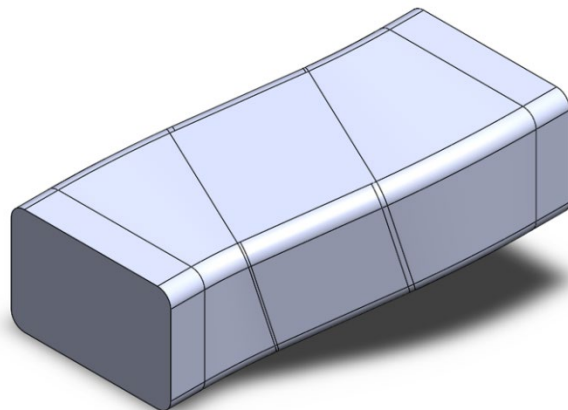
Figure 61. Rendering of the bent rectangular duct used as a representative tool geometry for this study

Table 20 outlines the geometry parameters required as user inputs in the specifications module, and their respective values for the two chosen geometries. The TEM requires the bounding box dimensions (length, width, and height) of the tool geometries and the geometries' volumes and external surface areas. All of these parameters are intended to be taken from existing CAD models. The bounding box dimensions are primarily used to determine the number of ceramic sand blocks required to bond together to make the ceramic preform for machining of a conventional tool. The geometry volumes and surface areas are used

for a number of calculations, such as the quantity of material to be removed during machining or the required amount of print material.

Table 20. Geometry Input Parameters Used in the Specifications Module

Geometry Parameters		
	Geometry #1	**Geometry #2**
Description	Small bent duct	Large bent duct
Bounding Box Length (in)	9.00	18.00
Bounding Box Width (in)	6.00	12.00
Bounding Box Height (in)	12.00	24.00
Final Geometry Volume (in^3)	304.80	2,438.10
Final Geometry Surface Area (in^2)	232.50	992.00

3.5.2.2 Conventional Tooling Parameters

Table 21 shows the conventional tooling parameters and their values for Geometry #1 and Geometry #2, respectively. These parameters are intended to be direct inputs specific to the conventional subtractive manufacturing approach for washout tools. First are the dimensions of the ceramic blocks that are bonded together to create the larger preform, as well as an oversize percentage. This parameter ensured that when the blocks are bonded together, the preform is larger than the bounding box of the final tool. From these parameters and the geometry parameters in Table 20, the number of ceramic blocks required, the number of bond lines, bond line surface area, and the amount of material to be removed during machining were calculated.

Table 21. Conventional Tooling Input Parameters for the Two Geometries with Calculated Parameters in Red Text

Conventional Tooling Parameters		
	Geometry #1	**Geometry #2**
Ceramic block width (in)	10.00	20.00
Ceramic block length (in)	10.00	14.00
Ceramic block thickness (in)	3.00	3.00
Oversize percentage (%)	10	10
Ceramic blocks required	5	9
Bond lines required	4	8
Bond line surface area (in^2)	400.00	2,240.00
Ceramic material to be removed (in^3)	1,195.00	5,122.00
Block preparation rate (min/block)	30	30
Block bonding rate (min/bond line)	15	15
Adhesive waste percentage (%)	20	20
CNC setup time (min)	30	30
Bulk CNC material removal rate (in^3/min)	10	25
CNC surface finishing rate (in^2/min)	10	10
Sanding finishing rate (in^2/min)	10	10

Sealing rate (in²/min)	10	10
Sealing overlap percentage (%)	25	25
Quality control time proportion (%)	10	10
Tool washout rate (in³/min)	10	10

The rest of the input parameters all relate to the manufacturing process steps. Block preparation time was an estimated time per block to face the ceramic blocks and prepare them for bonding. The bond rate was also estimated. Adhesive waste was also included because the cost of the spray adhesive used could have an influence on the overall material costs of the tool. Common machining parameters were included so that good estimates can be made for machining time, the main ones being setup time for the machine, bulk material removal rate, and the rate of surface finishing. Sanding finishing rate, whether by hand or with a pneumatic sander, were also included to calculate tool finishing times. Sealing rate and sealing overlap percentage related to the final sealing process with PTFE tape. When the tape is laid down, there will always be an overlap, so this parameter allowed for a more accurate material cost calculation. Quality control time was a more complex parameter. Often aerospace companies relate quality control requirements as a proportion of their overall workforce. In this case, quality control was estimated to be 10 % of the overall labor requirements. Therefore, this was the metric used to calculate the quality control process time and cost. Finally, tool washout rate was assumed to be constant to calculate the costs for the final process step.

3.5.2.3 3D Printing Tooling Parameters

Table 22 shows the 3D printing parameters and their associated values for the two geometries in the specifications module. First, there was an option to define the number of segments the tool will be printed in. As mentioned previously, the size of the tool may exceed the build volume of the 3D printer being used. Next was the print in-fill percentage (v_{fill}). Often 3D prints are not printed as solid pieces. It is common to reduce the fill within thick portions of the geometry to decrease printing times and material usage. In this case, it was defined as a percentage. This was defined by the research conducted at CSU to determine optimum in-fills for elevated temperature autoclave processing. Options were also provided for support material and oversize as a percentage of overall part volume (v_{excess} and $v_{support}$). Printed supports were not required for these specific geometries. Excess percentage was an option available in cases where prints must be oversized and then machined down to final specification and was not required in this case. These parameters, along with the initial geometry volume (V_T), were used to calculate the 3D print volumes (V_{3DP}) and required support volumes ($V_{support}$) using Eq. 1 and Eq. 2. These parameters worked as intended in this case, but it is common for engineers to specify wall thicknesses for prints. For large print geometries, such as Geometry #2, it may also be more efficient to print the tool as a shell rather than a solid volume. In this case, the in-fill percentage for Geometry #2 was reduced significantly to account for this. This was done by shelling out the geometry using CAD software to a shell thickness of 0.75 in (see Figure 62). This shell thickness was arbitrary and should be properly determined through structural analysis for actual composite tools to ensure dimensional stability. From this shell, the in-fill percentage was applied to calculate a final print volume. The in-fill percentage in the TEM was changed, so the print volume in the model matched the shell estimate. In the future, it would be logical to account for these design parameters in further iterations of the TEM.

$$V_{3DP} = V_T v_{fill}(1 + v_{excess}) \qquad (1)$$

$$V_{support} = V_{3DP} v_{support} \qquad (2)$$

Table 22. 3D-Printed Tooling Input Parameters for the Two Geometries with Calculated Parameters in Red Text

3D-Printed Tooling Parameters		
	Geometry #1	**Geometry #2**
Number of segments	2	4
In-fill percentage (%)	40	12
Support material percentage (%)	0	0
Excess percentage (%)	0	0
3D print volume (in^3)	121.92	292.57
3D print support volume (in^3)	0.00	0.00
Deposition rate (in^3/hour)	8	8
Print preprocessing time (min)	30	30
Printer warmup time (min)	30	30
Segment bonding rate (min/segment)	15	15
Surface finishing rate (in^2/min)	5	5
Sealing rate (in^2/min)	10,000	10,000
Sealing overlap percentage (%)	0	0
Quality control time proportion (%)	10	10
Tool washout rate (in^3/min)	0.5	0.5
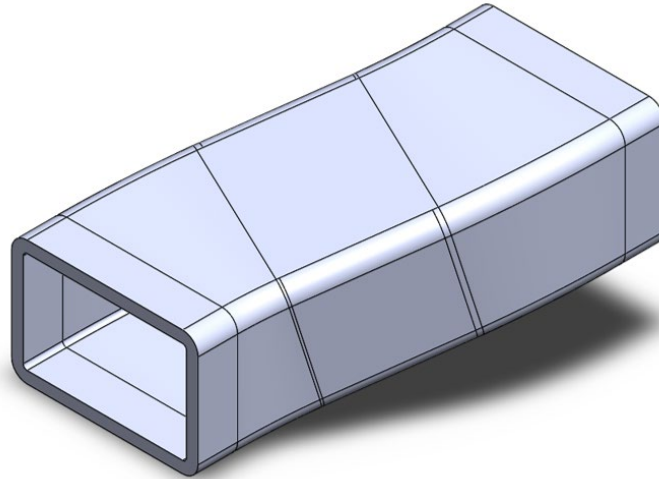
Figure 62. Rendering of Geometry #2 with a 0.75 in. shell thickness to optimize 3D print material usage and 3D printing times

The rest of the parameters in Table 22 generally relate to various processing times in the manufacturing process. Deposition rate is related to how fast a 3D printer can extrude polymer filament to build a geometry and varies between different models of printer and diameters of printer nozzles. Print preprocessing times and printer warmup time are the times taken for a printer to slice a CAD file and warm up the nozzles, print bed, and print chamber before starting the printing process. Like the conventional tooling parameters, 3D-printed tool parameters include segment bonding, surface finishing, and sealing rates. In this case, CSU developed a procedure whereby they could finish and seal their 3D prints using an ironing process with the

nozzle of the 3D printer. Therefore, only segment bonding rate and surface finishing rate were used. Sealing rate was set at a very high number to make the process step negligible during the process time and labor cost calculations because the finishing process with an iron is assumed to provide an adequate seal. Also, sealing overlap percentage is set to zero because no materials were required for sealing the print surface. Quality control time is defined in the same way as for the conventional tooling parameters. Finally, tool washout rate was set at 0.5 in^3/min. This is a lot lower than for conventional tools. As mentioned in Section 5.5.1, polymer 3D prints typically need a heated detergent bath to dissolve, which is a much slower dissolution process.

3.5.2.4 General Costs and Rates

Table 23 shows the final general costs and rates associated with the TEM. These relate to fixed labor costs, energy costs, and project-specific requirements. Energy costs were set at a fixed rate of $0.10 per kWh (kilowatt-hour), although in a manufacturing environment it is expected that energy costs may vary. This was less of a concern because energy requirements for tool manufacturing are generally considered negligible when compared to autoclave processing. Both labor and energy costs were best estimates for the year 2020. As was mentioned in Section 5.5.1, aerospace composite manufacturing facilities and their capital equipment are not fully dedicated to manufacturing molds. Also, a wide variety of mold geometries may be manufactured at any given time. Therefore, an appropriate method for calculating capital equipment costs needed to be outlined. This was aided by defining the molds based on specific projects. To do this, the user can define the number of tools to be manufactured for a project and the project's runtime. More details on how to use these parameters to calculate capital equipment costs are given in Section 5.5.5.

Table 23. General Costs and Rate Input Parameters for the Two Geometries

General Costs and Rates		
	Geometry #1	**Geometry #2**
Technician labor cost ($/hour)	75	75
Energy cost ($/kWh)	0.10	0.10
Number of tools for project	30	30
Project run time (months)	3	3

3.5.3   Materials and Equipment

The materials and equipment modules served as master lists of all the pertinent details for various direct and consumable materials used and capital equipment needed for the tool manufacturing processes. The TEM pulls information from these lists to calculate material, equipment, and energy costs for each geometry and manufacturing process. They are intended to be revised when required for new materials and variations in manufacturing processes that may require different equipment.

Table 24 shows the list of direct materials used for this study specifically, as well as important details and their uses. The list includes all of the 3D print materials that CSU researchers were investigating for their manufacturing trials. They found that the ST-130 material from Stratasys was the most appropriate for the given autoclave temperatures and pressures for composite processing. The list also includes a 3D print support material and tool washout solution specifically for the ST-130 print material. The last three materials are more related to the conventional tooling process, with ceramic core material and an estimate of its retail cost per cubic inch, as well as a typical contact adhesive and PTFE tape for sealing. The price for the adhesive is a best estimate for bond surface area coverage. All material costs were best estimates for the year 2020.

Table 24. Direct Materials List Used in the Materials Module of the TEM

Material	Supplier	Cost	Solvent	Density	Purpose
BVOH	Prusa	$160/kilogram (kg)	Water	1.20 g/cm^2	3D print
AquaSys 120	Infinite	$180/kg	Water (80 °C)	1.35 g/cm^2	3D print
Chamberlay 130	Filaments.ca	$260/kg	Water	1.19 g/cm^2	3D print
ST-130	Stratasys	$175/kg	Base (70 °C)	1.18 g/cm^2	3D print
PVA HT	3D Prima	$200/kg	Water	1.20 g/cm^2	3D print
Ionic	MatterHackers	$200/kg	Water	1.20 g/cm^2	3D print
GSM	Stratasys	$175/kg	Base (70 °C)	1.18 g/cm^2	3D print support
WaterWorks	Stratasys	$12.50/kg	-	-	3D print washout
Ceramic core	Soltec	$0.35/in^3	Water	-	Conventional tool
77 Rubber Adhesive	3M	$0.01/in^2	-	-	Ceramic block bonding
PTFE tape	3M	$0.25/in^2	-	-	Sealing

Table 25 shows the master list of consumable materials included in the materials module of the TEM. Most are related to personal protective equipment (PPE) and are fairly insignificant costs. Others, such as end mills, can be a relevant contribution to the overall tool costs. Prices of end mills vary, and a variety of different kinds may be used in the production of one tool. In this case, an average end mill cost was used, which could be more specific in the future.

Table 25. Consumable Materials List Used in the Materials Module of the TEM

Material	Unit	Cost per Unit
PPE: Tyvek suit	each	$5.00
PPE: goggles	each	$1.00
PPE: gloves	pair	$0.10
PPE: footwear	pair	$0.50
PPE: tape	roll	$0.25
PPE: ear protection	pair	$0.15
PPE: powered air purifying respirator (PAPR) filters	each	$20.00
End mills	each	$50.00
Sanding disks	each	$0.10
Razor blades	each	$0.15

The equipment module was split into two different lists, one for the conventional tool manufacturing process (Table 26) and one for the 3D-printed tool manufacturing process (Table 27). These were also intended to be master lists that the user can add to at any time. The tables include all the most important capital equipment required for the processes. Particularly important equipment related to the machining and printing processes are the CNC mill, 3D printer, dust collection systems, air compressors, and quality inspection equipment, such as the 3D laser scanner and drag profilometer for inspecting surface quality of

the tools. The user can also input useful life of the equipment, which is used to determine overall capital equipment costs. Service and maintenance costs were not included in the unit costs in this case, and all costs were best estimates for the year 2020 with no adjustment for inflation over their useful life. Power required was also included in this module, which is ultimately used to determine energy costs for the manufacturing process steps. It currently assumes that the required power for a piece of capital equipment is constant, although this is generally not the case.

Table 26. Capital Equipment Master List Used for Conventionally Manufactured Washout Tools

Equipment	Unit Cost	Useful Life (years)	Power Required (kilowatts [kW])
CNC mill	$300,000	20	10
Vacuum system	$7,000	15	15
Dust collection system	$50,000	20	10
Air compressor	$20,000	20	5
CNC software	$10,000	1	0
3D laser scanner	$100,000	10	0.5
Forklift	$25,000	20	0
Height gage	$5,000	25	0
Stock tank	$400	10	0

Table 27. Capital Equipment Master List Used for 3D-Printed Washout Tools

Equipment	Unit Cost	Useful Life (years)	Power Required (kW)
3D printer	$300,000	15	10
3D printing software	$1,000	1	0
Cleaning bath	$10,000	15	10
Air compressor	$20,000	20	5
Dust collection system	$50,000	20	10
3D laser scanner	$100,000	10	0.5
Forklift	$25,000	20	0
Pneumatic palm sander	$200	5	0
Drag profilometer	$5,000	10	0.25

3.5.4 Labor Costs

As described previously, defining the main process steps of the conventional and 3D-printed tool manufacturing processes formed the foundation of the TEM. The labor costs module specifically defines the process steps outlined in Figure 60. General costs and rates used in the modeling are given in Table 23. For simplicity, a technician labor cost of $75/hr was used for all processes. The module uses the related parameters from the specifications module to calculate labor costs, labor times, and process times for each process step for each geometry and manufacturing process, respectively. Generally, labor times and process times were considered equal, but some instances, such as 3D printing and machining, were not because these operations are often unattended.

3.5.4.1 Conventional Tooling

Table 28 and Table 29 show the calculated process times, labor times, and labor costs for the conventional manufacturing process for Geometry #1 and Geometry #2, respectively. All labor costs were calculated using Eq. 3, where n_T is the number of technicians required, c_T is the technician labor rate from the specifications module, and t_L is the labor time.

$$Labor\ cost = n_T c_T t_L \tag{3}$$

For the first three process steps (ceramic block preparation, ceramic block bonding, and CNC setup and preprocessing), labor times were considered equal to process times. These times were calculated using their respective rates per block (r_{bp}) or per bond line (r_{bb}) from the specifications module and then multiplied by the number of ceramic blocks (n_{block}) or bond lines (n_{bond}). This is shown in Eq. 4 and Eq. 5, where $P_{T,bp}$ is the block preparation process time and $P_{T,bb}$ is the block bonding process time. CNC setup and preprocessing ($P_{T,pp}$) is a fixed parameter in the specifications module. The CNC machining process time ($P_{T,CNC}$) is calculated using the material to be removed (n_{mr}) parameter calculated in the specifications module divided by the CNC material removal rate parameter (r_{mr}) shown in Eq. 6. In this case, the labor time was chosen as a set value of 60 minutes for both geometries, which is an estimate for unattended operation with occasional check-ins and some clean-up time afterward. Final finishing process time ($P_{T,ff}$) is calculated as a function of the geometry surface area (S_A), CNC finishing rate ($r_{f,CNC}$), and sanding finishing rate ($r_{f,sand}$) shown in Eq. 7. Final finishing labor time is considered to be equal to the process time with an additional 30-minute clean-up time. Sealing process time ($P_{T,seal}$) is the geometry surface area divided by the tool sealing rate (r_{seal}) parameter provided in the specifications module (see Eq. 8). Labor time is equal to process time. As previously described in Section 5.5.2.2, quality control times ($P_{T,qc}$) in the aerospace industry are commonly described as a proportion of total labor requirements. For the TEM, this is defined as the sum of the process times multiplied by the quality control proportion (v_{qc}) entered in the specifications module (see Eq. 9). Labor time is equal to process time in this case. Finally, the tool washout process step was kept separate from the tool manufacturing process steps for analysis purposes. Tool washout process time ($P_{T,wash}$) is calculated as the geometry volume (V_T) divided by the tool washout rate (r_{wash}) defined in the specifications module (see Eq. 10).

$$P_{T,bp} = r_{bp} n_{block} \tag{4}$$

$$P_{T,bb} = r_{bb} n_{bond} \tag{5}$$

$$P_{T,CNC} = {n_{mr}}/{r_{mr}} \tag{6}$$

$$P_{T,ff} = {S_A}/{(r_{f,CNC} + r_{f,sand})} \tag{7}$$

$$P_{T,seal} = {S_A}/{r_{seal}} \tag{8}$$

$$P_{T,qc} = \left(P_{T,bp} + P_{T,bb} + P_{T,pp} + P_{T,CNC} + P_{T,ff} + P_{T,seal}\right)v_{qc} \tag{9}$$

$$P_{T,wash} = {V_T}/{r_{wash}} \tag{10}$$

Table 28. Calculated Process Time, Labor Time, and Labor Cost for the Conventional Manufacturing of Geometry #1

Process Step	Number of Technicians	Process Time (min)	Labor Time (min)	Labor Cost
Ceramic block preparation	1	150	150	$188
Ceramic block bonding	1	60	60	$75
CNC setup and preprocessing	1	30	30	$38
CNC machining	1	120	60	$75
Final finishing	1	47	77	$96
Sealing	1	23	23	$29
Quality inspection	1	43	43	$54
Tool washout	1	30	30	$38

Table 29. Calculated Process Time, Labor Time, and Labor Cost for the Conventional Manufacturing of Geometry #2

Process Step	Number of Technicians	Process Time (min)	Labor Time (min)	Labor Cost
Ceramic block preparation	1	270	270	$338
Ceramic block bonding	1	120	120	$150
CNC setup and preprocessing	1	30	30	$38
CNC machining	1	341	60	$75
Final finishing	1	198	198	$286
Sealing	1	99	99	$124
Quality inspection	1	106	106	$132
Tool washout	1	244	244	$305

3.5.4.2 Additive Tooling

Table 30 and Table 31 show the calculated process times, labor times, and labor costs for the newly developed, 3D-printed tool manufacturing process for Geometry #1 and Geometry #2, respectively. Like the conventionally manufactured tool process times and labor costs, they were broken into the process steps defined in Figure 60 and calculated from the user-defined parameters in the specifications module. Process times and labor times were calculated similarly to the conventional tooling times and costs. Labor costs were calculated using Eq. 3. The process time for print preprocessing ($P_{T,pre-print}$) was defined as the number of segments (n_s) multiplied by the preprint processing time ($t_{pre-print}$) outlined in the specifications module (see Eq. 11). In this case, labor time was equal to process time. The tool print process time ($P_{T,print}$) was calculated using Eq. 12. This equation accounts for the number of segments to be printed and includes the time for the printer to warm up for each segment to be printed (t_{warm}). The general print time was calculated based on the overall print volume (V_{print}) and the printer deposition rate (r_{dep}). Printing is an unattended operation, so labor time was defined as 30 minutes to allow for regular check-ins to ensure that the mold is printing correctly. As mentioned previously, supports did not need to be printed for the example geometries and therefore did not need to be cleaned, although process and labor times ($P_{T,clean}$) were still included in the process steps in case more complex geometries are used in the future. In that case,

the cleaning of support material would be similar to that of tool washout. The process time for secondary bonding and finishing ($P_{T,finish}$) was calculated using the number of printed segments, the segment bonding rate (r_{bond}), geometry surface area, and the surface finishing rate (r_f) given in the specifications module (see Eq. 13). Labor time for this process step was considered equal to the process time. As mentioned in Section 5.5.2.3, CSU utilized a technique to finish and seal the tool surface simultaneously using their 3D printer. Therefore, sealing time and costs are zero. If an alternative method, such as PTFE tape, were used, then the process and labor times would be calculated using Eq. 8. Quality control process and labor times were calculated in the same way as for conventional tooling (see Eq. 14). Finally, the washout process time was calculated in the same way as for conventional tools (see Eq. 15), but labor time was not. Washout for 3D-printed tools is a longer but more hands-off process. In this case, labor time was set to 20 minutes for periodic check-ins.

$$P_{T,pre-print} = n_s t_{pre-print} \tag{11}$$

$$P_{T,print} = n_s t_{warm} + {}^{V_{print}}\!/_{r_{dep}} \tag{12}$$

$$P_{T,finish} = (n_s - 1)r_{bond} + {}^{S_A}\!/_{r_f} \tag{13}$$

$$P_{T,qc} = \left(P_{T,pre-print} + P_{T,print} + P_{T,clean} + P_{T,finish} + P_{T,seal}\right)v_{qc} \tag{14}$$

$$P_{T,wash} = {}^{V_{print}}\!/_{r_{wash}} \tag{15}$$

Table 30. Calculated Process Time, Labor Time, and Labor Cost for the Additive Manufacturing of Geometry #1

Process Step	Number of Technicians	Process Time (min)	Labor Time (min)	Labor Cost
Print preprocessing	1	60	60	$75
Printing	1	974	30	$38
Cleaning support material	1	0	0	$0
Secondary bonding and finishing	1	62	62	$77
Sealing	1	0	0	$0
Quality inspection	1	110	110	$137
Tool washout	1	244	20	$25

Table 31. Calculated Process Time, Labor Time, and Labor Cost for the Additive Manufacturing of Geometry #2

Process Step	Number of Technicians	Process Time (min)	Labor Time (min)	Labor Cost
Print preprocessing	1	60	60	$75
Printing	1	2,314	30	$38
Cleaning support material	1	0	0	$0
Secondary bonding and finishing	1	243	243	$304
Sealing	1	0	0	$0
Quality inspection	1	268	268	$335
Tool washout	1	585	20	$25

3.5.5 Material Costs

The material cost module was used to calculate both the direct and consumable material costs for tools manufactured from both conventional ceramic sand blocks and 3D-printed tools, for both chosen example geometries. Parameters from the specifications module and from the master list in the materials module, as well as some user inputs, were used to calculate the costs.

3.5.5.1 Conventional Tooling

Table 32 shows the chosen direct materials and their calculated cost for the conventional manufacturing of both Geometry #1 and Geometry #2. The amount of ceramic core required was calculated based on the number of ceramic blocks required and their dimensions from the specifications module (Table 21). The amount of spray adhesive required ($Q_{adhesive}$) was based on the bond line surface area (S_{bl}) and adhesive waste percentage (v_{aw}) defined in the specifications module (see Eq. 16). The total amount of PTFE tape required (Q_{seal}) to seal the mold was calculated in a similar way with the tool surface area (S_A) and the sealing overlap percentage ($v_{overlap}$), also defined in the specifications module (see Eq. 17).

$$Q_{adhesive} = (1 + v_{aw})S_{bl} \tag{16}$$

$$Q_{seal} = (1 + v_{overlap})S_A \tag{17}$$

Table 32. Direct Materials, Quantities, and Their Costs for the Conventional Manufacturing of Geometry #1 and Geometry #2

Material	Geometry #1		Geometry #2	
	Quantity	Cost	Quantity	Cost
Ceramic core	1500 in^3	$525	7560 in^3	$2646
77 rubber adhesive	480 in^2	$4.80	2688 in^2	$26.90
PTFE tape	291 in^2	$72.70	1240 in^2	$310

Table 33 shows the chosen consumable materials, their quantities, and calculated costs for the conventional manufacturing of both Geometry #1 and Geometry #2. Quantities were intended to be a user input based on best estimates and knowledge of the manufacturing process. Of course, these numbers could vary widely among technicians, especially the PPE usage.

Table 33. Consumable Materials, Quantities, and Costs for the Conventional Manufacturing of Geometry #1 and Geometry #2

Material	Geometry #1		Geometry #2	
	Quantity	Cost	Quantity	Cost
PPE: Tyvek suit	2	$10.00	2	$10.00
PPE: goggles	2	$2.00	2	$2.00
PPE: gloves	2	$0.20	2	$0.20
PPE: footwear	2	$1.00	2	$1.00
PPE: tape	4	$1.00	4	$1.00
PPE: ear protection	2	$0.30	2	$0.30
PPE: PAPR filters	1	$20.00	1	$20.00
End mills	2	$100.00	4	$200.00
Razor blades	5	$0.75	10	$1.50

3.5.5.2 Additive Tooling

Table 34 shows the direct material requirements for the 3D printing of Geometry #1 and Geometry #2. The direct material requirements for additively manufactured tools were brief. Only the print material and adhesive for bonding of segments were required to be included. In the TEM, the user can choose the print material from the material master list in the form of a drop-down menu. In this case, ST-130 was chosen because CSU determined it to be the most appropriate material for in-autoclave composite processing. The quantity required (Q_{print}) was calculated based on the print volume (V_{print}) and the density of the print material (ρ_{print}), which were defined in the specifications and materials modules (see Eq. 18). The quantity of adhesive required was calculated with Eq.19 and the number of printed segments (n_s), adhesive waste percentage (v_{aw}), and the tool bounding box width (w) and height (h). The equation is not perfect because the bond line surface area may vary depending on how the user chooses to segment the tool, but the adhesive costs were insignificant in comparison to the print material costs, so no further definition was required in this instance. Although technically a consumable material, the print washout solution was included in the direct material cost in Table 34. It was assumed that 1 kg of cleaning solution was enough to dissolve approximately 150 in^3 of print material.

$$Q_{print} = V_{print}\rho_{print} \tag{18}$$

$$Q_{adhesive} = (1 + v_{aw})(n_s - 1)lw \tag{19}$$

Table 34. Direct Materials, Quantities, and Their Costs for the Additive Manufacturing of Geometry #1 and Geometry #2

Material	Geometry #1		Geometry #2	
	Quantity	Cost	Quantity	Cost
ST-130	2.36 kg	$412.57	5.66 kg	$990.04
77 rubber adhesive	86.4 in^2	$0.86	1037 in^2	$10.37
WaterWorks solution	1.00 kg	$12.50	2.00 kg	$25.00

Table 35 shows the chosen consumable materials, their quantities, and calculated costs for additive manufacturing of both Geometry #1 and Geometry #2. Like the direct material requirements, the consumable material requirement for additively manufactured tools was also minimal. Very little was required in terms of PPE or disposable tools, because it is a contained process where most process steps are conducted within the printer itself.

Table 35. Consumable Materials, Quantities, and Their Costs for the Additive Manufacturing of Geometry #1 and Geometry #2

Material	Geometry #1		Geometry #2	
	Quantity	Cost	Quantity	Cost
PPE: Tyvek suit	1	$5.00	1	$5.00
PPE: goggles	1	$1.00	1	$1.00
PPE: gloves	1	$0.10	1	$0.10
PPE: footwear	1	$0.50	1	$0.50
PPE: tape	1	$0.25	1	$0.25
PPE: ear protection	1	$0.15	1	$0.15
PPE: PAPR filters	1	$20.00	1	$20.00

3.5.6 Equipment Costs

The goal of the equipment cost module was to determine capital equipment costs per tool. Properly accounting for capital equipment costs in the TEM required some important considerations. As mentioned previously, composite manufacturing facilities, like Ability Composites, and their capital equipment are not dedicated to the tool manufacturing process. Critical pieces of capital equipment, such as CNC mills, air compressors, and dust collection systems, are often utilized for other operations. Proper accommodations needed to be made to account for these variations. To do this, information from the general costs and rates section of the specifications module (Table 23), the equipment module, and a significant amount of user input were required. To estimate capital equipment costs ($C_{eq,i}$), the user must define the equipment used from the master list for each individual process step, as well as estimate its percentage use on that specific process step over the run time of the project ($v_{eq,i}$). From these user inputs, as well as the number of that piece of equipment required ($n_{eq,i}$), the total number of tools for the project (n_{tool}), project run time (t_{proj}), the individual equipment cost ($c_{eq,i}$), and its associated useful life ($t_{life,i}$), the cost per tool for a piece of capital equipment was calculated using Eq. 20, where the subscript i refers to an individual piece of equipment in a process step. From this, the total capital equipment costs for each process step ($C_{eq,T}$) can be calculated from Eq. 21, where n is the number of pieces of capital equipment required for a specific process step.

$$C_{eq,i} = \left(n_{eq,i} c_{eq,i} v_{eq,i} t_{proj}\right) \Big/ \left(t_{life,i} n_{tool}\right) \tag{20}$$

$$C_{eq,T} = \sum_{i=1}^{n} C_{eq,i} \tag{21}$$

3.5.6.1 Conventional Tooling

Table 36 shows the equipment used for each process step associated with the conventional manufacturing of Geometry #1, and Table 37 shows the number of said equipment required for each process step, as well as proportional usage and calculated capital equipment costs. Table 38 and Table 39 show the same for the conventional manufacturing of Geometry #2. The required equipment for Geometry #1 and Geometry #2 were almost the same, with the addition of a forklift for the CNC setup and preprocessing step for Geometry #2, because the tool is significantly larger and would be too heavy for one person to lift.

The proportional usage of each piece of equipment for each process step was based on best estimates over the defined 3-month run time of the project. In reality, these may vary significantly depending on the manufacturing facility and a varying workload from contractors. For Geometry #2 the proportional usage was increased slightly to reflect the larger geometry and increased process times calculated in the labor costs module. In the future, it may be possible to integrate this into the TEM itself.

Table 36. Capital Equipment Selection for the Conventional Manufacturing of Geometry #1

Process Step	Operation	Equipment 1	Equipment 2	Equipment 3	Equipment 4
1	Ceramic block preparation	CNC mill	Vacuum system	Dust collection system	Air compressor
2	Ceramic block bonding	-	-	-	-
3	CNC setup and preprocessing	CNC software	Height gage	Forklift	-
4	CNC machining	CNC mill	Vacuum system	Dust collection system	Air compressor
5	Final finishing	Vacuum system	Dust collection system	Air compressor	-
6	Sealing	-	-	-	-
7	Quality inspection	3D laser scanner	-	-	-
End	Tool washout	Stock tank	-	-	-

Table 37. Number of Each Piece of Individual Equipment Required, Proportional Use, and Calculated Costs for the Conventional Manufacturing of Geometry #1

Process Step	$n_{eq,1}$	$v_{eq,1}$	$C_{eq,1}$	$n_{eq,2}$	$v_{eq,2}$	$C_{eq,2}$	$n_{eq,3}$	$v_{eq,3}$	$C_{eq,3}$	$n_{eq,4}$	$v_{eq,4}$	$C_{eq,4}$	$C_{eq,T}$
1	1	25%	$31.25	1	17%	$0.66	1	8%	$1.74	1	8%	$0.69	$34.34
2	-	-	-	-	-	-	-	-	-	-	-	-	$0.00
3	1	50%	$41.67	1	20%	$0.33	-	-	-	-	-	-	$42.00
4	1	25%	$31.25	1	17%	$0.66	1	8%	$1.74	1	8%	$0.69	$34.34
5	1	17%	$0.65	1	8%	$1.74	1	8%	$0.69	-	-	-	$3.08
6	-	-	-	-	-	-	-	-	-	-	-	-	$0.00
7	1	50%	$41.67	-	-	-	-	-	-	-	-	-	$41.67
End	1	50%	$0.17	-	-	-	-	-	-	-	-	-	$0.17

Table 38. Capital Equipment Selection for the Conventional Manufacturing of Geometry #2

Process Step	Operation	Equipment 1	Equipment 2	Equipment 3	Equipment 4
1	Ceramic block preparation	CNC mill	Vacuum system	Dust collection system	Air compressor
2	Ceramic block bonding	-	-	-	-
3	CNC setup and preprocessing	CNC software	Height gage	Forklift	-
4	CNC machining	CNC mill	Vacuum system	Dust collection system	Air compressor
5	Final finishing	Vacuum system	Dust collection system	Air compressor	-
6	Sealing	-	-	-	-
7	Quality inspection	3D laser scanner	-	-	-
End	Tool washout	Stock tank	-	-	-

Table 39. Number of Each Piece of Individual Equipment Required, Proportional Use, and Calculated Costs for the Conventional Manufacturing of Geometry #2

Process Step	$n_{eq,1}$	$v_{eq,1}$	$C_{eq,1}$	$n_{eq,2}$	$v_{eq,2}$	$C_{eq,2}$	$n_{eq,3}$	$v_{eq,3}$	$C_{eq,3}$	$n_{eq,4}$	$v_{eq,4}$	$C_{eq,4}$	$C_{eq,T}$
1	1	35%	$43.75	1	20%	$0.78	1	15%	$3.13	1	15%	$1.25	$48.90
2	-	-	-	-	-	-	-	-	-	-	-	-	$0.00
3	1	50%	$41.67	1	30%	$0.50	-	15%	$1.56	-	-	-	$43.73
4	1	35%	$43.75	1	20%	$0.78	1	15%	$3.13	1	15%	$1.25	$48.90
5	1	20%	$0.78	1	15%	$3.13	1	15%	$1.25	-	-	-	$5.15
6	-	-	-	-	-	-	-	-	-	-	-	-	$0.00
7	1	60%	$50.00	-	-	-	-	-	-	-	-	-	$50.00
End	1	75%	$0.25	-	-	-	-	-	-	-	-	-	$0.25

3.5.6.2 Additive Tooling

Table 40 shows the equipment used for each process step associated with the additive manufacturing of Geometry #1, and Table 41 shows the number of said equipment required for each process step, as well as proportional usage and calculated capital equipment costs. Table 42 and Table 43 show the same for the additive manufacturing of Geometry #2. Exactly the same capital equipment was used for both Geometry #1 and Geometry #2. Unlike the conventional tool manufacturing process, a forklift was not added for moving the larger Geometry #2 because it was designed as a shell and would be light enough for one person to lift. The percentage equipment usages were increased for Geometry #2, because the calculated process times for each process step had increased significantly in the labor costs module. Again, these were just estimates and have not been directly linked to process times. Future iterations of the TEM may be able to include these features. The capital equipment requirements for 3D printing of washout tools were significantly less than that of conventional subtractive manufacturing, which highlights one of the main benefits of additive manufacturing.

Process Step	Operation	Equipment 1	Equipment 2	Equipment 3	Equipment 4
1	Print preprocessing	3D printing software	-	-	-
2	Printing	3D printer	-	-	-
3	Cleaning support material	-	-	-	-
4	Secondary bonding and finishing	Air compressor	Dust collection system	-	-
5	Sealing	-	-	-	-
6	Quality inspection	3D laser scanner	Drag profilometer	-	-
End	Tool washout	Cleaning bath	-	-	-

Table 41. Number of Each Piece of Individual Equipment Required, Proportional Use, and Calculated Costs for the 3D Printing of Geometry #1

Process Step	$n_{eq,1}$	$v_{eq,1}$	$C_{eq,1}$	$n_{eq,2}$	$v_{eq,2}$	$C_{eq,2}$	$n_{eq,3}$	$v_{eq,3}$	$C_{eq,3}$	$n_{eq,4}$	$v_{eq,4}$	$C_{eq,4}$	$C_{eq,T}$
1	1	60%	$5.00	-	-	-	-	-	-	-	-	-	$5.00
2	1	60%	$100.00	-	-	-	-	-	-	-	-	-	$100.00
3	-	-	-	-	-	-	-	-	-	-	-	-	$0.00
4	1	8%	$0.67	1	8%	$1.67	-	-	-	-	-	-	$2.33
5	-	-	-	-	-	-	-	-	-	-	-	-	$0.00
6	1	60%	$41.67	1	60%	$2.50	-	-	-	-	-	-	$44.17
End	1	60%	$3.33	-	-	-	-	-	-	-	-	-	$3.33

Table 42. Capital Equipment Selection for the 3D Printing of Geometry #2

Process Step	Operation	Equipment 1	Equipment 2	Equipment 3	Equipment 4
1	Print preprocessing	3D printing software	-	-	-
2	Printing	3D printer	-	-	-
3	Cleaning support material	-	-	-	-
4	Secondary bonding and finishing	Air compressor	Dust collection system	-	-
5	Sealing	-	-	-	-
6	Quality inspection	3D laser scanner	Drag profilometer	-	-
End	Tool washout	Cleaning bath	-	-	-

Table 43. Number of Each Piece of Individual Equipment Required, Proportional Use, and Calculated Costs for the 3D Printing of Geometry #2

Process Step	$n_{eq,1}$	$v_{eq,1}$	$C_{eq,1}$	$n_{eq,2}$	$v_{eq,2}$	$C_{eq,2}$	$n_{eq,3}$	$v_{eq,3}$	$C_{eq,3}$	$n_{eq,4}$	$v_{eq,4}$	$C_{eq,4}$	$C_{eq,T}$
1	1	75%	$6.25	-	-	-	-	-	-	-	-	-	$6.25
2	1	75%	$125.00	-	-	-	-	-	-	-	-	-	$125.00
3	-	-	-	-	-	-	-	-	-	-	-	-	$0.00
4	1	15%	$1.25	1	15%	$3.13	-	-	-	-	-	-	$4.38
5	-	-	-	-	-	-	-	-	-	-	-	-	$0.00
6	1	75%	$62.50	1	75%	$3.13	-	-	-	-	-	-	$65.63
End	1	75%	$4.17	-	-	-	-	-	-	-	-	-	$4.17

3.5.7 Energy Costs

The final processing portion of the TEM was the energy costs module, which used information from the capital equipment usage and process times to determine the energy requirements for the manufacturing processes. The energy costs module was fully automated and required no user input to calculate final energy requirements and costs. The total energy costs for each individual process step (C_{energy}) were calculated as a sum of the energy costs for each individual piece of capital equipment, which was a function of the process step process time (P_T), the power requirements of each piece of equipment (p_i) from the equipment module, and the cost of energy (r_{energy}) from the general costs and rates table in the specifications module (see Table 23). Their relationship is shown by Eq. 22, where i and n refer to the same nomenclature used in Eq. 20 and Eq. 21. This equation assumed that the energy cost was constant and that the energy usage by the capital equipment was a constant rate throughout each process step. Realistically, this is not the case but was the best method to use without overcomplicating the calculations.

$$C_{energy} = r_{energy} \sum_{i=1}^{n} P_T p_i \tag{22}$$

3.5.7.1 Conventional Tooling

Table 44 shows the energy usage and energy costs for each process step for the conventional manufacturing of Geometry #1 and Geometry #2. It shows that most energy costs were associated with the ceramic block preparation and CNC machining process steps. They both use the same equipment, which is relatively energy intensive. In comparison, the ceramic block bonding, CNC setup and preprocessing, sealing, and tool washout process steps require no energy at all, because their capital equipment requirements are negligible.

Table 44. Energy Usage and Energy Costs Associated with Each Process Step for the Conventional Manufacturing of Geometry #1 and Geometry #2

Process Step	Geometry #1			Geometry #2		
	Process Time (hours)	Energy Use (kWh)	Energy Cost	Process time (hours)	Energy Use (kWh)	Energy Cost
1	2.50	100.00	$10.00	4.50	180.00	$18.00
2	1.00	0.00	$0.00	2.00	0.00	$0.00
3	0.50	0.00	$0.00	0.50	0.00	$0.00
4	1.99	79.68	$7.97	5.69	227.64	$22.76
5	0.78	23.25	$2.33	3.31	99.20	$9.92
6	0.39	0.00	$0.00	1.65	0.00	$0.00
7	0.72	0.36	$0.04	1.77	0.88	$0.09
End	0.51	0.00	$0.00	4.06	0.00	$0.00

3.5.7.2 Additive Tooling

Table 45 shows the energy usage and energy costs for each process step for the 3D printing of Geometry #1 and Geometry #2. In this case, most energy usage and costs were associated with the printing and tool washout process steps. The printer itself and the cleaning bath required for the washout process have relatively high power requirements for heating. They are also very time-consuming process steps and require a lot of energy. In contrast, the print preprocessing, secondary bonding and finishing, and sealing steps require much less energy, because they are relatively short steps, the equipment use is minimal, and several operations can be completed simultaneously, such as the final finishing and sealing.

Table 45. Energy Usage and Energy Costs Associated with Each Process Step for the 3D printing of Geometry #1 and Geometry #2

Process Step	Geometry #1			Geometry #2		
	Process Time (hours)	Energy Use (kWh)	Energy Cost	Process time (hours)	Energy Use (kWh)	Energy Cost
1	1.00	0.00	$0.00	2.00	0.00	$0.00
2	16.24	162.40	$16.24	38.57	385.72	$38.57
3	0.00	0.00	$0.00	0.00	0.00	$0.00
4	1.03	15.38	$1.54	4.06	60.85	$6.09
5	0.00	0.00	$0.00	0.00	0.00	$0.00
6	1.03	1.37	$0.14	4.46	3.35	$0.33
End	4.06	40.64	$4.06	9.75	97.52	$9.75

3.5.8 Presentation and Discussion of Results

Finally, all of the cost results calculated in the labor cost, material cost, equipment cost, and energy cost modules were directed toward the results module for analysis. The separation of the modules allowed for cost breakdowns and a deeper analysis of the significant differences between the manufacturing processes and the two different geometries. Tracking processing times in the labor cost module also allowed for process time comparisons, which can be a significant driver in manufacturing operations and can inform future decisions for composite manufacturers.

3.5.8.1 Cost Comparison

Table 46 and Figure 63 show the overall cost breakdowns and comparison for conventional manufacturing and additive manufacturing of Geometry #1, based on labor, material, energy, and equipment costs in 2020. In this comparison, costs associated with the washout process have been subtracted to properly compare the tool manufacturing processes on their own. On comparison of the totals given in Table 46 and Figure 63, it is clear that the additive manufacturing process developed by CSU is significantly cheaper than subtractive manufacturing of ceramic sand for composite washout tool manufacturing. In fact, manufacturing Geometry #1 with a 3D printer and the Stratasys ST-130 filament is almost a 40% reduction in cost when compared to conventional in-house manufacturing techniques. On further inspection, it is evident that the main cost differences come from the labor and material costs. Additive manufacturing is very much a hands-off process. Very little labor is required aside from preparing the printer and minor finishing operations. The conventional manufacturing of ceramic tools is more involved, especially in terms of preparing the ceramic blocks and the bulk preform to be machined. It is also a messy process. Significant labor time is required for the cleanup of the ceramic sand after machining and final finishing.

The calculated material costs associated with additive manufacturing were significantly cheaper as well. This is also one of the main benefits of additive manufacturing. Only the required amount of material for the final tool form is used. It also allows for more optimization to further reduce material costs. In the case of Geometry #1, a 40% in-fill was used to calculate the required amount of ST-130 filament. In comparison, a lot more material is needed to manufacture a conventional tool from ceramic blocks. Table 21 shows how much material would be wasted during the CNC machining process. In addition, the subtractive manufacturing process does not allow for as much optimization to reduce material usage.

The equipment and energy costs for the two manufacturing processes were much less significant and only accounted for 18% of the costs total. They were relatively similar between conventional and additive manufacturing. For equipment, the 3D printer cost used was very similar to the CNC machine cost, which accounted for a large proportion of the equipment costs (see Table 37 and Table 41). Also, because the conventional machining is a dirtier process, there are greater requirements for vacuum systems and dust collection systems. The energy costs were also relatively comparable but should be taken with caution. As mentioned in Section 5.5.7, the method of calculating these costs were based on some broad assumptions and will require more refinement in future iterations of the TEM.

Table 46. Cost Breakdowns and Comparisons for the Conventional and Additive Manufacturing of Geometry #1

Module	Conventional Manufacturing		Additive Manufacturing	
	Cost	Cost Share	Cost	Cost Share
Labor	$553.35	37.7%	$326.39	34.4%
Materials	$737.71	50.3%	$452.93	47.7%
Equipment	$155.43	10.6%	$151.50	16.0%
Energy	$20.33	1.4%	$17.91	1.9%
Total:	**$1,466.81**	**Total:**	**$948.74**	
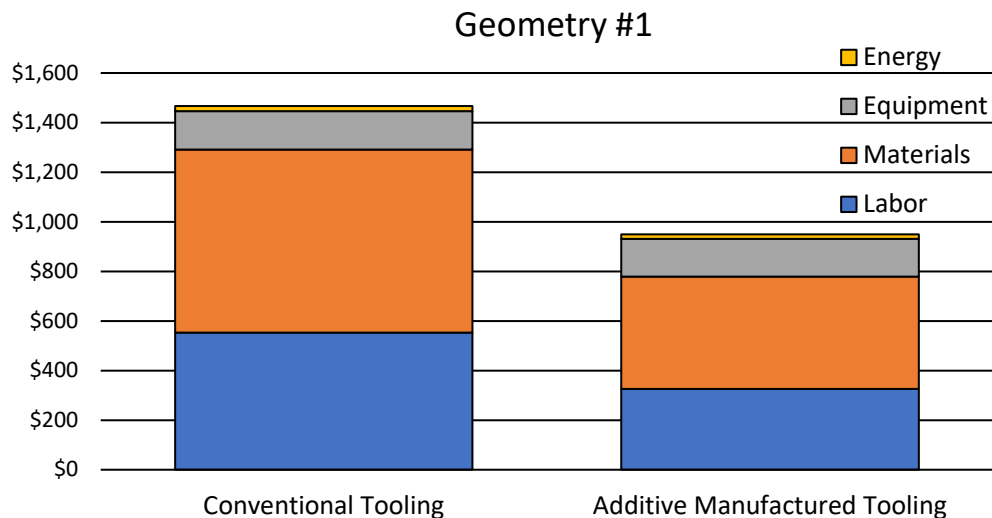
Figure 63. Cost share comparison for the conventional and additive manufacturing of Geometry #1

Table 47 and Figure 64 show the overall cost breakdowns and comparison for conventional manufacturing and additive manufacturing of Geometry #2, based on labor, material, energy, and equipment costs in 2020. Again, tool washout costs were removed from these cost breakdowns to be analyzed separately. The cost totals for Geometry #2 showed similar differences to those for Geometry #1. Conventional manufacturing of Geometry #2 as a washout tool was significantly more than that with additive manufacturing. In fact, the difference was even greater with additive manufacturing being almost 55% cheaper than conventional manufacturing methods. Again, the largest differences were due to labor and material costs. The labor costs actually show a smaller percentage difference when compared with those from Geometry #1. This was probably because Geometry #2 was specified to be printed in four separate pieces rather than two, requiring more hands-on labor.

The material costs show the most significant differences. Again, conventional manufacturing using ceramic blocks does not allow for much optimization in terms of reducing materials usage. In the case of Geometry #2, it was modified significantly to expedite the additive manufacturing process. It was shelled out to a 0.75 in shell thickness, and then the density was reduced even further with a 40% in-fill. To compare, approximately 8,400 in^3 of ceramic sand would be required to make the conventional preform versus only 300 in^3 for the optimized additively manufactured tool. Turning the geometry into a shell was possible in this instance because the geometry was a single duct, which allows for the easy application of a vacuum bag through the mold cavity. For ducts with multiple inlets and outlets, this kind of optimization may not always be possible.

The equipment and energy costs were still relatively comparable, although slightly less for additive manufacturing. This was expected, because the equipment requirements for both manufacturing processes were largely unchanged from Geometry #1, aside from the addition of a forklift for the conventional manufacturing and slight modifications in capital equipment usage over the project run time.

Table 47. Cost Breakdowns and Comparisons for the Conventional and Additive Manufacturing of Geometry #2

Module	Conventional Manufacturing		Additive Manufacturing	
	Cost	Cost Share	Cost	Cost Share
Labor	$1,141.88	24.8%	$826.60	38.9%
Materials	$3,218.88	69.8%	$1,052.41	49.5%
Equipment	$196.69	4.3%	$201.25	9.5%
Energy	$50.77	1.1%	$44.99	2.1%
Total:	**$4,608.22**	**Total:**	**$2,125.25**	
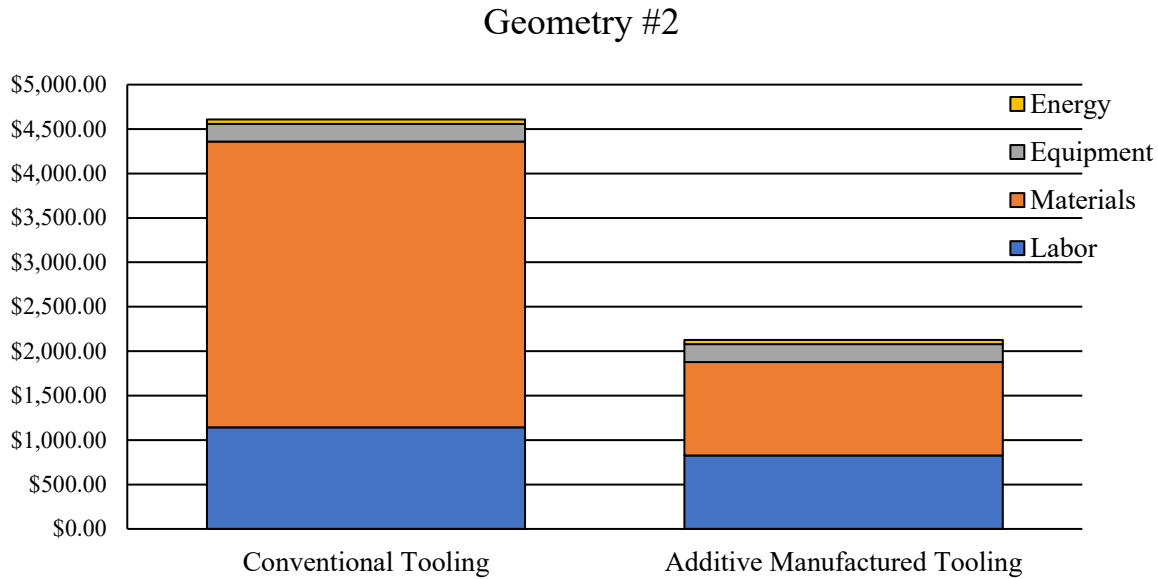
Geometry #2

Figure 64. Cost share comparison for the conventional and additive manufacturing of Geometry #2

Finally, Figure 65 shows a comparison of the TEM results for washout costs for both manufacturing processes and geometries, based on labor, material, energy, and equipment costs in 2020. For Geometry #1, washout costs were relatively comparable between conventional and additive manufacturing processes and insignificant when compared to the overall tool manufacturing processes. For conventional manufacturing, the main costs originated from labor, because a technician has to wash out the tool manually, whereas the additively manufactured tool washout costs were more a combination of labor for a technician to set up the cleaning bath and materials (the cleaning solution). The washout costs for Geometry #2 showed much greater differences in costs. The washout costs for a conventionally manufactured ceramic sand tool significantly increased. This was all attributed to labor costs. More medium would need to be washed out, so a technician would have to spend more time on the operation. In comparison, washout costs for an additively manufactured tool increased but not by anywhere near as much. The labor costs did not change (see Table 31), but more cleaning solution would be required for a longer time in the cleaning bath, which means higher energy usage. The additive manufacturing washout costs do not account for disposal for the basic cleaning solution. Although it is a light detergent and can often be diluted and disposed of with general wastewater, environmental impacts should be considered carefully, and proper disposal methods should be applied when dissolving large amounts of polymer-based 3D prints in basic solutions.

Tool Washout Costs

Figure 65. Comparison of washout costs for the conventional and additive manufacturing of Geometry #1 and Geometry #2

3.5.8.2 Process Time Comparison

Table 48 and Figure 66 show process step times and their respective time shares and totals for the conventional and additive manufacturing of Geometry #1. Again, tool washout times were removed for separate analysis. The differences in total process times show that the conventional tool manufacturing process is much faster. A single tool can be manufactured in less than 8 hours, whereas it would take more than 20 hours with additive manufacturing. The process times were relatively evenly distributed over each process step for the conventional manufacturing process. With additive manufacturing, however, the process times were largely associated with the printing process itself. Even though no support cleaning was necessary, and surface finishing and sealing of the tool could be completed simultaneously with the printing process, the printing of the tool would still take more than 16 hours. This highlights a crucial downside to the additive manufacturing process, especially with filament extrusion-type 3D printers. Despite this, there is plenty of room to expedite the additive manufacturing process in the future. For example, optimizing the geometry to reduce material costs would also reduce print times. Other methods, such as using multiple extrusion heads with different nozzle diameters, could also increase material deposition rates and reduce print times.

Table 48. Process Time, Time Share, and Total Process Time Comparisons for the Conventional and Additive Manufacturing of Geometry #1

Process Step	Conventional Manufacturing		Additive Manufacturing	
	Process Time (hours)	Time Share	Process Time (hours)	Time Share
1	2.50	31.77%	1.00	4.98%
2	1.00	12.71%	16.24	80.83%
3	0.50	6.35%	0.00	0.00%
4	1.99	25.31%	1.03	5.10%
5	0.78	9.85%	0.00	0.00%
6	0.39	4.92%	1.83	9.09%
7	0.72	9.09%		
Total:	7.87	Total:	20.09	
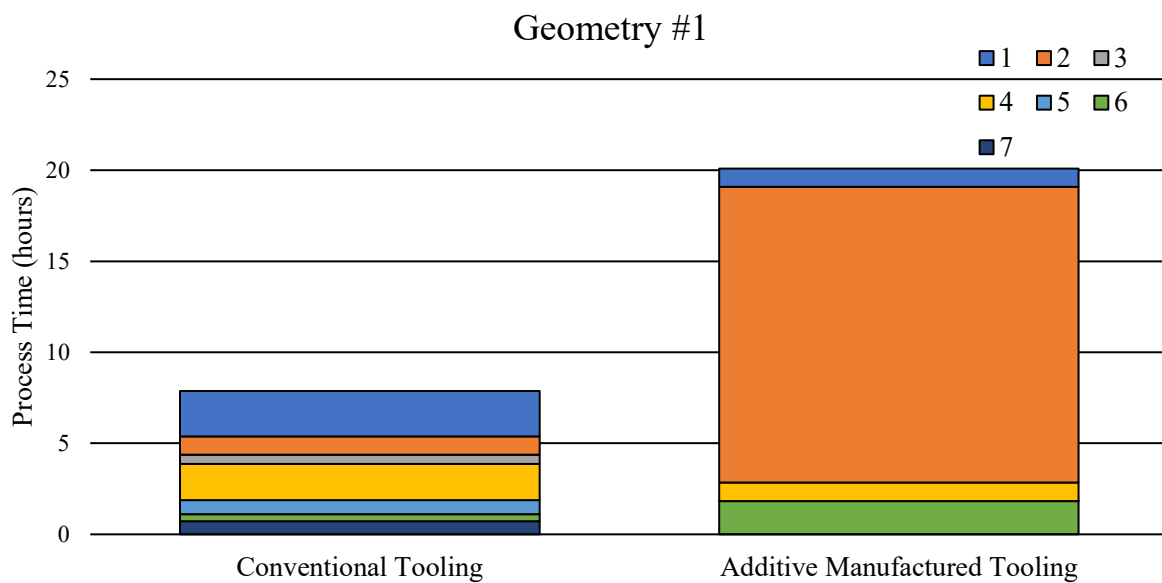
Figure 66. Time share comparison for the conventional and additive manufacturing of Geometry #1

Table 49 and Figure 67 show process step times and their respective time shares and totals for conventional and additive manufacturing of Geometry #2 with times for the washout process steps removed for separate analysis. The process time breakdown for Geometry #2 showed similar relationships to those of Geometry #1. Process times for the conventional manufacturing process were still relatively evenly distributed across all process steps, whereas the additive manufacturing process was still heavily weighted toward the printing process step. Also, this was with a large amount of the tool volume removed to leave a shell. If this had not been done, then the print times would be infeasible. Even with a reduced print volume, the print time at almost 40 hours could still be excessively long under some circumstances, but there is certainly room for improvement in this area.

Process Step	Conventional Manufacturing		Additive Manufacturing	
	Process Time (hrs)	Time Share	Process Time (hrs)	Time Share
1	4.50	23.18%	2.00	4.07%
2	2.00	10.30%	38.57	78.57%
3	0.50	2.58%	0.00	0.00%
4	5.69	29.31%	4.06	8.26%
5	3.31	17.03%	0.00	0.00%
6	1.65	8.52%	4.46	9.09%
7	1.77	9.09%		
Total:	19.42	Total:	49.09	
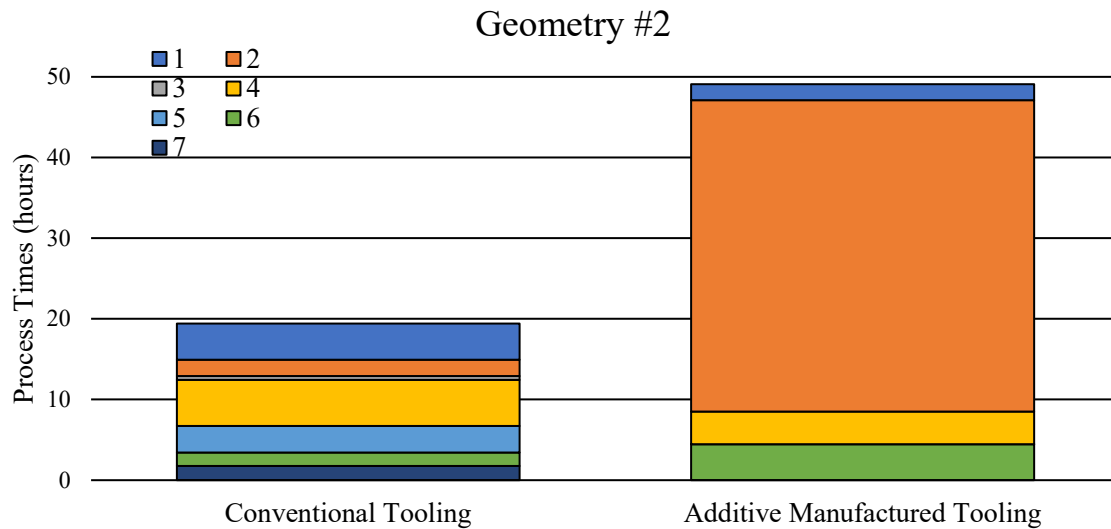
Figure 67. Time share comparison for the conventional and additive manufacturing of Geometry #2

Finally, Figure 68 shows a comparison of the TEM results for washout times for both manufacturing processes and geometries. Like the main manufacturing processes, the tool washout process was also much slower for the additively manufactured tools when compared to the conventionally manufactured tools. The Stratasys ST-130 filament used in this study had a much slower dissolution rate than the ceramic sand, even in an elevated temperature bath with basic detergent solution and reduced print density. Again, there is room for improvement for the additively manufactured tool washout process. If the print volume of the tools can be reduced further with optimization, then washout times could also be significantly reduced.
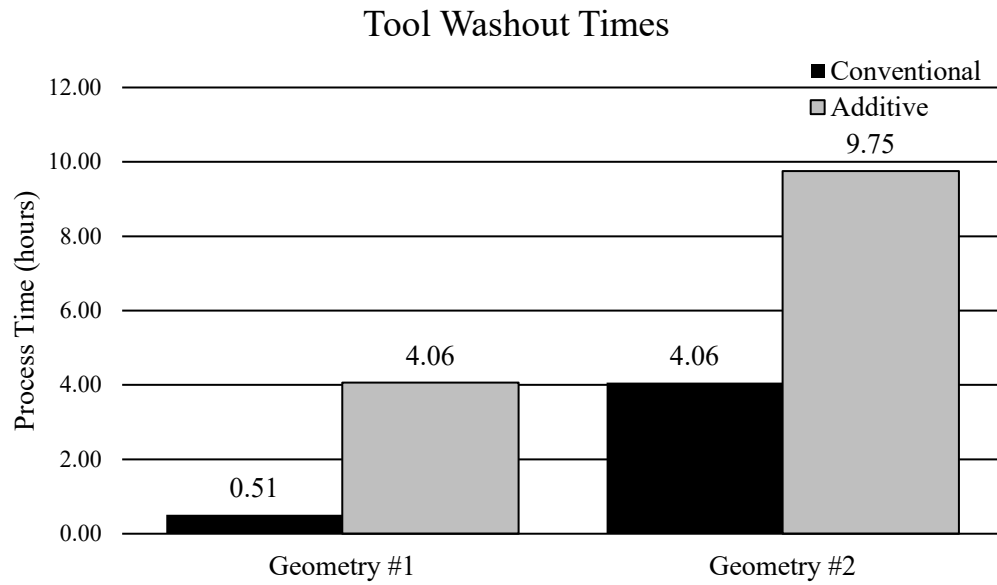
Tool Washout Times

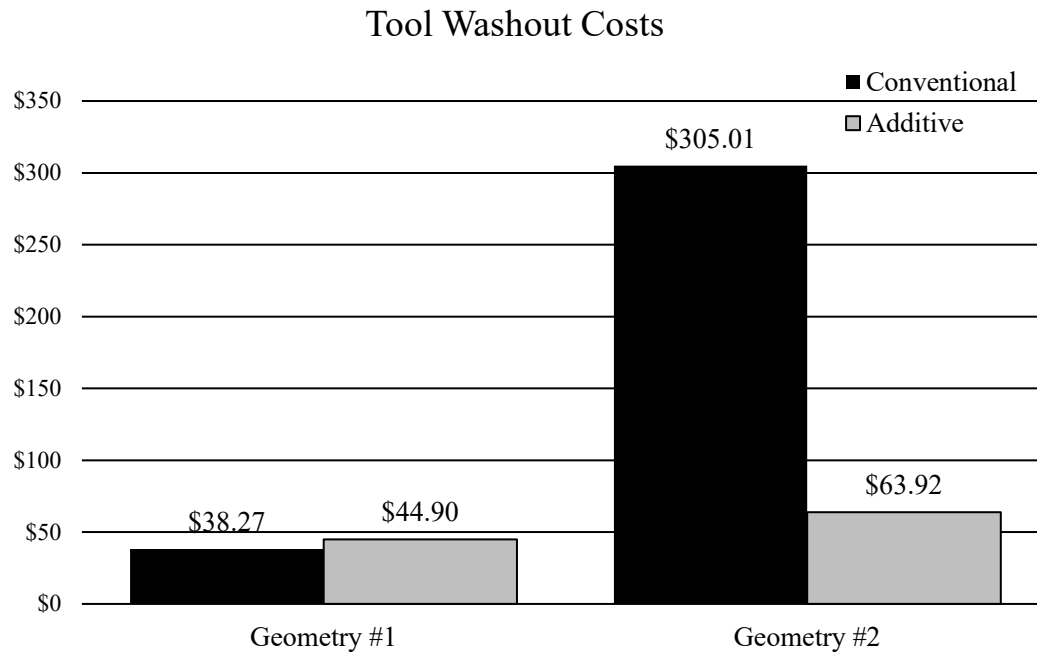*Figure 68. Comparison of washout times for the conventional and additive manufacturing of Geometry #1 and Geometry #2*

4 CONCLUSIONS

4.1 Physical Development of Dissolvable Tooling

The desire to move toward rapid manufacture of tooling for the processing of composite parts is complimented well by the benefits of additive manufacturing. The potential benefits of 3D printed tooling increase further as the geometric complexity increases. This is particularly true for composite parts produced on sacrificial tooling, which offer opportunities for even greater geometric complexity as the need for multiple tool or mold segments and the associated parting planes disappears.

Of the dissolvable candidate materials examined, the most successful tooling material, from a geometric fidelity standpoint, was Stratasys ST-130. However, it also requires a basic solution for washout, and it has a significant CTE that requires careful incorporation into tool design to generate accurate dimensions in the final composite part. AQ-180 was also identified as a successful dissolvable tooling material, stable at temperatures slightly less than ST-130. It can be dissolved in water and has a lower CTE. This material, in circumstances where slightly lower temperature cure cycles are permissible, may be preferable to ST-130 and moving to higher infill densities may extend the composites processing window. Processing challenges for ST-130 and AQ-180 include requiring a need for a heated build chamber, approaching the glass transition temperatures of the materials, and moisture absorption during storage and printing. The most important parameter for controlling the tool robustness was infill density. Between gyroid and quarter-isogrid infill patterns, it was found that gyroid outperformed the quarter-isogrid pattern in crush testing. However, alternative tooling configurations that allow full density were recognized to be preferred.

The results of curing composites on the square pyramid tools showed that the tool remained rigid enough to support the composite during the 121 °C/345kPa cure, with deviations of approximately +/- 0.25 mm (0.010"). It was seen that the surface geometry and roughness of the tool transferred to the cured part. The use of surface smoothing routines holds promise for improving the surface finish of completed parts, making the use of a secondary surface treatment step unnecessary. The deviations from the nominal part geometry were likely caused by a combination of 3D printer inaccuracy, CTE driven deformation during cure, and tool softening during cure.

The complex bent duct tooling studies showed that the elevated cure temperature of 160 °C and pressure of 420kPa used in the Ability Composites autoclave trials exceed the capabilities of the 3D printed tooling materials in this study. However, the study also showed how a hollow duct geometry may provide significant savings in manufacturing time and material usage, while also reducing tool structural requirements and enabling satisfactory composite part production. The associated TEM indicated that this hollow tool approach was less than half the cost of the corresponding conventional washout tool.

The dissolution studies included, AQ-180 and ST-130, as well as conventional washout material. The conventional washout material could be removed from a duct with light labor using hand tools after soaking in water for several hours. By drilling a hole in an AQ-180 sample, it was shown that the gyroid infill could successfully be flooded, greatly reducing the washout time. The ST-130 used a trisodium phosphate solution, but future trials including WaterWorks or EcoWorks may improve washout times.

Complex duct-like geometries should be made hollow during printing, if possible, for benefits including reduced material use, reduced manufacturing time, and thin-walled tooling allowing for faster heat-up rates in autoclave processes. The vacuum bagging utilized for the hollow geometries showed a reduced, but existent, need for highly structural tools. Tooling with relatively thin walls still showed good performance

even at temperatures much higher than the tool's HDT. Overall, the 3D printed dissolvable tooling shows good promise for the lack of need for surface sealing, the geometric complexity that becomes possible, and the ability to utilize hollow tooling. However, significant attention should be paid to the tradeoffs between material usage and structural requirements during cure. Because the tooling is a thermoplastic, the structural properties decrease as the temperatures increase. Therefore, careful consideration of the tradeoffs between structural integrity and material usage (infill density), as well as of the cure temperature, CTE, and vacuum bagging approach should be made to ensure composite part fidelity.

4.2 Techno-Economic Modeling

A TEM was developed to assess the costs and viability of utilizing additive manufacturing for producing washout composite tools for manufacturing complex composite features, such as ducts and other components where internal surface quality is critical. The goal of the TEM was to compare conventional washout tool manufacturing processes with the additive manufacturing process being developed at CSU. It utilized information in the form of geometry and process parameters to determine the costs associated with four main categories: labor, materials, capital equipment, and energy. The TEM was also able to calculate process times for the two manufacturing processes.

To assess the TEM and the viability of additively manufactured washout tooling, two geometries were used for comparison. Geometry #1 was a bent rectangular duct, and Geometry #2 was the same duct but double the scale. Knowledge and experience were provided by Ability Composites and CSU to define the process parameters that would be associated with the two geometries. The results have clearly shown that the additive manufacturing process developed at CSU would reduce washout tool manufacturing costs significantly. Material costs were lower as well as associated labor costs. Additive manufacturing requires little supervision, so tools can be manufactured with little in the way of labor costs. The additive manufacturing approach also allows for a large amount of design optimization for the tools, as was demonstrated by the shell approach to Geometry #2. This showed potential for even greater savings on material costs.

The analysis of process times, however, indicated a potential disadvantage to the additive manufacturing approach. Print times for the specified geometries were calculated to be significantly longer than the process times for conventional manufacturing of washout tools. Despite this, tool design optimization has the potential to reduce these print times and make them more comparable to the conventional manufacturing processes.

Finally, the tool washout process was compared between the two manufacturing techniques. Again, the TEM indicated that the additive manufacturing approach is generally cheaper because it requires minimal labor, at the expense of longer process times. The selected 3D print medium dissolves much slower than the ceramic sand used in the conventional manufacturing process.

Overall, the developed TEM operated as expected and was successful in highlighting the advantages and disadvantages of additively manufacturing washout tools when compared with conventional manufacturing techniques. The results matched up well with the hands-on manufacturing research conducted by CSU and Ability Composites. Despite this, a number of features were highlighted as potential improvements for future iterations of the TEM. In future research, the 3D print geometry parameters could be expanded to allow for better definition of 3D print-optimized tool geometries. Only print in-fill was used in this case, but the parameters could be extended to use print wall thicknesses and shell thicknesses. Also, better definition of 3D print deposition rates would be a useful feature, especially if this research moves toward

using multiple print nozzles of different diameters to reduce printing times. Another minor difficulty encountered was properly accounting for capital equipment costs. Because not all capital equipment was dedicated to the tool manufacturing process, special considerations had to be made for their proportional usage on specific tool manufacturing runs. In this case, the parameters were provided as user inputs, which led to a lot of rough estimates. Future iterations of the TEM could include equations linking process and labor times to proportional usage of capital equipment. This would reduce the requirement for rough user inputs. Finally, the energy calculations were based on the assumptions that the cost of energy is linear, and that capital equipment would have constant power requirements throughout process steps. The results of this study showed that energy costs accounted for very small proportions of the total manufacturing costs, but future studies may require greater refinement.

Ultimately, the TEM produced for this project has shown to be very useful for comparing and assessing tool manufacturing costs for the additive manufacturing and conventional manufacturing techniques. It was also built in such a way that future users should be easily able to make changes and modifications to suit their manufacturing process requirements.

5 ACCOMPLISHMENTS

The accomplishments developed from this work include:
1. Publication submitted:
   Murdy, P., Snowberg, D., Berry, D., Radford, D. and Morris, I., "Subtractive or Additive Manufacturing? A Techno-economic Comparison for Soluble Composite Tooling", *The International Journal of Advanced Manufacturing Technology*
2. CAMX 2021 conference proceedings.
   Morris, I. and Radford, D., "Development of Additively Manufactured Dissolvable Tooling for Autoclave Cured Composites." *CAMX 2021,* Dallas, TX. 2021.
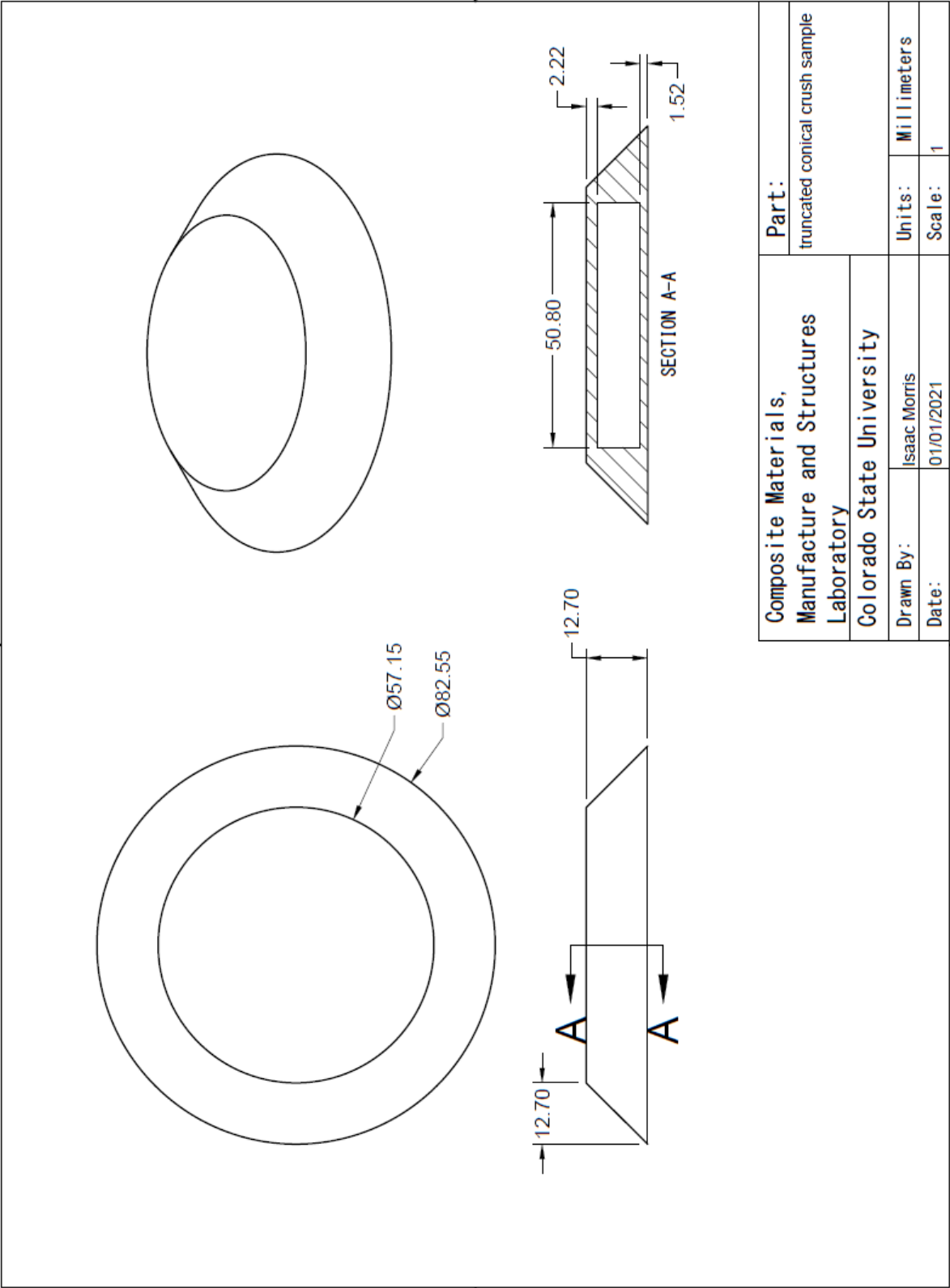3. Thesis content applied to one graduate student's work, in progress.

6 REFERENCES

1. Post, B., Richardson, B., Lloyd, P., Love, L., Nolet, S., & Hannan, J. (2017). Additive Manufacturing of Wind Turbine Molds.

2. Stratasys. (2017). FDM for Composite Tooling 2.0: Design Guide.

3. Türk, D.-A., Kussmaul, R., Zogg, M., Klahn, C., Leutenecker-Twelsieka, B. and Meboldt, M., "Composites Part Production with Additive Manufacturing Technologies." *1st CIRP Conference on Composite Materials Parts Manufacturing*. 2017. Elsevier. [DOI: 10.1016/j.procir.2017.03.359]

4. Hassen, A.A., Lindahl, J., Chen, X., Post, B., Love, L. and Kunc, V., "Additive Manufacturing of Composite Tooling using High Temperature Thermoplastic Materials." *SAMPE 2016*, Long Beach, CA. 2016.

5. Kunc, V., Lindahl, J., Dinwiddie, R., Post, B., Love, L. Duty, C., Matlack, M., Fahley Jr., R.L. and Hassen, A.A., "Investigation of In-Autoclave Additive Manufacturing Composite Tooling." *CAMX*, Anaheim, CA. 2016.

6. Stickland, J., Martinez, P., Noel, A., Nolan, P., Cheung, A., and Ursenbach, D., "Design, Analysis, and Manufacturing of a Fiber Reinforced Composite Hard Upper Torso for the Exploration Space Suit." *SAMPE 2021*, Long Beach, CA. 2021. Türk, D.-A., Ebnöther, A., Zogg, M. and Meboldt, M., "Additive Manufacturing of Structural Cores and Washout Tooling for Autoclave Curing of Hybrid Composite Structures." *Journal of Manufacturing Science and Engineering* 140 (2018). [DOI: 10.1115/1.4040428]

7. Wallen, M., Rossfeldt, J., Aune, C., and Wing, Z. N., "Flexible Manufacturing of Hollow Composites via Soluble Tooling." *SAMPE 2013,* Long Beach, CA. 2013.

8. Thompson, Eric J., "Design of a multi-piece removable mandrel mold tool to fabricate and control inner mold surface contour of a composite wing spar" (2010). *Graduate Theses, Dissertations, and Problem Reports*. 4664.

9. Wing, Z. N. and Vaidyanathan, R., "Evaluation of Out of Autoclave Composite Properties Manufactured from a Soluble Self-Pressurizing Tooling." *SAMPE 2016*, Long Beach, CA. 2016.

10. Türk, D.-A., Triebe, L., and Meboldt, M., "Combining Additive Manufacturing with Advanced Composites for Highly Integrated Robotic Structures." *26th CIRP Design Conference*. 2016. Elsevier. [DOI: 10.1016/j.procir.2016.04.202]

11. Türk, D.-A., Einarsson, H., Lecomte, C. and Meboldt, M., "Design and Manufacturing of High-Performance Prostheses with Additive Manufacturing and Fiber-Reinforced Polymers." *Production Engineering* 12 (2018):203-213. [DOI: 10.1007/s11740-018-0799-y]

12. Tosto, C., Latteri, A., Pergolizzi, E., Giordano, D., Abramo, G., Catenaro, R., Pignotti, N., and Cicala, G., "Additive Manufacturing of Plastics: An Efficient Approach for Composite Tooling." *Macromolecular Symposia*. 2020. Wiley. [DOI: 10.1002/masy.201900069]

13. Biedermann, M., Widmer, M. and Meboldt, M., "Additive Manufactured Break-out Cores for Composite Production: A Case Study with Motorcycle Parts." *Munich Symposium on Lightweight Design*. 2020. Springer Berlin Heidelburg. [DOI: 10.1007/978-3-662-63143-0_7]

14. Baker, A., McCoy, J., Majumdar, B., Rumley-Ouellette, B., Wahry, J., Marchi, A., Barnardin, J., & Spernjak, D. "Measurement and Modelling of Thermal and Mechanical Anisotropy of Parts Additively Manufactured Using Fused Deposition Modelling (FDM)." *Eleventh International Workshop on Structural Health Monitoring.* Stanford, CA, 2017. Kopsaftopoulos, F., Chang, F. [DOI:10.12783/SHM2017/13917]

15. Roy, M. and Dickens, T.J., "Additive Technology of Soluble Mold Tooling for Embedded Devices in Composite Structures: A Study on Manufactured Tolerances." *Additive Manufacturing* 15 (2017): 78-86.

16. Sardinha, M., Vicente, C. M. S., Frutuoso, N., Leite, M., Ribeiro, R., & Reis, L. (2020). Effect of the ironing process on ABS parts produced by FDM. Material Design & Processing Communications, n/a(n/a), e151. doi:https://doi.org/10.1002/mdp2.151

7 APPENDICES

The appendices show the geometries manufactured by the CMMS Lab at CSU and by Ability Composites to compare the fidelity of 3D printed tooling to traditional ceramic washout tooling.

Appendix A. Crush sample geometry

SECTION A-A

2.22

1.52

50.80

12.70

12.70

Ø57.15

Ø82.55

A

A

Composite Materials, Manufacture and Structures Laboratory
Colorado State University

Part:	truncated conical crush sample	
Drawn By:	Isaac Morris	Units: Millimeters
Date:	01/01/2021	Scale: 1

Appendix B. Truncated Square Pyramid - PETG

SECTION A-A

Composite Materials, Manufacture and Structures Laboratory	Part: half size truncated square pyramid	
Colorado State University		
Drawn By: Isaac Morris	Units: Millimeters	
Date: 01/01/2021	Scale: 1	

76.20

50.80

12.70

12.70

50.80

76.20

1.27

.60

.60
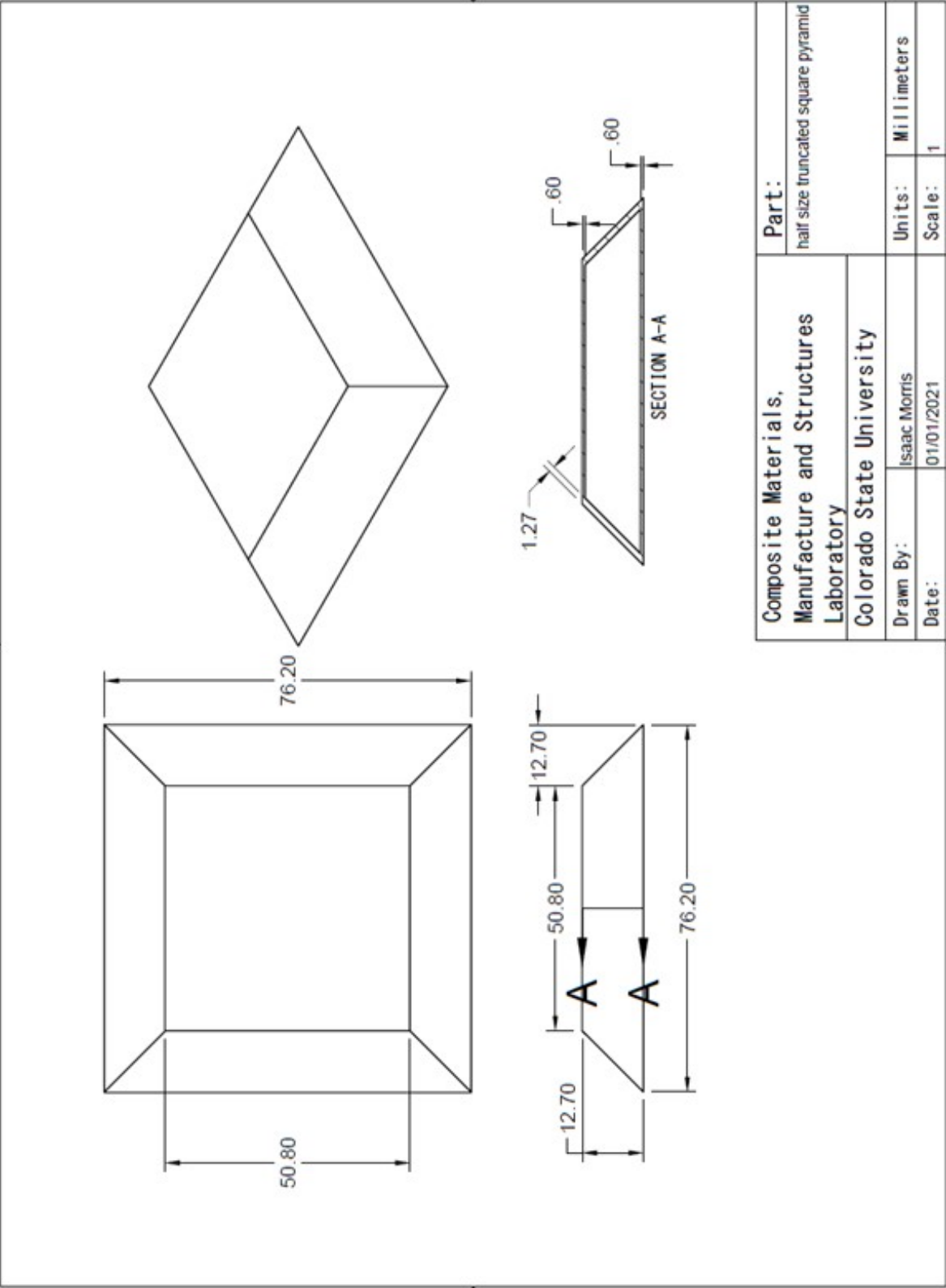
Appendix C. Truncated Square Pyramid – Composite Manufacturing Trials

SECTION A-A

3.28

2.82

1.91

152.40

101.60

25.40

101.60

152.40

25.40

A

A

Composite Materials, Manufacture and Structures Laboratory	Part:
	truncated square pyramid
Colorado State University	
Drawn By: Isaac Morris	Units: Millimeters
Date: 01/01/2021	Scale: 1:2
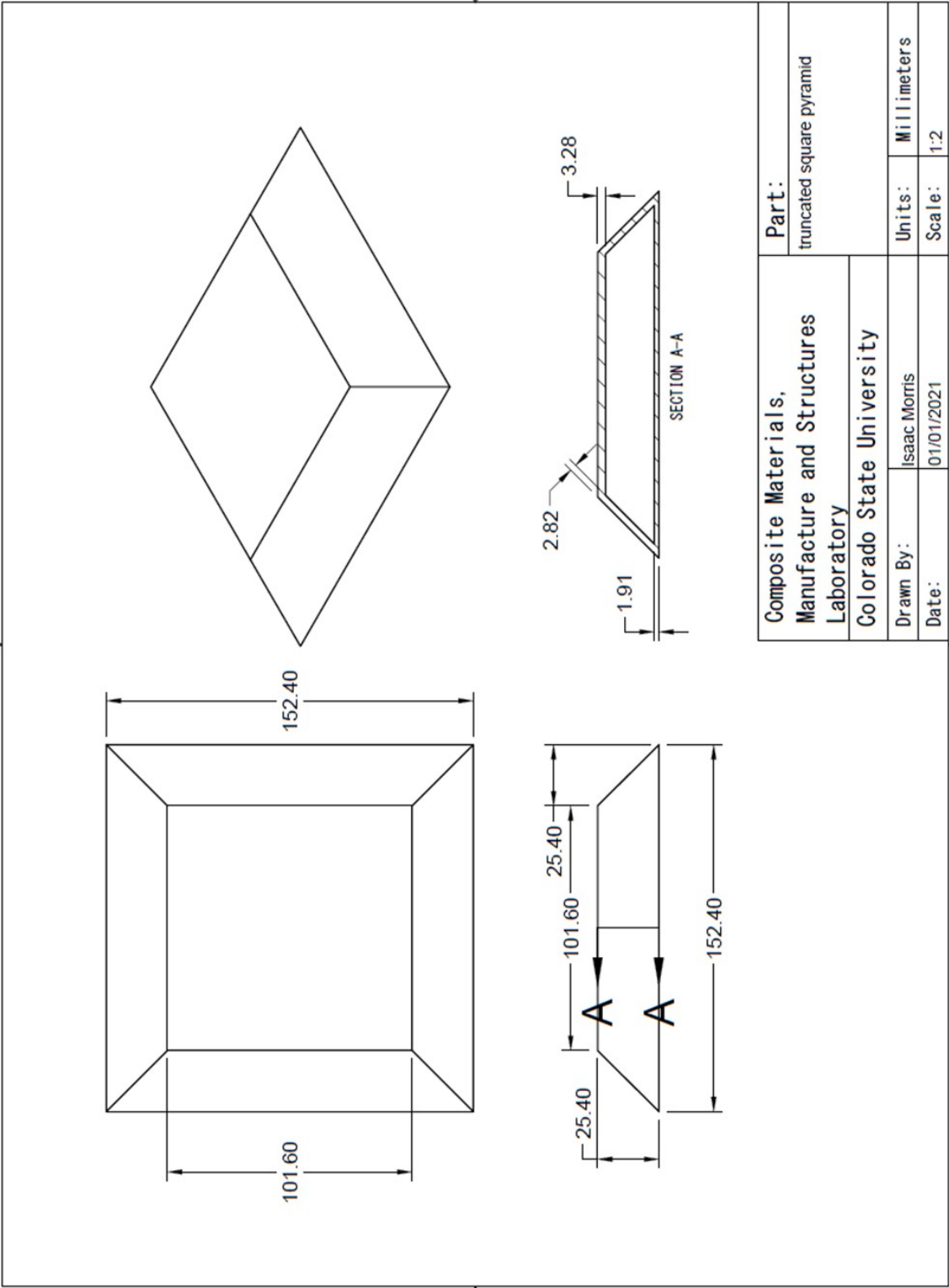
Appendix D. Bent Duct Tooling

Part: bent duct 12.5 inch

Composite Materials, Manufacture and Structures Laboratory

Colorado State University

| Drawn By: | Isaac Morris |
| Date: | 01/01/2021 |

Units: Millimeters

Scale: 1:6

Dimensions shown: 101.60, 38.61, 88.46, R387.90, 88.45, 38.61, R388.01, R119.82, R12.70, 38.61, R81.13, 93.72, R278.51, 152.40, 38.61, 152.40, Ø12.70, R278.49, 93.73, R81.17, 101.60
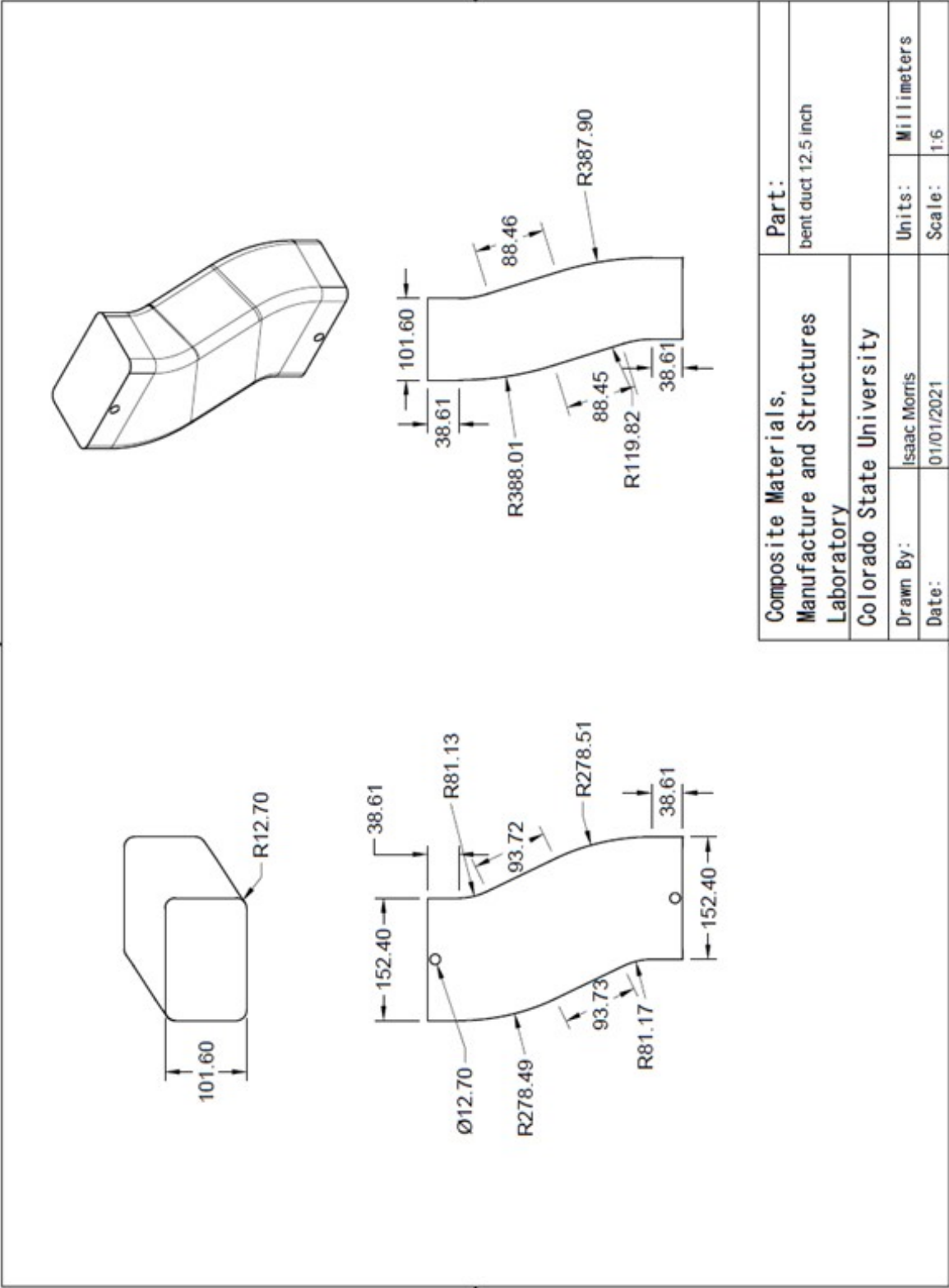
Appendix E. Top Half – Longitudinally Split Duct

Composite Materials, Manufacture and Structures Laboratory	Part:
	bent duct 12.5 inch top
Colorado State University	
Drawn By: Isaac Morris	Units: Millimeters
Date: 01/01/2021	Scale: 1:6

76.20

25.40

152.40

152.40

R12.70

317.50
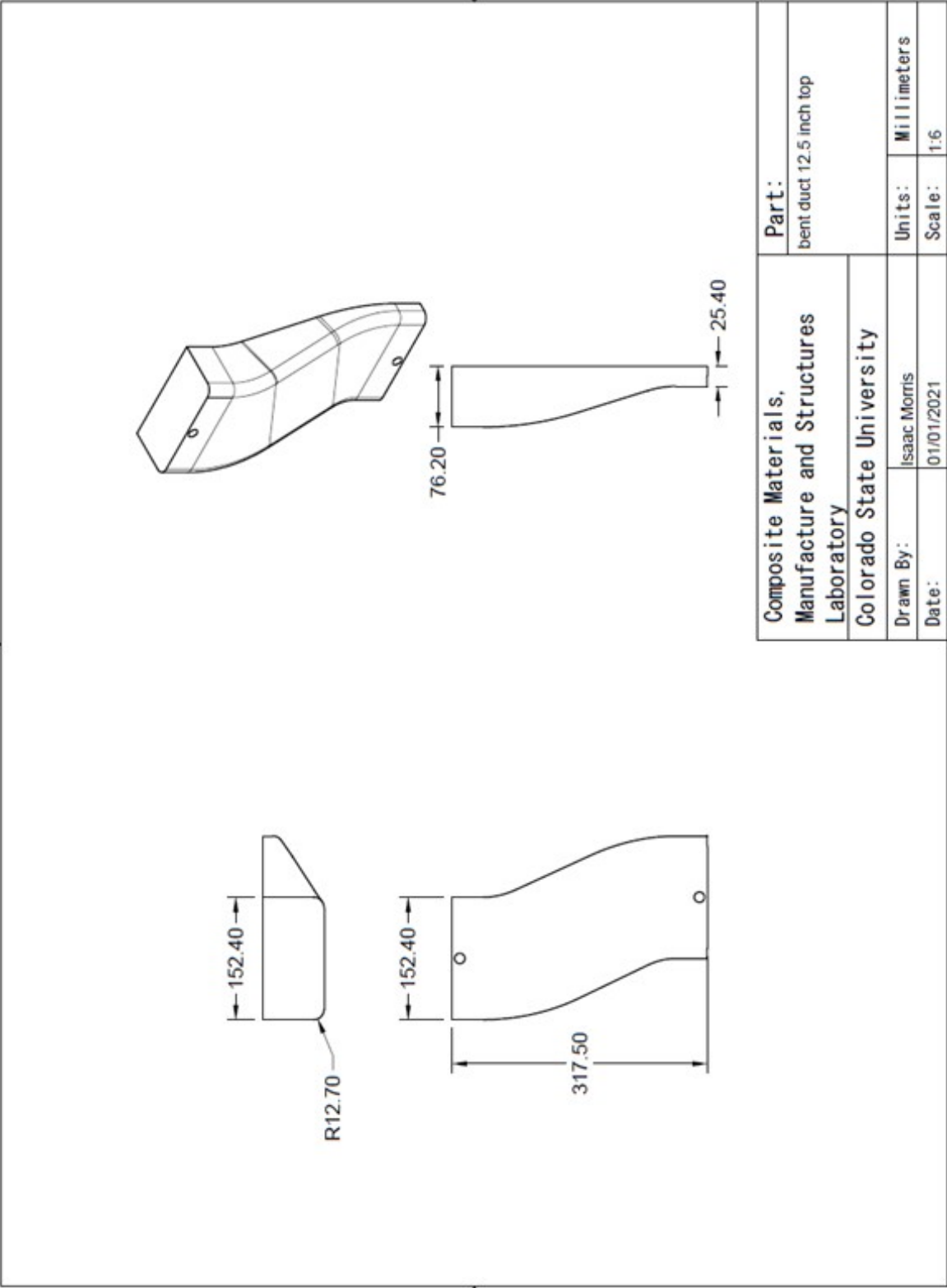
Appendix F. Bottom Half – Longitudinally Split Duct

Composite Materials, Manufacture and Structures Laboratory

Colorado State University

Part:	bent duct 12.5 inch bottom
Drawn By:	Isaac Morris
Date:	01/01/2021
Units:	Millimeters
Scale:	1:6

R12.70

152.40

152.40

317.50

228.60

76.20

25.40